Water-based Synthesis of Oxide Semiconductor Fine Particles for Efficient Photocatalyst Systems

Sayuri Okunaka

2016

Water-based Synthesis of Oxide Semiconductor Fine Particles for Efficient Photocatalyst Systems

Sayuri Okunaka

Department of Energy and Hydrocarbon Chemistry
Graduate School of Engneering
Kyoto University
Kyoto, Japan

2016

Table of Contents

General Introduction

1. Objective of this thesis

In recent decades, environmental problems such as global warming and the depletion of energy resources have become more serious than ever. To address these issues, the development of clean energy carrier that is independent from any fossil fuels, not only the technologies for the utilization of renewable energies, has been strongly desired and thus extensively studied. Although hydrogen is considered as one of the most promising energy carrier for clean generation of electricity and/or heat *via* technologies such as fuel cells, most hydrogen is currently produced from fossil resources, mainly methane in natural gas, *via* steam-reforming reaction.[1] Therefore, the development of the technology that can produce hydrogen from non-fossil resources such as water by using renewable energy is strongly desired. Water splitting using semiconductor photocatalysts is considered as one of the promising technologies that can produce hydrogen cleanly and directly from water by harvesting abundant solar light energy, thus has been extensively studied.[2-10] For the practical application of this technique for commercial hydrogen production, however, significant enhancement in the solar-light to hydrogen conversion efficiency is still indispensable.[10] Semiconductor photocatalysts can also be applied to decompose and/or neutralize various pollutants (toxic organic compounds, NOx, SOx, etc.) in environments, by utilizing the energy of solar light (or other artificial light sources in some cases).[11–13] As for such environmental purification, the products with photocatalytic ability, such as TiO_2-coated glass or WO_3-coated glass, have been already commercialized on some levels. To expand the use of photocatalysts in environmental purification, however, the development of highly active and scalable photocatalyst materials that are low-cost and abundant still required. Additionally, the development of technologies for effective immobilization of photocatalyst in a cost-effective and environmentally-friendly way is essential to further expand such application because photocatalyst particles are basically immobilized on a substrate (e.g., glass or silicon) in practical applications. Such effective immobilization is also indispensable for the practical application of photocatalytic water splitting in near future, because the simple scale-up of the present suspension-base system results in the necessity of huge energy for keeping the photocatalyst particles suspended in solutions.[14]

To address the above mentioned problems, the present thesis focused on (1) the development of environmentally-friendly water-based synthesis processes of fine oxide semiconductor particles that exhibit high photocatalytic activities for water splitting and/or environmental purification, and (2) the immobilization of these particles onto substrates with maintenance of their high activities. Highly

active photocatalyst particles with diameters below 100 nm were synthesized by controlling the particle growth during calcinations process using appropriate chelate agents in precursor aqueous solutions. The prepared active photocatalyst particles with homogeneously small size are also utilized to fabricate efficient photocatalyst films *via* simple spin-coating or screen-printing method for demonstrating the feasibility of large-scale application.

2. History of research on semiconductor photocatalysts

Table 1. Major topics in the photocatalytic reactions.

	Decomposition of organic pollutants	Energy conversion (water splitting)
1950	1940~ : *Photodegradation of paint by TiO_2*	
1960		1960~: *Semiconductor electrodes under illumination*[20] (Gerischer)
1970		1972 : *PEC water splitting using TiO_2 single crystal* [21] (Fujishima, Honda)
		1977 : *PEC water splitting using "photochemical diode"* [22] (Nozik)
1980	1980: *Photodecomposition of water including organic compounds using TiO_2* [15] (Kawai, Sakata)	1980 : *Photocatalytic water vapor splitting over Pt/TiO_2 particles*[23] (Sato, White) *Photocatalytic water vapor splitting over RuO_2/TiO_2 particles* [24] (Kawai, Sakata) *Photocatalytic water splitting over $NiOx/SrTiO_3$ particles*[25-26] (Domen)
		1986~: *Metal oxides with structural regularities* [27-31] (Domen, Inoue)
1990		
	1997: *Superhydophilicity TiO_2* [16,17] (Hashimoto, Watanabe, TOTO Ltd.)	1995~: *Highly active tantalate photocatalysts* [32-34](Kudo) *Visible-light-driven photocatalysts*[35-39] (Kudo, Domen)
2000	2001: *Decomposition of organic compounds over anion-doped TiO_2*[18] (Toyota Central R&D Labs., Inc.)	2001 : *Z-scheme water splitting over $SrTiO_3$:Cr/Ta + WO_3*[40,41] (Abe, Sayama)
		2004 : *Z-scheme water splitting over $SrTiO_3$:Rh + $BiVO_4$* [42] (Kudo)
	2008: *Decomposition of organic compounds over Pt/WO_3*[19] (Abe)	*Direct water splitting under visible-light over GaN-ZnO* [43-46] (Maeda, Domen)
2010		

Table 1 summarizes the major history of researches on photocatalytic reactions.[15–46] One pioneering study was done by Fujishima and Honda, who demonstrated that overall water splitting can be achieved using a photoelectrode system consisting of photoanode of single-crystal TiO_2 with a rutile phase, and a platinum (Pt) cathode under ultraviolet (UV) irradiation with an external bias (Figure 1 (a)).[21] In such photoelectrochemical (PEC) water splitting with n-type semiconductor (e.g., TiO_2), the water splitting is initiated by the absorption of the photon having higher energy that the band-gap of semiconductor, leading water oxidation on the semiconductor by photo-generated holes and the migration of photo-excited electrons *via* the outer-circuit to the counter where water reduction takes place by the electrons. Although PEC water splitting requires externally applied bias between the counter electrode, considerable fraction of photon energy can be converted and stored as hydrogen if

the applied bias is smaller than the theoretical value for electrochemical water splitting (1.23 V).[20–22, 47–50]

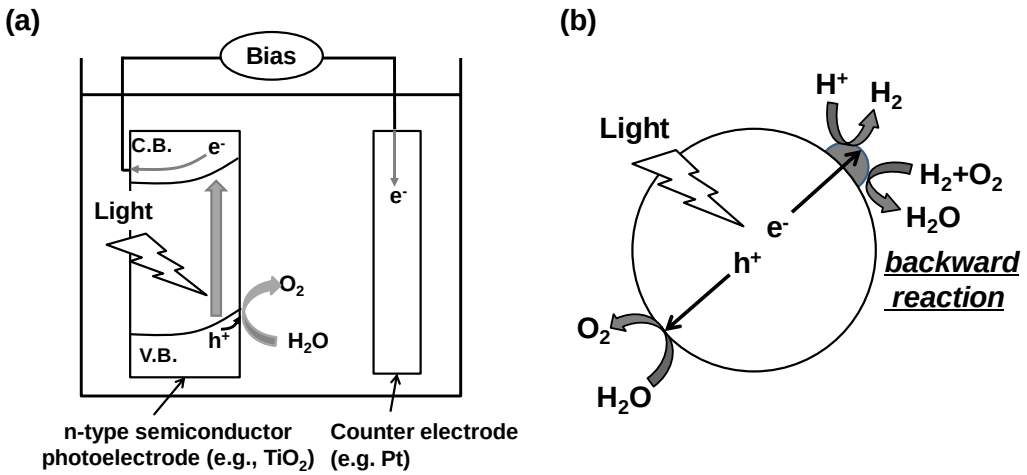

Figure 1. Overall water splitting over (a) a photoelectrochemical system using n-type semiconductor (e.g., TiO_2) photoelectorode and (b) a heterogeneous photocatalytic system under light irradiation.

On the other hand, heterogeneous photocatalytic systems that employ semiconductor particles (Figure 1 (b)) have several advantages over PEC systems, including greater simplicity and lower cost. Heterogeneous photocatalysts have been extensively investigated by research groups in Japan. During the early stages of research, photocatalytic splitting of water was extensively attempted by using TiO_2 particles loaded with Pt co-catalyst (denoted as Pt/TiO_2).[23,51,52] However, simultaneous generation of H_2 and O_2 had not been achieved for more than 10 years, basically due to the occurrence of rapid backward reaction of H_2 and O_2 on the loaded metal co-catalyst such as Pt.[51] Sato et al. have first reported photocatalytic H_2 and O_2 evolution from water vapor over Pt/TiO_2 particles or NaOH-coated Pt/TiO_2 particles, on which the NaOH layers on Pt co-catalyst effectively suppressed the backward reaction.[23,52] However, the photocatalytic water splitting in suspended system, in which photocatalyst particles (e.g., Pt/TiO_2) are suspended in water, was still difficult due to the rapid backward reaction between the evolved H_2 and O_2 on such metal co-coatalyst before they escape from the suspension to gas phase. To address this intrinsic issue, Domen et al. have developed a new core-shell type NiOx co-catalyst, on which the backward reaction is effectively suppressed whereas water reduction to H_2 is efficiently enhanced, and demonstrated water splitting into H_2 and O_2 under the UV irradiation to the suspension of NiOx-loaded $SrTiO_3$ photocatalyst particles in pure water.[25,26]

3. Basic principle of photocatalytic reaction

The applications of semiconductor photocatalysts can be generally classified into two categories: environmental purifications and light energy conversions.[4] The photocatalytic reactions that are involved in such applications can be classified by the difference in the change in Gibbs free energy before and after the reaction, as shown in Figure 2. Since the former reactions involved in environmental purifications, such as oxidative decomposition of organic compounds, are basically accompanied by decrease in the Gibbs free energy, they are classified to downhill reactions (Figure 2 (a)). On the other hand, the reactions involved in light energy conversions, such as water splitting, is undoubtedly accompanied by a large positive change in the Gibbs free energy. Thus they are classified to uphill reactions (Figure 2 (b)), in which a part of photon energy is converted into chemical energy, in analogy with the photosynthesis in green plants.

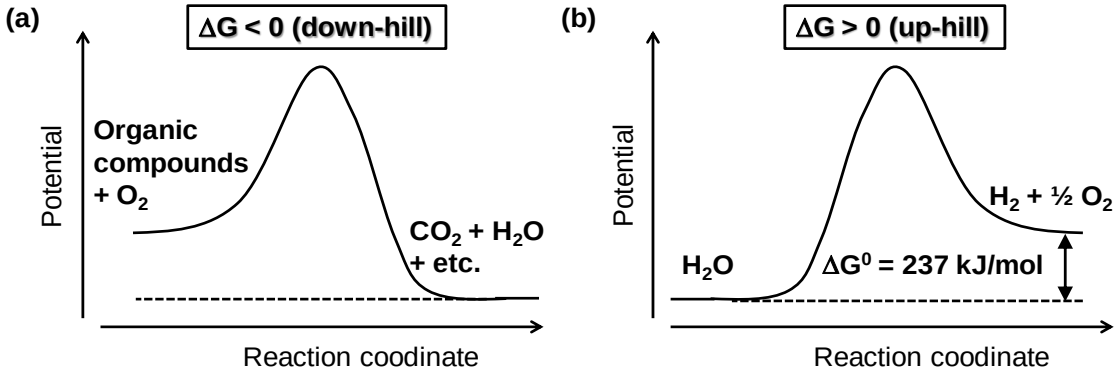

Figure 2. Energy diagrams of photocatalytic reactions for (a) environmental purifications and (b) light energy conversions.

Figure 3 describes the main processes involving in photocatalytic reactions on semiconductor photocatalysts. When the semiconductor absorbs the photons having higher energy than the bandgap, some electrons in the valence band (VB) are excited to the conduction band (CB), thereby generating holes in the VB (Figure 3, Step 1). A part of the photo-exited carriers separate each other and migrate to the surface without recombination (Figure 3, Step 2). The photo-excited electrons in CB can reduce some substances, whereas the holes in the VB can oxidize some substances, if the reactions are fulfill the thermodynamical requirements. (Figure 3, Step 3).

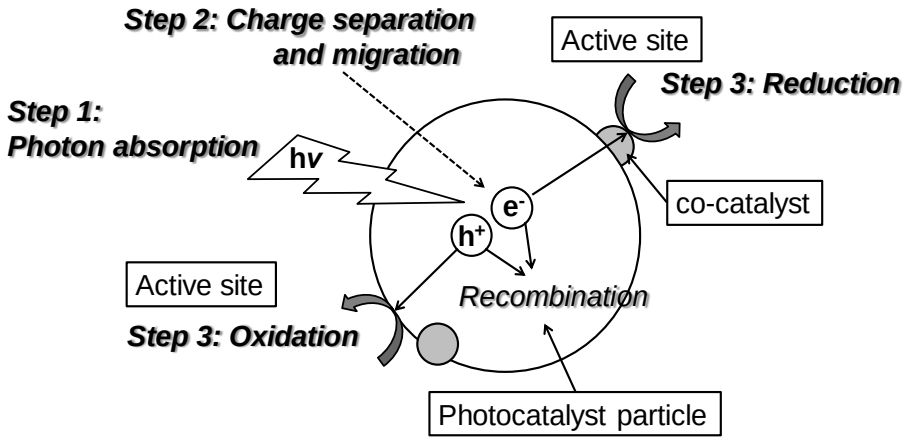

Figure 3. Reaction steps in the photocatalytic reactions on semiconductor photocatalysts.

3.1 Basic principles and applications of semiconductor photocatalysts for environmental purification

Environmental purification using semiconductor photocatalysts is caused by (a) photocatalytic oxidation reactions and/or (b) photo-induced super-hydrophilic phenomena[16]. One of the essential requirements for semiconductor photocatalysts to drive the reaction (a) is the more negative conduction band minimum (CBM) than the reduction potential of oxygen molecule (O_2) (e.g., production of superoxide radical anions, $O^{\bullet-}/O_2$, –0.05V vs. NHE). Simultaneously, the valence band maximum (VBM) must be more positive than the oxidation potential of water molecule to produce hydroxyl radical ($^{\bullet}OH$) which can subsequently oxidize various organic pollutants, while direct oxidation by photo-genetated holes is also occurred in some cases through the adsorption of organic compounds on the surface of photocatalyst (Figure 4 (a)).[12] Photo-induced super-hydrophilicity (b) is a phenomenon that decreases the water contact angle, which is defined as the angle between the solid surface and the tangent line of the liquid phase at the interface of the solid-sliquid-gas phases[53], less than ca. 5° on the surface of photocatalyst-coated film by light irradiation.[16,17] It has been suggested that the decrease in the contact angle up to ca. 10° is mainly caused by the removal of hydrophobic organic compounds from the surface through the reaction (a) (i.e., oxidative decomposition of organic compounds). It has been also suggested that the further decrease in the water contact angle below 10° is mainly caused by changes in the surface structure (i.e., increase of hydroxyl groups) through the self-oxidative reaction of photo-generated holes with the lattice oxygen (Figure 4 (b)).[54-56]

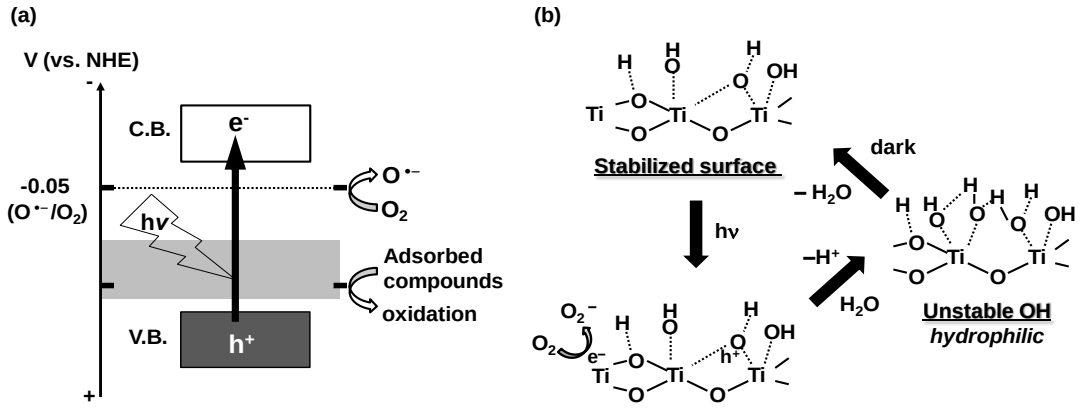

Figure 4. (a) Schematic energy diagram of a semiconductor photocatalyst for environmental purification. (b) Schematic illustration of changes in amounts of hydroxyl groups on a TiO_2 film under UV light irradiation and in the dark.

The reaction (a) can be used for the purification of air and/or water that contains contaminants (organic or inorganic), whereas the reaction (b) can be used for self-cleaning process combined with reaction (a), in which the organic contaminants on the surface are more easily removed by the photo-induced super-hydrophilicity of surface with additional water such as rain. The application of such self-cleaning effect of TiO_2-coated substrates has been extensively studied since the first report in 1997.[57] Some products having such self-cleaning effects (basically based on TiO_2 or its related materials) have been already commercialized. However, the development of technologies for both the synthesis of highly active photocatalyst materials and the immobilization of them onto some substrate through a cost-effective and environmentally-friendly way is essential to further expand such application, and therefore are still extensively studied.[58–61]

3.2 Basic principles of water splitting reaction on a heterogeneous photocatalyst

Although the photocatalytic environmental purifications, in which TiO_2-based photocatalysts are mainly employed, can contribute to solve some environmental issues by reducing the required energy through the utilization of energy of solar light (or some cheap artificial light), it is difficult for them to radically solve the energy issues. Thus, the development of efficient photocatalyst systems with energy conversion type reaction (e.g., water splitting) is indispensable.

When a heterogeneous semiconductor photocatalyst is used for water splitting, two thermodynamical conditions must be satisfied: (a) the more negative (i.e., higher) CBM than water

reduction potential to produce H_2 (H^+/H_2, 0 V vs. NHE), and (b) the more positive (i.e., lower) VBM than water oxidation potential to produce O_2 (O_2/H_2O, 1.23 V vs. NHE) (Figure 5 (a)).

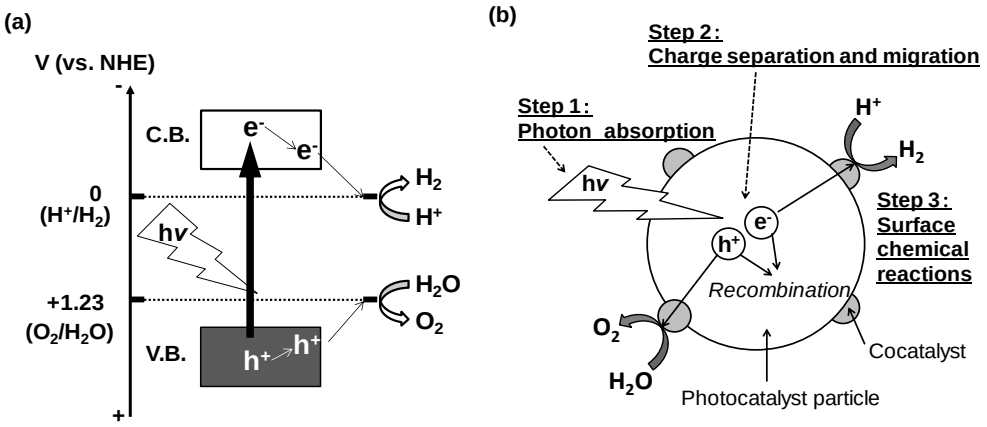

Figure 5. (a) Schematic energy diagram of a semiconductor photocatalyst for water splitting reaction, and (b) key steps for photocatalytic overall water splitting on heterogeneous photocatalyst.

However, even if the semiconductors fulfill the above thermodynamical conditions, they cannot split water into H_2 and O_2 in most cases.[62] Other three important requirements must be fulfilled. Firstly, the charge separation and the migration to the surface's active sites must be occurred efficiently (Figure 5 (b), Step 2). The crystal structure, crystallinity, and size of the photocatalysts particles influence this process. The use of small photocatalyst particles is useful in the elementary sense to shorten the migration length of carrier to reach the surface active sites, thereby decreasing the probability of recombination of the photogenerated electrons and holes during their migration. On the other hand, crystal defects such as oxygen vacancies in the photocatalyst particles generally work as trapping sites of electrons or holes, which often facilitate the recombination of photogenerated electrons and holes (Figure 5 (b)), lowering the photocatalytic activity. Therefore, the photocatalyst particles having both the small particle size and high crystallinity (i.e., low concentration of crystal defects) are highly desired to achieve efficient photocatalysis. Secondary, the surface chemical reactions (i.e., reduction and oxidation of water) must proceed efficiently (Figure 5 (b), Step 3). After protons are reduced to H_2 by photo-excited electrons and water is oxidized to O_2 by holes, a water splitting reaction can take place. However, photo-generated electrons and holes can easily recombine with each other if there are no active sites on the surface, even if the thermodynamical requirements for water splitting are fulfilled. Thus, the quality and the numbers of active sites dramatically influence this process. A general strategy for introducing such effective active sites is loading of fine metal particles (e.g., Pt, Ru) or metal oxide

partilcles (e.g., RuO_2, CoO_x) as "co-catalysts" on the surface of photocatalyst particles. Finally, the produced H_2 and O_2 must escape from the surface of photocatalyst particles (from co-catalyst surface in some cases) into the solution and then into the gas phase without being react each other to form H_2O catalytically on the surface of metal co-catalyst surface. The competitive reduction of O_2 on the reduction site also lowers the efficiency of water splitting. As mentioned above, it is important to design and control the properties of both the semiconductor bulk and the surface active sites to achieve highly efficient water splitting.

Photocatalytic H_2 or O_2 evolution from aqueous solutions containing sacrificial reagents, which are "half-reactions" of the overall water splitting reaction, are often used to evaluate the possibility of application of a semiconductor material to water splitting. The reaction schemes are shown in Figure 6.

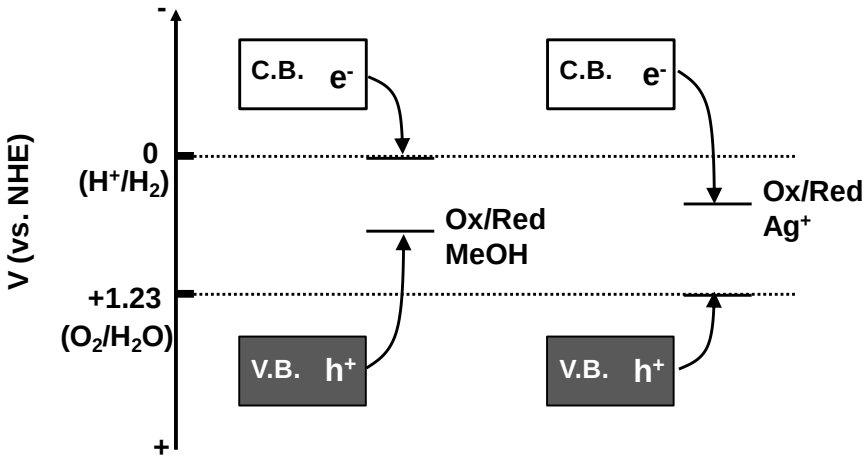

Figure 6. Schematic energy diagrams of photocatalytic reactions in the presence of sacrificial reagents (e.g., methanol and silver ion).

When the photocatalytic reaction is carried out in an aqueous solution with a reducing reagent (e.g., alcohols or sulfide ions), photo-generated holes irreversibly oxidize the reducing reagent instead of water, generating only H_2 if the material has enough CBM to reduce water. The addition of oxidizing reagents (e.g., Ag^+ and Fe^{3+}) enhance the consumption of photo-excited electrons and thereby facilitate the O_2 evolution, if the material has sufficient VBM for water oxidation as well as high stability against self-oxidative deactivation. Although these half reactions in the presence of sacrificial reagents are downhill reactions and are different from overall water splitting reactions, they can be often used for the feasibility test whether a certain photocatalyst satisfies the thermodynamic and kinetic potentials for H_2 or O_2 evolution.

4. Overall water splitting using visible-light-driven semiconductor photocatalysts

Overall water splitting (i.e., simultaneous H_2 and O_2 evolution from water in the stoichiometric ratio 2:1) has been demonstrated under UV light using various semiconductor photocatalysts, mainly metal oxides. Various oxide semiconductors consisting of transition metal cation with d^0 configuration (Ti^{4+}, Ta^{5+}, Nb^{5+}, and Zr^{4+}) or those consisting of typical metal cation with d^{10} -configuration (Ga^{3+}, In^{3+} Ge^{4+}, Sn^{4+}, and Sb^{5+}) have been reported to show activities for water splitting reactions under UV light irradiation.[63-73] Such metal oxides are generally highly stable against photocorrosion and therefore have been extensively studied as UV-light-driven photocatalysts. However, the solar energy conversion efficiency of water splitting reactions using such UV-light-driven photocatalysts remains below 1%,[47,74] mainly due to their wide bandgaps (> 3.0 eV) that limit the utilization of solar light spectrum to only small fraction of UV region. In order to improve the solar energy conversion efficiency, it is necessary to use visible light from 400–800 nm, which accounts for about half (ca. 54%) of the solar spectrum. Although the use of photons in UV light limit the total energy conversion efficiency of solar to hydrogen up to ca. 2% at maximum, the efficient utilization of photons in visible light region drastically improves the ideal conversion efficiency; e.g., to ca. 16% by harvesting all of the photons up to 600 nm and to ca. 32% up to 800 nm.[47] Therefore, the development of photocatalysts that can split water into H_2 and O_2 by harvesting visible light is indispensable to show the feasibility of efficient solar hydrogen production. Although the demonstration of overall water splitting under visible light had been quite challenging task in 20th century, some breakthroughs have been accomplished at the start of 21th century. Visible-light-induced water splitting has been demonstrated in two different systems, one-step or two-step[7,75] excitation systems, as shown in Figure 7.

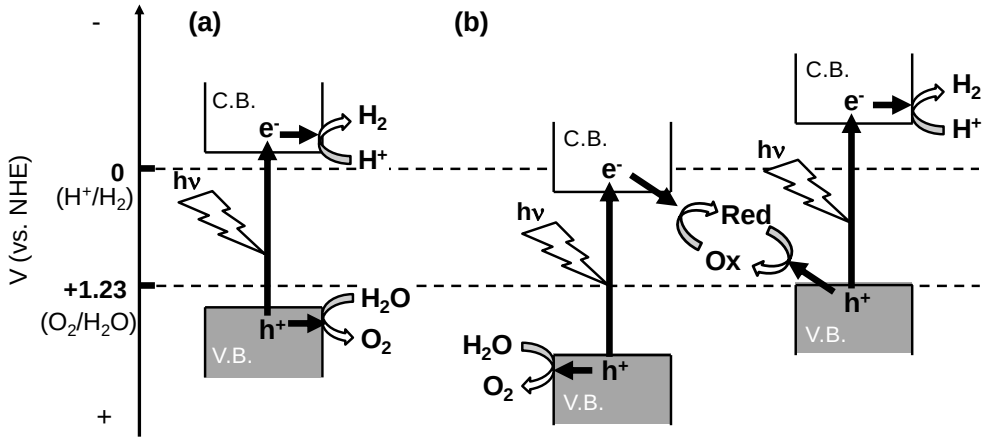

Figure 7. Schematic energy diagrams of the photocatalytic overall water splitting on (a) a one-step and (b) two-step systems.

The one-step excitation system uses a single photocatalyst material to induce water splitting. Maeda and Domen et al. demonstrated overall water splitting under visible light irradiation in 2004 using a GaN-ZnO solid-solution photocatalyst ($(Ga_{1-x}Zn_x)(N_{1-x}O_x)$, x=0.05–0.42).[43-46] Kudo et al. have succeeded to split water under visible light in 2014 using Rh,Sb co-doped $SrTiO_3$ ($SrTiO_3$:Rh,Sb).[76] Most recently, Takata and Domen et al. demonstrated overall water splitting under visible light using $LaMg_xTa_{1-x}O_{1+3x}N_{2-3x}$ (x = 0–2/3), which can utilize visible light up to 600 nm.[77] Although water splitting using a single photocatalyst is important from a scientific viewpoint, the requirement for the band structure on the photocatalyst is very strict; therefore, there are few photocatalysts suitable for the one-step system.

The two-step excitation system consists of two photocatalysts with smaller band gaps and reversible redox reagents (e.g., IO_3^-/I^-, Fe^{3+}/Fe^{2+}).[7,75] This system is inspired by photosynthesis and thus has been given the name "Z-scheme water splitting" due to the similarity between the excitation and transfer processes of photo-excited electrons.[78,79] One photocatalyst works like photosystem II (PSII) in photosynthesis, as the reduction of redox reagents and the oxidation of water occur on this photocatalyst. The other photocatalyst works like photosystem I (PSI), as the oxidation of redox regents and the reduction of protons (or water molecules) take place on this photocatalyst. Because the energy required to drive each photocatalyst is significant lowered compared to that in conventional one-step system, the utilization of photons in visible light region becomes much easier. In other words, it becomes possible to apply a semiconductor with a potential for either water reduction or oxidation on one side of this two-step (Z-scheme) water splitting system. Although most of visible light-responsive oxide semiconductors such as tungsten oxide (WO_3) and bismuth vanadate ($BiVO_4$) cannot generate H_2 due to their lower CBM than water reduction potential, they can generate O_2 from water accompanied by reduction of some oxidant in the solution. Sayama and Abe et al. have reported water splitting under visible light for the first time in the world by constructing a Z-scheme system consisting of WO_3 as O_2-evolving photocatalyst, Cr,Ta-co-doped $SrTiO_3$ (Pt/$SrTiO_3$:Cr,Ta) as H_2-evolving photocatalyst, and an IO_3^-/I^- redox as electron mediator.[40,41] After the report of this pioneering work, various Z-scheme photocatalyst systems have been demonstrated to split water into H_2 and O_2 under visible light irradiation (see Table 2). Among the combinations of photocatalysts reported so far, the combination of $SrTiO_3$:Rh (loaded with Pt or Ru cocatalyst for H_2 evolution) and $BiVO_4$ photocatalysts is worth of attention, because it can work in the presence of various electron mediators,

not only redox couples such as Fe^{3+}/Fe^{2+}, $[Co(bpy)_3]^{3+/2+}$, or $[Co(phen)_3]^{3+/2+}$ but also solid conductive materials such as reduced graphene oxide (RGO) or Au metal.[42,80-85] Interestingly, this combination can split water even without a redox mediator through direct electron transfer between them *via* the redox cycle of Rh species contained in the $SrTiO_3$:Rh particle (Figure 8).[86,87]

Table 2. Various Z-scheme photocatalyst systems that can split water under visible light.

photocatalyst (available wavelength)		redox mediator	max apparent quantum yield/%	ref (year)
H_2	O_2			
Pt/TiO_2 anatase (<380 nm)	TiO_2 rutile (<410 nm)	IO_3^-/I^-	1 (350 nm)	78(2001)
Pt/$SrTiO_3$:Cr/Ta (<550 nm)	PtO_x/WO_3 (<460 nm)	IO_3^-/I^-	1 (420 nm)	40(2001)
Pt/$SrTiO_3$:Rh (<520 nm)	$BiVO_4$ (<520 nm)	Fe^{3+}/Fe^{2+}	0.4 (420 nm)	42(2004)
Pt/$SrTiO_3$:Rh (<520 nm)	WO_3 (<460 nm)	Fe^{3+}/Fe^{2+}	0.4 (420 nm)	42(2004)
Ru/$SrTiO_3$:Rh (<520 nm)	$BiVO_4$ (<520 nm)	Fe^{3+}/Fe^{2+}	0.3 (420 nm)	81,82(2008)
Ru/$SrTiO_3$:Rh (<520 nm)	$BiVO_4$ (<520 nm)	$[Co(bpy)_3]^{3+/2+}$	2.1 (420 nm)	83(2013)
Ru/$SrTiO_3$:Rh (<520 nm)	$BiVO_4$ (<520 nm)	$[Co(phen)_3]^{3+/2+}$	No data	83(2013)
Ru/$SrTiO_3$:Rh (<520 nm)	$BiVO_4$ (<520 nm)	PRGO	1.0 (420 nm)	84(2011)
Ru/$SrTiO_3$:Rh (<520 nm)	$BiVO_4$ (<520 nm)	none	1.7 (420 nm)	86,87(2009)
Ru/$SrTiO_3$:Rh (<520 nm)	Ir/CoOx/Ta_3N_5 (<600 nm)	none	No data	88(2013)
Ru/$SrTiO_3$:La,Rh (<520 nm)	Ir/CoOx/Ta_3N_5 (<600 nm)	none	1.1 (420 nm)	85(2014)
coumarin dye-adsorbed Pt/$H_2K_2Nb_6O_{17}$ (<750 nm)	IrO_2-Pt/WO_3 (<460 nm)	I_3^-/I^-	<0.1 (500 nm) for H_2 evolution	89,90(2009)
Pt/TaON (<520 nm)	PtO_x/WO_3 (<460 nm)	IO_3^-/I^-	0.5 (420 nm)	91,92(2005)
Pt/$BaTaO_2N$ (<660 nm)	PtO_x/WO_3 (<460 nm)	IO_3^-/I^-	0.1 (420-460 nm)	93,94(2008)
Pt/ZrO_2/TaON (<520 nm)	PtO_x/WO_3 (<460 nm)	IO_3^-/I^-	6.3 (420 nm)	95,96(2008)

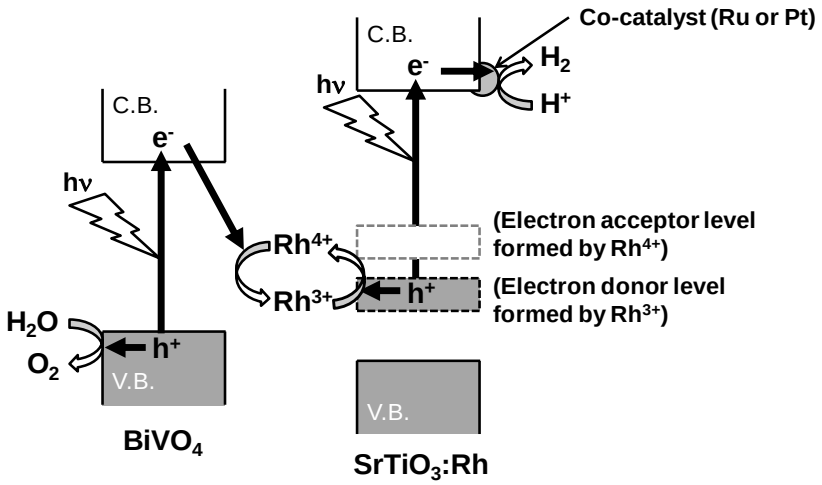

Figure 8. Schematic images of the photocatalytic water splitting using the Z-scheme photocatalysis system driven by electron transfer between co-catalyst loaded $SrTiO_3$:Rh and $BiVO_4$.

5. Strategy for development of visible-light-driven photocatalysts

Conventional metal oxide photocatalysts such as TiO_2 and $SrTiO_3$ cannot absorb visible light due to their wide band gaps (Figure 9 (a)). In general, the conduction bands of such metal oxide photocatalysts generally consist of empty orbitals (LUMOs) of metal cations, whereas the valence bands usually consist of O-2p orbitals forming the VBM at ca. +3 V vs. NHE.[97] Consequently, the CBMs of the oxide semiconductors with visible light absorption (bandgap < 3.0 eV) are inevitably lower than water reduction potential, ruling out H_2 evolution on these materials (Figure 9 (b)). Indeed, visible-light-responsive metal oxides such as WO_3 and $BiVO_4$ show photocatalytic no activity for H_2 evolution even in the presence of strong electron donors, whereas they can efficiently generate O_2 from water in the presence of appropriate electron acceptors under visible light.[98-103] On the other hand, some metal chalcogenides, such as CdS and CdSe, possess appropriate band levels for water reduction and oxidation. These metal chalcogenides, however, are generally unstable and easily become deactivated through photocorrosion or self-oxidation by photogenetated holes rather than evolving O_2 (Figure 9 (c)).[104,105]

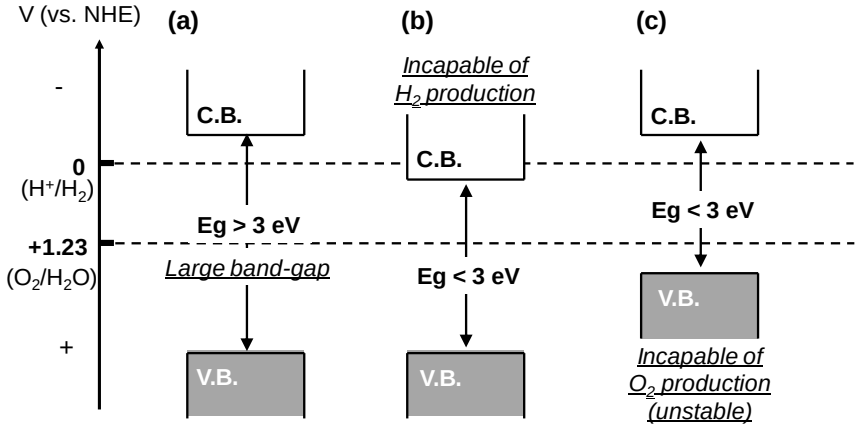

Figure 9. Schematic illustration of the band structures of some semiconductor photocatalysts.

To demonstrate water splitting under visible light, therefore, the semiconductor materials that fulfill the following three requirements are needed; (1) band gap energy lower than 3 eV, (2) suitable CBM and VBM for water splitting in one-step or two-step with appropriate redox, and (3) high durability toward chemical and/or photochemical reduction and oxidation. Kudo and Abe have suggested four strategies for developing such visible-light-responsive photocatalysts ((a) transition metal-doping, (b) formation of hybridized valence band, (c) formation of solid-solution, and (d) sensitization of wide bandgap oxide , as shown in Figure 10).[4]

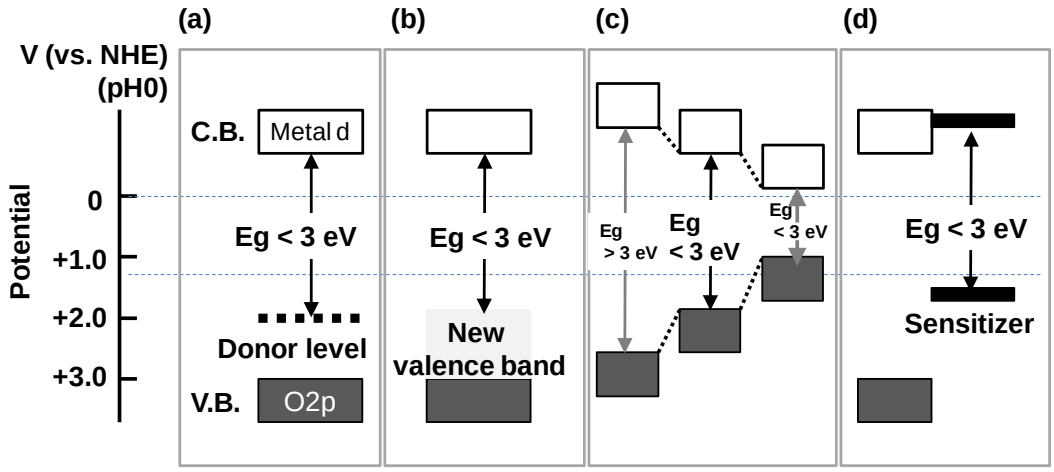

Figure 10. Band engneering of heterogeneous photocatalyst.

The doping of transition metal cations (e.g., Cr^{3+}) into the lattice of wide bandgap oxide semiconductors (e.g., TiO_2) had been extensively studied as an effective way to sensitize them in the early stage of research from 80s to 90s.[34] Although doping of appropriate cation indeed enables such wide bandgap oxides to absorb visible light by forming impurity level in the forbidden band (Figure 10 (a)), such doping by cations with different valences creates the defects that often works as recombination centers between photo-generated electrons and holes, consequently decreases the photocatalytic activity in most cases. Furthermore, the impurity levels are usually discrete, which would appear to be disadvantageous for the migration of photo-generated holes. Doping of cations such as Cr^{3+}, Ni^{2+}, Rh^{3+} and Ir^{3+} into TiO_2 or $SrTiO_3$ have been found to form electron donor levels in their forbidden band and thereby giving them ability of visible light absorption, however, the doping of these di- or tri- balance cations unbalance the charge in the host material by partial replacement of Ti^{4+}, creating defects and losing their photocatalyst activities under visible light.[34, 106-110] Kudo et al. have first proven that appropriate co-doping such as Cr^{3+}/Ta^{5+}, Cr^{3+}/Sb^{5+}, Ni^{2+}/Ta^{5+} into $SrTiO_3$ (or TiO_2 in some cases), which replace a part of Ti^{4+}, is effective way to obtain visible-light-responsive photocatalysts with high activity by suppressing the formation of defect through the charge compensation.[34,106,107] Interestingly, Kudo et al. also found that the doping of Rh cations is effective creating the new visible-light-resonsive $SrTiO_3$ photocatalyst showing high activity for H_2 evolution.[108] It has been so far demonstrate that Rh-doped $SrTiO_3$ (denoted as $SrTiO_3$:Rh) photocatalysts exhibit high activity for H_2 evolution (e.g., 5.6% apparent quantum efficiency at 420 nm) under visible light irradiation without co-dopants to suppress charge imbalances.[108] The $SrTiO_3$:Rh material absorbs

visible light due to the transition from electron donor levels formed by Rh^{3+} ions to a conduction band composed of the Ti-3d orbital of $SrTiO_3$ host, making it a unique photocatalyst.[111] Although both the Rh^{3+} and Rh^{4+} cations are incorporated into the Ti^{4+} site in $SrTiO_3$, the Rh^{4+} species are reduced by photo-excited electrons under the photoirradiation. (Figure 11).[108] The $SrTiO_3$:Rh is quite unique visible light-responsive photocatalyst because this is the only material that can generate H_2 from water in the presence of Fe^{2+} electron donor as well as through interparticle electron transfer *via* redox cycle of Rh^{4+}/Rh^{3+}.

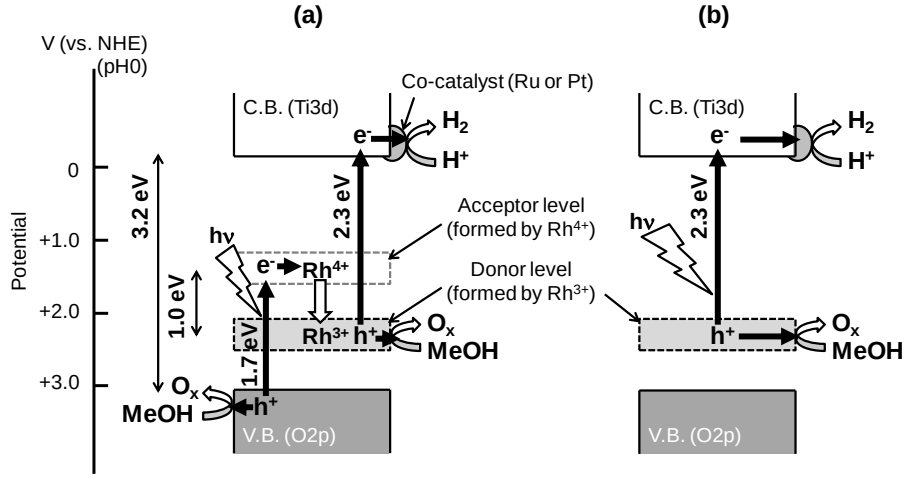

Figure 11. Band structures of the Rh-doped $SrTiO_3$ photocatalyst in H_2 evolution reaction, (a) at the induction period and (b) in the steady state, under visible-light irradiation.

Hybridization of O-2p orbital with other orbitals of cations, which have higher energy than that of O-2p, such as Bi^{3+}, Pb^{2+}, Ag^{+}, and Sn^{2+} has demonstrated to obtain promising materials for achieving water splitting under visible light (Figure 10 (b)).[100-103,112-115] Although some oxides containing these cations indeed exhibited activity for H_2 evolution under visible light in the presence of an electron donor or hole scavenger, but overall water splitting has not demonstrated by using these materials. $BiVO_4$ is classified to this kind of material, because it has been reported that the balance band of sheelite monoclinic $BiVO_4$ is consist of hybridization of O-2p with Bi-6s, resulting in negative shift of the VBM compared to those of conventional oxide semiconductors. Although the CBM of sheelite monoclinic $BiVO_4$ is still lower than water reduction potential even with the negative shift of VBM unfortunately, the sheelite monoclinic $BiVO_4$ is regarded as one of the most promising photocatalysts for O_2 evolution from an aqueous solution containing electron donors (Ag^{+} or Fe^{3+}) under visible light irradiation. Another strategy for creating visible light-driven photocatalysts is the hybridization of O-2p

orbital with other p-orbitals of anions having less electronegativity than O-2p, such as N-2p or S-3p (i.e., metal oxynitidides or oxysulfides). It has been reported that some metal oxynitrides can be applied to both one-step and two-step water splitting under visible light,[2,5] while their instability due to self-oxidation of these high energy anions (e.g., $2N^{3-} + 6h^{+} + N_2$) should be addressed and improved further for the practical application, as well as the improving their efficiency.

The formation of solid solutions from two materials having same crystal structure but different bandgaps is effective way to adjust the potentials of CBM and VBM as well as the bandgaps, and has been indeed proven to be available for creating new photocatalyst materials for water splitting under visible light.

As mentioned above, a large number of visible light responsive photocatalysts have been developmed through different strategies and many of them have been indeed demonstaret to show acivity for H_2 or O_2 evolution in the presence of sacrificial (or reversible in some cases) electron donor or acceptor, respectively. For practical use, however, to the significant improve in their efficiency is still indispensable.

6. Designing and synthesis of semiconductor photocatalyst oxide particles for highly active water splitting reaction under visible-light irradiation

As mentioned in Section 1.3, the photocatalytic reactions mainly consist of following three important processes: (1) absorption of photons having higher energy than the band-gap of semiconductor; (2) separation photo-generated electrons and holes and their subsequent migration to the surface of semiconductor particles; and (3) reduction/oxidation of substances (i.e., water or organic compounds) on the surface. Considering the reaction efficiency on the surface, the particle size should be as smaller as possible, while the total photocatalytic activity is generally influenced by various factors not only the particle size.[116] When both the light absorption and the migration of carriers in the bulk are considered, the smaller particles size also seems favorable. For example, it was reported that the diffusion lengths of photo-generated carriers in visible-light responsive photocatalysts are generally short (e.g., ~70 nm in $BiVO_4$, ~5 nm in Fe_2O_3).[117] These short diffusion lengths imply that most of the carriers generated in the bulk of large particles readily recombination and thereby cannot reach the surface. Thus, it can be assumed that the particles radius of photocatalyst should be similar or smaller than the diffusion length of carrier for achieving effective utilization of photons. Additionally, the

higher amount of crystal defects such as oxygen vacancies increases the number of donor (electron traps) in the n-type semiconductors, thereby further shortening the diffusion length of carriers by increasing the probability of recombination. Based on the essential processes in photocatalysis explained above, the basic guiding principles for developing highly efficient photocatalysts will be prepare semiconductor particles having both the small size (considering the diffusion length of carrier, if possible) and the reduced numbers of crystal defects. However, it is difficult to synthesize the photocatalyst particles satisfying both the requirement simultaneously. For example in the conventional solid-state synthesis, elevating calcination temperature can generally reduce the amount of crystal defects, however, increase the particle size (i.e., decrease the surface area) due to the crystal growth and aggregation of particles. Other alternative synthesis methods have therefore been employed to control the physicochemical properties of photocatalyst particles in an effort to achieve highly efficient photocatalysis. Table 3 briefly summarizes such typical synthetic method for metal oxide particles along with their advantages and disadvantages.

Table 3. Synthetic method of metal oxide particles along with their advantages and disadvantages.

Method	Advantage	Disadvantage
Solid-state reaction	Extremely simple	Difficult to control particle size
Sol-gel	Small particle size	Low crystallinity
Co-precipitation	Small particle size	Inhomogeneous
Hydrothermal/Solvothermal	Small particle size	Low crystallinity
Polymerized complex	Homogeneous	Particle aggrigation
Flux	High crystallinity	Large particle size

In general, metal-oxide photocatalysts are synthesized *via* a solid-state reaction. This method is extremely simple and does not require a large-scale device. The raw materials (e.g., metal oxides, alkali, and alkaline earth carbonates) are simply mixed and subsequently calcined at a high temperature under various conditions (e.g., air, N_2). The solid-state reaction proceeds with the interdiffusion of the ions at the point of contact with heterogeneous particles (Figure 12 (a)). It should be noted that the speed of diffusion of cations within a solid is extremely low. Therefore, to obtain homogeneous samples, repeated calcination, mixing, and grinding processes are required to reduce diffusion distance and thereby promote interdiffusion for long hours at a high temperature, inevitably resulting in the increase of particle size. Extended calcination at high temperatures causes evaporation of some cations and/or

anions in some cases, making it difficult to prepare products with precise stoichiometry. In addition, since the size of the obtained particles tend to depends on the particle sizes of the precursor particles, it is relatively difficult to control the particle size and size distribution.

Various liquid-phase synthesis methods have been extensively applied to synthesis of photocatalyst particles because they can produce desired small particles through calcination at relatively low temperatures. This favorable feature of liquid-phase synthesis is basically due to the much easier diffusion of precursor materials (cations and/or anions in some cases) in liquid phase. Such homogeneous mixing of precursors enables low temperature synthesis as well as controlling of particle size in some extent.

The sol-gel method can be applied to synthesize various homogeneous ceramics, in which various organic and/or inorganic compounds can be used as precursors in appropriate solutions.[118-121] Adding a small amount of water to the organic solvent triggers hydrolysis, condensation and polymerization, thereby producing gels with a continuous inorganic network (Figure 12 (b)). The obtained gel is dried completely and followed by calcination to yield metal-oxide particles with relatively small size, while the particle size basically depends on the calcination temperature.

The co-precipitation method is carried out as follows: ammonia water is added to a mixed solvent solution containing precursor metal salts, resulting in precipitation of particles due to the pH change.[122] However, differences in solubility and in the reaction rate between the precursors often produce the precipitates with inhomogeneous contents of precursor cations.

Hydrothermal or solvothermal synthesis involves the use of an aqueous/organic solvent to dissolve the precursor ions under high pressure and a high temperature (e.g., 100℃ 1 atm).[123] In these methods, the various properties such as crystals phase, crystal face orientation and the particle size can be controlled in some extent by changing the environment of dissolved and re-precipitated process; i.e., it is possible to control the properties of particles by employing appropriate additives such as surfactants.[124-125]

Although the above-mentioned synthesis methods enables to prepare semiconductor (metal oxide in most cases) particles with small size, the prepared particles generally have low crystallinity, which often leads to low activity in photocatalytic water splitting. For example, Osterloh et al. synthesized the NiO cocatalyst-loaded $SrTiO_3$ particles with nano-size (ca. 6.5 nm) *via* hydrothermal synthesis and demonstrated photocatalystic water splitting on these particles under UV light irradiation.[126] However,

the nano-sized $SrTiO_3$ particles exhibited lower activity on photocatalytic water splitting than large-sized $SrTiO_3$ particles prepared *via* conventional solid-state reaction. In order to improve crystallinity, post-calcination at a high temperature, is generally required, resulting in theparticle growth after all. Kato et al. also synthesized small $SrTiO_3$:Rh partcles with below 300 nm *via* hydrothermal synthesis, but calcined them at 1000℃ to enhance the photocatalytic activity.[82]

Polymerized complex (PC) method is another way to synthesize photocatalyst particles homogeneously at relatively low temperatures. This method was developed by Kakihana et al. and is based on a patent by Pechini et al..[127] Essentially, the first step involves the formation of the stable chelate complexes with an α-hydroxycarboxylic acid, such as citric acid (CA). Then, the esterification of carboxylic acid functional groups in CA with hydroxyl groups in polyhydroxy alcohol, such as ethyrene glycol (EG) at around 100–150℃ (Figure 12 (c)), producing the polyester-type resins in which metal ions are highly dispersed. Heat treatment in air at 300–450℃ decomposes the produced polymer, followed by the subsequent crystallization of the oxide at high temperatures (above 500℃), finally producing homogeneous composite oxide. Many perovskite-type metal oxides such as $SrTiO_3$, $La_2Ti_2O_7$, have been synthesized *via* the PC-method, which generally shows a higher photocatalytic activity on water splitting than that prepared by the SS-method.[82,127]

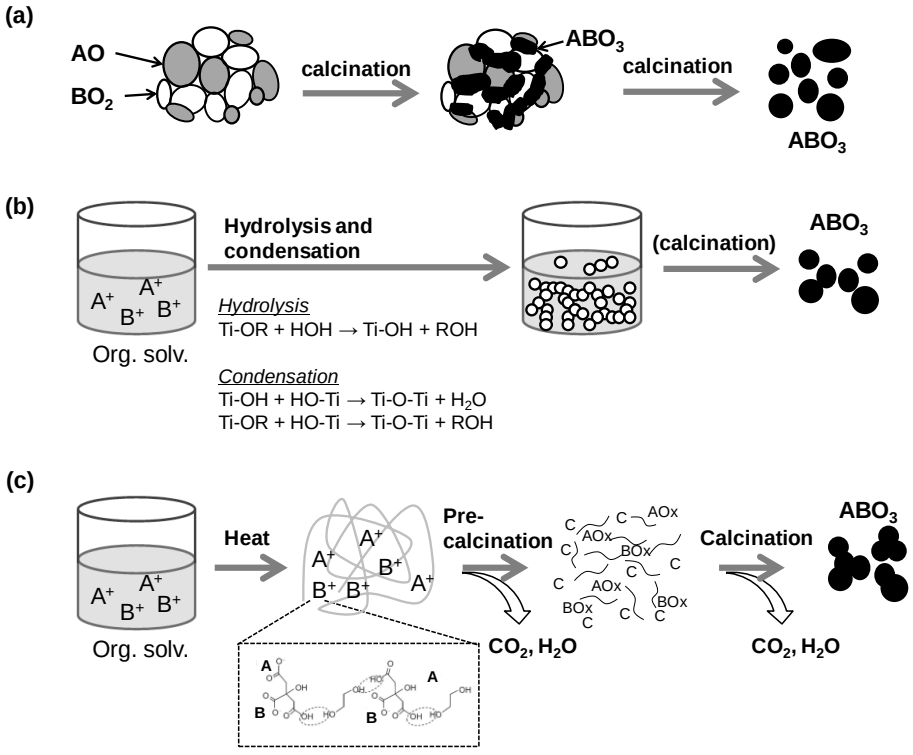

Figure 12. Illustrations of various synthetic methods for metal oxide particles; (a) solid-state reaction, (b) sol-gel, and (c) polymerized complex method.

Controlling the crystallinity of semiconductor particles is also important for highly active photocatalysts. The application of flux method was demonstrated by Teshima et al.[128] to be effective to obtain semiconductor particles with high crystallinity and relatively homogenous size, consequently affording high photocatalytic activity.

Although the improvement in photocatalytic activity of various semiconductor materials has been demonstrated by employing the above- mentioned method, it is still difficult to synthesize photocatalyst particles of a small size and a high degree of crystallization. For practical applications, it is also desirable to synthesize photocatalyst particles using a simple and environmentally friendly process. However, the organic solvents are often used in most of the liquid-phase methods. Such organic solvents have adverse effects on the human body (e.g., they are explosive, flammable, or carcinogenic). Additionally, organic solvents are generally used in large amounts, in comparison to solutes, and are often released into the atmosphere through evaporation or leakage. In contrast to organic solvents, water is an environmentally friendly solvent with no toxicity, and it is inexpensive and easy to obtain. Therefore, the water-based synthesis has excellent properties in terms of green chemistry, safety, and cost, compared to that based on organic solvents. As mentioned in Section 1.4, many oxide semiconductors including transition metal cation with d^0 configuration, such as Ti^{4+}, Ta^{5+}, and Nb^{5+}, shows high activity for water splitting under UV light and also can be host materials of visible-light-responsive photocatalyst though cation doping. However, most of the precursors of these cations are insoluble or instable in water solvent. For example, the alkoxides of these metal cations are highly susceptible to hydrolysis, producing precipitate immediately in water solvent. A water-based synthesis method has been reported by Kakihana et al., which uses some chelating ligands (e.g., peroxo-species, lactate) to stabilize precursor cations such as Ti^{4+} in water.[129-132] However, these complex aqueous solutions require a complicated preparation process. Thus, it is important to find a new method to synthesize composite oxides using a much more simple process.

7. Immobilization of photocatalyst particles onto substrates

As mentioned in the above sections, photocatalytic water-splitting reactions have mainly been studied using particle suspension systems, so far. However, when considering the practical application in large scale, such suspension systems have serious disadvantages to be solved. For example, such a heterogeneous system requires energy to suspend the semiconductor particles in the solution (e.g.,

mechanical stirring or gas bubbling) and to separate the particles for recycling or replacing.[126] Although photoelectrochemical systems can solve the problems of suspension system, there are associated cost disadvantages due to the cost of conductive substrates (e.g., conductive glass or metals) and external circuitry (e.g., the power source).[126] Therefore, development of new-type and low-cost photocatalyst system with high scalability is strongly desired.

As one of such new systems, photocatalyst panels, in which photocatalyst particles are fixed onto an inexpensive substrate such as glass, have recently been suggested (Figure 13 (a)).Water splitting into H_2 and O_2 on photocatalyst panels have been reported for the first time by Domen et al. in 2014, in which particles of a visible-light-responsive photocatalyst $Ga_{1-x}N_x$-$Zn_{1-x}O_x$ (GaN-ZnO, x = 0.18) solid-solution are fixed on glass substate via drop-casting or squeegee method.[127] This study also reported that the addition of photo-inactive SiO_2 particles as a hydrophilic binder created porosity suitable for mass transfer, resulting in higher H_2 and O_2 evolution than results obtained from GaN-ZnO panels without the addition of SiO_2; the addition of micrometer-sized SiO_2 was found to be more effective for photocatalytic water-splitting reactions afforiding comparable efficiency to that of suspension system.[127] These findings indicated that controlling film structures for efficient diffusion of the water is necessary to achieve efficient water splitting on photocatalyst panels. Recently, Wang et al. demonstrated simultaneous evolution of H_2 and O_2 on a photocatalyst sheet, where Rh and La co-doped $SrTiO_3$ ($SrTiO_3$:Rh,La) and $BiVO_4$ photocatalytic particles were immobilized onto a thin gold (Au) layer, which was deposited onto the substrate (Figure 13 (b)), and electron transfer between the two photocatalysts proceeded through the Au layer. [128]

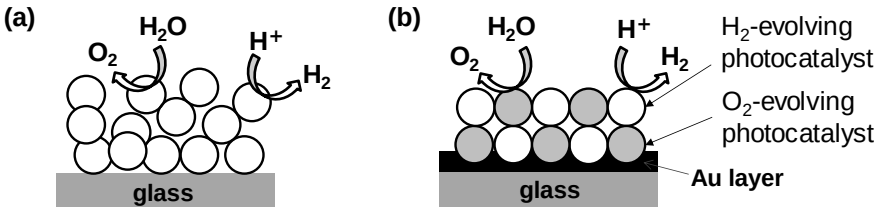

Figure 13. Water splitting systems in which photocatalyst particles are fixed onto an inexpensive substrate (e.g. glass); (a) photocatalyst panel and (b) photocatalyst sheet.

8. Configuration of the present thesis

The present thesis consists of general introduction, five chapters and summary as follows:

In General introduction, the background of the present research, basic principles of the

photocatalytic reaction for environmental purification and energy conversion on a heterogeneous photocatalyst, and the progress made in the development of visible-light responsive photocatalysts were described.

In Chapter 1, a novel stable aqueous titania sol was developed to prepare TiO_2 photocatalyst thin films that shows high activity for environmental purification such as photo-induced surface superhydrophilicity under UV-light irradiation. A detailed characterization of the aqueous titania sol and the photocatalytic reaction of the prepared TiO_2 films under UV-light irradiation were discussed.

In Chapter 2, the titania sols developed in Chapter 1 was use as stable precursor to prepare mixed metal oxide Rh-doped $SrTiO_3$ ($SrTiO_3$:Rh) particles with small and narrow size distributions, to improve the photocatalytic activity of for H_2 evolution under visible light irradiation compared to those prepared *via* conventional solid state synthesis. The effects of the preparation methods, preparation conditions, and Rh-doping concentrations on the physiochemical properties and photocatalytic water-splitting performance of $SrTiO_3$:Rh were investigated.

In Chapter 3, the highly active fine particles of $SrTiO_3$:Rh developed in Chapter 2 were utilized as precursor of porous photocatalyst panels that can efficiently generate H_2 under visible light irradiation. Attempt were made to control and optimize the porous structure and thickness of $SrTiO_3$:Rh films for affording comparable efficiency in visible-light-induced H_2 evolution to that in the corresponding suspension system.

In Chapter 4, a new aqueous chelating method was developed to synthesis sheelite monoclinic $BiVO_4$ particles with homogenously small size for demonstrating highly efficient photocatalytic O_2 evolution from water under visible light. The effects of the preparation methods, preparation conditions, and types of ligands on the physiochemical properties and photocatalytic water-splitting performance of $BiVO_4$ were investigated.

Chapter 5 described the fabrication photocatalyst panels that can split water into H_2 and O_2 under visible light through the interparticle Z-scheme mechanism. Composite-type films were prepared using simple screen-printing of $SrTiO_3$:Rh and $BiVO_4$ fine particles, which were described in Chapters 2 and 4. The structures of the prepared composite-type films were examined and water-splitting activities under visible light irradiation were discussed.

Finally, Summary and outlook summarizes the results described in the Chapters 1–5 and proposes future research and applications for the processes described in this thesis.

References

1. R. Trygve, F. H. Elisabet, J. S. V. Preben and U. Øystein, *Hydrogen Production and Storage*, International Energy Agency, Paris, 2006, p.1.
2. K. Maeda and K. Domen, *J. Phys. Chem. C*, 2007, **111**, 7851.
3. F. E. Osterloh, *Chem. Mater.* 2008, **20**, 35–54.
4. A. Kudo and Y. Miseki, *Chem. Soc. Rev.*, 2009, **38**, 253–278.
5. K. Maeda and K. Domen, *J. Phys. Chem. Lett.*, 2010, **1**, 2655–2661.
6. A. Kudo, *Mater. Res. Bull.*, 2011, **36**, 32–38.
7. R. Abe, *Bull. Chem. Soc. Jpn.*, 2011, **84**, 1000–1030.
8. K. Takanabe and K. Domen, *Chem Cat Chem.*, 2012, **4**, 1485–1497.
9. T. Takata, C. Pan and K. Domen, *Sci. Technol. Adv. Mater.*, 2015, **16**, 033506.
10. T. Hisatomi, K. Takanabe and K. Domen, *Catal. Lett.*, 2015, **145**, 95–108.
11. A. Fujishima, T N. Rao and D A. Tryk, *J. Photochem. Photobiol. C*, 2000, **1**, 1–21.
12. K. Hashimoto, H. Irie and A. Fujishima, *Jpn. J. Appl. Phys.*, 2005, **44**, 8269–8285.
13. K. Nakata and A. Fujishima, *J. Photochem. Photobiol. C*, 2012, **3**, 169–189.
14. B.Pinaud, J. Benck, L.Seitz, A. Forman, Z. Chen, T. Deutsch, B. James, K. Baum, G. Baum, S. Ardo, H. Wang, E. Miller and T. Jaramillo, *Energy Environ. Sci.*, 2013, **6**, 1983.
15. T. Kawai and T. Sakata, *Nature*, 1980, **286**, 474–476.
16. R. Wang, K. Hashimoto, A. Fujishima, M. Chikuni, E. Kojima, A. Kitamura, M. Shimohigoshi, T. Watanabe, *Nature*, 1997, **388**, 431–432.
17. R. Wang, K. Hashimoto, A. Fujishima, M. Chikuni, E. Kojima, A. Kitamura, M. Shimohigoshi, T. Watanabe, *Adv. Mater.*, 1998, **10**, 135.
18. R. Asahi, T. Morikawa, T. Ohwaki and Y. Taga, *Science*, **293**, 269–271.
19. R. Abe, H. Takami, N. Murakami and B. Ohtani, *J. Am. Chem. Soc.*, 2008, **130**, 7780–7781.
20. H. Gerischer, *J. Electrochem. Soc.*, 1966, **113**, 1174.
21. A. Fujishima and K. Honda, *Nature*, 1972, **238**, 37–38.
22. A. J. Nozik, *Appl. Phys. Lett.*, 1977, **39**, 567–569.
23. S. Sato, J. M. White, *Chem. Phys. Lett.*, 1980, **72**, 83–86.
24. T. Kawai and T. Sakata, *Chem. Phys. Lett.*, 1980, **72**, 87.
25. K. Domen, S. Naito, M. Soma, T Onishi, and K. Tamaru, *J. Phys. Chem.*, 1982, **86**, 3657.

26. K. Domen, A. Kudo and T. Onishi, *J. Catal.*, 1986, **102**, 92.
27. A. Kudo, K. Sayama, A. Tanaka, K. Asakura, K. Domen, K. Maruya and T. Onishi, *J. Catal*, 1989, **120**, 337.
28. K. Domen, A. Kudo, A. Shinozaki, A. Tanaka, K. Maruya, and T. Onishi, *J. Chem. Soc., Chem. Commun.*, 1986, **356**.
29. Y. Inoue, T. Nishiyama, and K. Sato, *Top. Catal.*, 1994, **1**, 137.
30. S. Ogura, M. Kohno, K. Sato, Y. Inoue, *Phys. Chem. Chem. Phys.*, 1999, **1**, 179.
31. S. Ogura, K. Sato, Y. Inoue, *Phys. Chem. Chem. Phys.*, 2000, **2**, 2449.
32. H. Kato, K. Asakura, and A. Kudo, *J. Am. Chem. Soc.*, 2003, **125**, 3082.
33. H. Kato, A. Kudo, *Catal. Today.*, 2003, **78**, 561.
34. T. Ishii, H. Kato, A. Kudo, *J. Photochem. Photobiol. A*, 2004, **163**, 181.
35. A. Ishikawa, T. Takata, J.N. Kondo, M. Hara, H. Kobayashi, K. Domen, *J. Am. Chem. Soc.*, 2002, **124**, 13547.
36. G. Hitoki, T. Takata, J.N. Kondo, M. Hara, H. Kobayashi, K. Domen, *Chem. Commun.*, 2002, 1698.
37. G. Hitoki, A. Ishikawa, T. Takata, J.N. Kondo, M. Hara, K. Domen, *Chem. Lett.*, 2002, **31**, 736.
38. A. Kasahara, K. Nukumizu, G. Hitoki, T. Takata, J.N. Kondo, M. Hara, H. Kobayashi, K. Domen, *J. Phys. Chem. A*, 2002, **106**, 6750.
39. D. Yamashita, T. Takata, M. Hara, J.N. Kondo, K. Domen, *Solid State Ionics*, 2004, **172**, 591.
40. K. Sayama, K. Mukasa, R. Abe, Y. Abe and H. Arakawa, *Chem. Commun.*, 2001, 2416–2417.
41. R. Abe, K. Sayama, and H. Sugihara, *J. Phys. Chem. B*, 2005, **109**, 16052–16061.
42. H. Kato, M. Hori, R. Konta, Y. Shimodaira and A. Kudo, *Chem. Lett.*, 2004, **33**, 1348–1349.
43. K. Maeda, T. Takata, M. Hara, N. Saito, Y. Inoue, H. Kobayashi, and K. Domen, *J. Am. Chem. Soc.*, 2005, **127**, 8286.
44. K. Maeda, K. Teramura, D. Lu, T. Takata, N. Saito, Y. Inoue and K. Domen, *Nature*, 2006, **440**, 295.
45. K. Maeda, K. Teramura, D. Lu, N. Saito, Y. Inoue and K. Domen, *J. Phys. Chem. C*, 2007, **111**, 7554.
46. K. Maeda, K. Teramura, and K. Domen, *J. Catal.*, 2008, **254**, 198.
47. R. Abe, *J. Photochem. Photobiol. C: Photochem. Rev.*, 2010, **11**, 179–209.

48. T. Hisatomi, J. Kubota, K. Domen, *Chem. Soc. Rev.*,2014, **43**, 7520.

49. F. E. Osterloh, *Chem. Soc. Rev.*, 2013, **42**, 2294.

50. A. J. Bard, *J. Photochem.*, 1979, **10**, 59–75.

51. A. J. Bard, *Science*, 1980, **207**, 139–144.

52. S. Sato, J. M. White, *J. Catal.*, 1981, **69**, 128–139.

53. R N. Wentzel, *Ind. Eng. Chem.*, 1936, **28** (8), 988–994.

54. N. Sakai, A. Fujishima, T. Watanabe and K. Hashimoto, *J. Phys. Chem. B*, 2003, **107**, 1028.

55. R. Nakamura, K. Ueda, and S. Sato, *Langmuir*, 2001, **17**, 2298.

56. R. D. Sun, A. Nakajima, A. Fujishima, T. Watanabe and K. Hashimoto, *J. Phys. Chem. B*, 2001, **105**, 1984.

57. A. Fujishima, K. Hashimoto and T. Watanabe, *TiO_2 Photocatalysis Fundamentals and Applications*, 1999 (BKC, Tokyo).

58. M. Miyauchi, A. Nakajima, A. Fujishima, K. Hashimoto, T. Watanabe, *Chem.Mater.*, 2000, **12**, 3.

59. M. Miyauchi, A. Nakajima, T. Watanabe, K. Hashimoto, *Chem.Mater*.2002, **14**, 2812–2816.

60. H. Tokudome and M. Miyauchi, *Chem. Lett.*, 2004, **33**, 1108–1109.

61. Y. Huogen, Y. Shimodaira, Y. Hosogi, Y. Kuroda, M. Miyauchi, and K. Hashimoto, *J. Phys. Chem. C*, 2010, **114**, 16481–16487.

62. X. Yang, A. Wolcott, G. Wang, A. Sobo, R.C. Fitzmorris, F. Qian, J. Z. Zhang, Y. Li, *Nano Lett.*, 2009, **9**, 2231.

63. K. Sayama and H. Arakawa, *J. Phys. Chem*, 1993, **97**, 531.

64. T. Takata, K. Shimohara, A. Tanaka, M. Hara, J.N. Kondo, and K. Domen, *J. Photochem. Photobiol. A*, 1997, **106**, 45.

65. H. Takahashi, M. Kakihana, Y. Yamashita, K. Yoshida, S. Ikeda, M. Hara, and K. Domen, *J. Allows Compd.*, 1999, **285**, 77.

66. J. Sato, N. Saito, H. Nishiyama, Y. Inoue, *J. Phys. Chem.*, 2001, **105**, 6061.

67. K. Igarashi, J. Sato, H. Kobayashi, N. Saito, H. Nishiyama, Y. Inoue, *J. Phys. Chem. B*, 2002, **106**, 9048.

68. J. Sato, N. Saito, H. Nishiyama, Y. Inoue, *J. Photochem. Photobiol. A*, 2002, **148**, 85.

69. J. Sato, H. Kobayashi, N. Saito, H. Nishiyama, Y. Inoue, *J. Photochem. Photobiol. A*, 2003, **158**, 139.

70. J. Sato, N. Saito, H. Nishiyama, Y. Inoue, *J. Phys. Chem. B*, 2003, **107**, 7965.
71. S. Ikeda, T. Itani, K. Nango and M. Matsumura, *Catal. Lett.*, 2004, **98**, 229.
72. J. Sato, H. Kobayashi, K. Igarashi, N. Saito, H. Nishiyama, Y. Inoue, *J. Phys. Chem. B*, 2004, **108**, 4349.
73. R. Abe, M. Higashi, K. Sayama, Y. Abe, H. Sugihara, *J. Phys. Chem. B*, 2006, **110**, 2219.
74. B. Sorenson, *Renewable Energy, Academic Press*, 1979, p.316.
75. K. Maeda, *ACS Catal.*, 2013, 3, 1486–1503.
76. R. Asai, H. Nemoto, Q. Jia, K. Saito, A. Iwase and A. Kudo, *Chem. Commun.*, 2014, **50**, 2543–2546.
77. C. Pan, T. Takata, M. Nakabayashi, T. Matsumoto, N. Shibata, Y. Ikuhara and K. Domen, *Angew. Chem.*, 2015, **127**, 2998–3002.
78. R. Abe, K. Sayama, K. Domen, H. Arakawa, *Chem. Phys. Lett.*, 2001, **344**, 339–344.
79. K. Sayama, K. Mukasa, R. Abe, Y. Abe and H. Arakawa, *J. Photochem. Photobiol., A*, 2002, 148, 71–77.
80. H. Kato, Y. Sasaki, A. Iwase and A. Kudo, *Bull. Chem. Soc. Jpn.*, 2007, **80**, 2457–2464.
81. Y. Sasaki, A. Iwase, H. Kato and A. Kudo, *J. Catal.*, 2008, **259**, 133–137.
82. H. Kato, Y. Sasaki, N. Shirakura and A. Kudo, *J. Mater. Chem. A*, 2013, **1**, 12327–12333.
83. Y. Sasaki, H. Kato and A. Kudo, *J. Am. Chem. Soc.*, 2013, **135**, 5441.
84. A. Iwase, Y. H. Ng, Y. Ishiguro, A. Kudo and R. Amal, *J. Am. Chem. Soc.*, 2011, **133**, 11054–11057.
85. Q. Wang, T. Hisatomi, S. S. K. Ma, Y. Li, K. Domen, *Chem. Mater.*, 2014, **26**, 4144–4150.
86. Y. Sasaki, H. Nemoto, K. Saito and A. Kudo, *J. Phys. Chem. C*, 2009, **113**, 17536–17542.
87. Q. Jia, A. Iwase, A. Kudo, *Chem. Sci.*, 2014, **5**, 1513–1519.
88. S. S. K. Ma, K. Maeda, T. Hisatomi, M. Tabata, A. Kudo and K. Domen, *Chem.–Eur. J.*, 2013, **19**, 7480–7486.
89. R. Abe, K. Shinmei, K. Hara, B. Ohtani, *Chem. Commun*. 2009, 3577.
90. R. Abe, K. Shinmei, N. Koumura, K. Hara, B. Ohtani, *J. Am. Chem. Soc*. 2013, **135**, 16872.
91. R. Abe, T. Takata, H. Sugihara, K. Domen, *Chem. Commun*.2005, 3829.
92. R. Abe, M. Higashi, K.Domen, *Chem Sus Chem.* 2011, **4,** 228.
93. M. Higashi, R. Abe, K. Teramura, T. Takata, B. Ohtani, K. Domen, *Chem. Phys. Lett.* 2008, **452**,

120.

94. M. Higashi, R. Abe, T. Takata, K. Domen, *Chem. Mater*. 2009, **21**, 1543.
95. K. Maeda, H. Terashima, K. Kase, M. Higashi, M. Tabata, K. Domen, *Bull. Chem. Soc. Jpn.* 2008, **81**, 927.
96. K. Maeda, M. Higashi, D. Lu, R. Abe, K. Domen, *J. Am. Chem. Soc*. 2010, **132**, 5858.
97. D. E. Scaife, *Solar Energy*, 1980, **25**, 41.
98. J.R. Darwent, A. Mills, *J. Chem. Soc., Faraday Trans.*, 1982, **2**, 359.
99. W. Erbs, J. Desilvestro, E. Borgarello, M. Grätzel, *J. Phys. Chem.*, 1984, **88**, 4001.
100. A. Kudo, K. Ueda, H. Kato, *Catal. Lett.*, 1998, **53**, 229.
101. A. Kudo, K. Omori, H. Kato, *J. Am. Chem. Soc*., 1999, **121**, 11459.
102. S. Tokunaga, H. Kato, A. Kudo, *Chem. Mater*., 2001, **13**, 4624.
103. J.Q. Yu, A. Kudo, *Adv. Funct. Mater*., 2006, **16**, 2163.
104. R. Williams, *J. Chem. Phys.*, 1960, **32**, 1505–1514.
105. A.B. Ellis, S.W. Kaiser, J. M. Bolts, M. S. Wrighton, *J. Am. Chem. Soc*., 1977, **99**, 2839–2848.
106. H. Kato, A. Kudo, *J. Phys. Chem. B*, 2002, **106**, 5029.
107. R. Niishiro, H. Kato, A. Kudo, *Phys. Chem. Chem. Phys*., 2005, **7**, 308.
108. R. Konta, T. Ishii, H. Kato and A. Kudo, *J. Phys. Chem. B*, 2004, **108**, 8992–8995.
109. R. Niishiro, R. Konta, H. Kato, W.-J. Chun, K. Asakura, A. Kudo, *J. Phys. Chem. C*, 2007, **111**, 17420.
110. A. Iwase, K. Saito, A. Kudo, *Bull. Chem. Soc. Jpn*., 2009, **82**, 514.
111. S. Kawasaki, K. Akagi, K. Nakatsuji, S. Yamamoto, I. Matsuda, Y. Harada, J. Yoshinobu, F. Komori, R. Takahashi, M. Lippmaa, C. Sakai, H. Niwa, M. Oshima, K. Iwashina and A. Kudo, *J. Phys. Chem. C*, 2012, **116**, 24445–24448.
112. J. Yoshimura, Y. Ebina, J. Kondo, K. Domen, A. Tanaka, *J. Phys. Chem.*, 1993, **97**, 1970.
113. J. Yu, Y. Zhang, A. Kudo, *J. Solid State Chem.*, 2009, **182**, 223.
114. R. Konta, H. Kato, H. Kobayashi, A. Kudo, *Phys. Chem. Chem. Phys*., 2003, **5**, 3061.
115. Y. Hosogi, Y. Shimodaira, H. Kato, H. Kobayashi, A. Kudo, *Chem. Mater*., 2008, **20**, 1299.
116. B. Ohtani, O. Mahaney, F. Amano, N. Murakami and R. Abe, *J. Adv. Oxid. Technol.*, 2010, **13**, 247–261.

117. F.F. Abdi, T.J. Savenije, M.M. May, B. Dam, R. Krol, *J. Phys. Chem. Lett.*, 2013, **4**, 2752–2757.

118. J. Livage, M. Henry, C. Sanchez, *Prog. Solid St. Chem*., 1988, 18, 259–341.

119. C. Sanchez, J. Livage, M. Henry, F. Babonneau, *J. Non-Cryst. Solids.*, 1988, **100**, 65–76.

120. U. Schubert, *J. Mater. Chem.*, 2005, **15**, 3701–3715.

121. J. Livage, C. Sanchez, *J. Non-Cryst. Solids.*, 1992, **145**, 11–19.

122. M. Kakihana, *J. Sol-Gel Sci Technol.*, 1996, **6**, 7–55.

123. S. H. Yu, *J. Ceram. Soc. Jpn*., 2001, **109**, 65.

124. H. Uchiyama, K. Matsumoto, H. Kozuka, *Chem. Lett*., 2010, **39**, 445–447.

125. C. J. Barbe, F. Arendse, P. Comte, M. Jirousek, F. Lenzmann, V. Shkolver, M. Grätzel, *J. Am. Ceram. Soc.*, 1997, **80** (12), 3157–3171.

126. T. K. Townsend, N.D. Browning, E.E. Osterloh, *ASC Nano*, 2012, **6**, 7420–7426.

127. M. Kakihana, K. Domen, *MRS bulletin*, 2000, 27.

128. Y. Moriya, T. Takata, K. Domen, *Coord. Chem. Rev.*, 2013, **257**, 1957.

129. M. Kakihana, M. Yoshimura, *Bull. Chem. Soc. Jpn.*, 1999, **72**, 1427.

130. T. Ohya, M. Ito, K. Yamada, T. Ban, Y. Ohya, Y. Takahashi, *J. Sol-Gel Sci. and Tech.* 2004, **30**, 71–81.

131. M. Kakihana, M. Kobayashi, K. Tomita, V. Petrykin, *Bull. Chem. Soc. Jpn.*, 2010, **83**, 11, 1285–1308.

132. M. Kakihana, M. Tada, M. Shiro, V. Petrykin, M. Osada,Y. Nakamura, *Inorg. Chem.*, 2001, **40**, 891–894.

133. D. M. Fabian, S. Hu, N. Singh, F. A. Houle, T. Hisatomi, K. Domen, F. E. Osterloh and S. Ardo, *Energy Environ. Sci.*, 2015, **8**, 2825.

134. A. Xiong, G. Ma, K. Maeda, T. Takata, T. Hisatomi, T. Setoyama, J. Kubota, K. Domen, *Catal Sci Technol.*, 2014, **4**, 325–328.

135. Q. Wang, Y. Li, T. Hisatomi, M. Nakabayashi, N. Shibata, J. Kubota, K. Domen, *J. Catal.*, 2015, **328**, 308–315.

Chapter 1

Facile Preparation of Stable Aqueous Titania Sols for Fabrication of Highly Active TiO_2 Photocatalyst Thin Films

1.1 Introduction

It is well known that titanium dioxide (TiO_2) induces various useful photocatalytic reactions such as water splitting, decomposition of organic compounds[1] and photo-induced surface superhydrophilicity[2] under UV light irradiation. Owing to its excellent photocatalytic activity, sufficient chemical stability, nontoxic property and abundance as natural resources, various TiO_2-related photocatalyst products have been already put to practical use, on which TiO_2 thin films are coated as the active layer. For example, the glass plates coated with transparent TiO_2 thin films can work as highly-functional glasses that display both antifogging and self-cleaning effects.

Sol-gel techniques are typically used as a facile and cost-effective method to form transparent TiO_2 thin films on substrates such as glass.[3-6] The coated titanium precursors or TiO_2 nano-colloids are often subjected to post-calcination at relatively low temperatures for forming densely-packed TiO_2 fine particles with enough photocatalytic activity and mechanical strength. The conventional sol-gel methods for TiO_2 thin films generally employ an alkoxide (e.g., $Ti(OEt)_4$, $Ti(OiPr)_4$) or a chloride (e.g., $TiCl_4$) as a titanium source, dissolved in an appropriate organic solvent such as ethanol. However, the high reactivity of these titanium sources toward hydrolysis makes it difficult to store these solutions for long periods under ambient condition, and therefore limits the use of them for lab-scale experiments or comparatively-small-scale practical applications. Thus, the development of water-based TiO_2-precursor solution with enough stability is strongly desired to widen a range of applications and also to reduce environmental burdens such as the volatilization of organic solvents. It has been reported that some titanium complexes such as titanium lactate ($Ti(OH)_2[OCH(CH_3)COOH]_2$)[7] and titanium(IV)-peroxo-citrate ($(NH_4)_4[Ti_2(C_6H_4O_7)_2(O_2)_2]\cdot 4H_2O$)[8,9] can be stabilized in water and thus used as water-based titanium precursors solutions for preparation of TiO_2 thin films. However, the preparation of these stable titanium precursor solutions generally requires complicated multistep procedures. Another water-based sol-gel technique is the use of TiO_2 colloids that are stabilized in water. However, the stabilization generally requires highly acidic condition to suppress the aggregation of TiO_2 colloids.[10-15] The strong acidity of the precursor sols is environmentally-unfriendly. In addition, the conventional acidic titania sols dominantly contain TiO_2 particles having non-uniform particle sizes larger than 10 nm,[12-15] making it difficult to prepare densely-packed TiO_2 thin films with retaining transparency and mechanical strength.

In this chapter, the facile preparation of aqueous sols that can stabilize amorphous titanium oxide particles with ca. 4 nm of average size even under mild acidic condition (~ pH 4), by simply mixing titanium(IV) tetraisopropoxide (TIPT) and acetylacetone (acac) in aqueous acetic acid (AcOH) solution, was developed. The role of these additives for stabilizing titania colloidal particles in water solvent was discussed on the basis of detailed characterization of the solutions. Transparent TiO_2 thin films were prepared on quartz substrates by mean of simple spin-coating of the newly-developed titania sol and subsequent calcination in air, and their photocatalytic activities were evaluated on photo-induced surface superhydrophilicity under UV light irradiation.

1.2 Experimental

1.2.1 Materials

Titanium(IV) tetraisopropoxide (TIPT) (95.0%), acetylacetone (acac) (99.0%), acetic acid (AcOH) (99.7%), and lactic acid (85.5–94.5%) were purchased from Wako Pure Chemical Industries, Ltd., Osaka, Japan. Titanium(IV)-peroxo-citrate complex ($(NH_4)_4[Ti_2(C_6H_4O_7)_2(O_2)_2]\cdot 4H_2O$) was purchased from Furuuchi Chemical Corporation. All reagents were used as received, and all the experiments were carried out under ambient condition without eliminating the water from the atmosphere.

1.2.2 Preparation of aqueous titania sols

TIPT (20.0 mmol) was added to acac (20.0 mmol) slowly under continuous stirring at room temperature. The mixture was stirred for 10 minutes. The resulting yellow solution of TIPT/acac precursor was added dropwise to an aqueous solution of AcOH (0.40 mol/L, 50.0 mL) under continuous stirring for 1 hour at room temperature, yielding yellow transparency solutions. This titania sol will be denoted as AA-sols hereafter. For comparison, other aqueous solutions were prepared from TIPT in the same procedure but without either of acac or AcOH.

Additionally, aqueous solution of titanium lactate was obtained by adding TIPT (20.0 mmol) into an aqueous solution of lactic acid (0.8 mol/L, 50.0 mL) under continuous stirring at room temperature for 7 days. Aqueous solution of titanium-peroxo-citrate was also obtained by adding titanium(IV)-peroxo-citrate complex (ca. 10.0 mmol) to water (50.0 mL).

1.2.3 Characterization of AA sols

The particle sizes of titania colloids in sols were estimated by means of dynamic light scattering (DLS, ELSZ-1000, Otsuka Eletronics Co., Ltd). Infrared absorption spectra of the sols were obtained by means of Fourier transform infrared spectroscopy (FT/IR-4600, JASCO) using a transmission-type cell equipped with BaF_2 windows. Spectra were obtained in the range 2000–800 cm^{-1}, by integrating 64 scans at an effective resolution of 4 cm^{-1}. For comparison, FT-IR spectra of aqueous solutions of AcOH (0.40 mol/L), acac (0.40 mol/L), and their mixture were also measured. Differential spectra were obtained by subtracting the spectrum of water. ^{1}H NMR and ^{13}C NMR spectra were recorded on a JMN-ECA 500 spectrometer (JEOL). For ^{1}H NMR spectrum measurements, sodium 3-(trimethylsilyl)propionate-2,2,3,3-d_4 in D_2O (0.4 vol%) was used as an external reference in a capillary tube. For ^{13}C NMR spectrum measurements, $CDCl_3$ was used for an external referencing (77.23 ppm) and locking. For comparison, ^{1}H NMR and ^{13}C NMR spectra of aqueous solutions of AcOH (0.40 mol/L), acac (0.40 mol/L), and 2-propanol (1.6 mol/L) were also measured.

1.2.4 Preparation of TiO_2 films

Thin films of TiO_2 were prepared by spin-coating method: a cleaned quart substrate (5×5 cm) was dropped with the AA sols (ca. 1 mL), and then rotated at 500 rpm for 5 seconds and subsequently 2,000 rpm for 10 seconds. The coated film was dried at room temperature for 10 min and then at 60°C for 10 minutes. The set of spin coating and drying was further repeated once again. The as-prepared film was then heated at different temperatures ranging from 600 to 900°C for 5 hours to yield TiO_2 thin films, which will be denoted as AA-*T* (*T* = 600–900) films hereafter. In addition, the TiO_2 thin films prepared from aqueous solutions of titanium lactate complex or titanium(IV)-peroxo-citrate complex will be denoted as L-*T* or P- *T* (*T* = 600–900) films, respectively. The thickness of each film was adjusted ca. 50 nm.

1.2.5 Characterization of TiO_2 films

The morphologies of TiO_2 films were observed using a laser microscope (Shimazu, OLS4000), scanning electron microscope (SEM, HITACHI, S-4100), and scanning probe microscope (SII, Nanocute) with a self-sensitive cantilever (SII, PRC-DF40P).

Changes in the crystal phase were monitored using X-ray diffraction (XRD, PANalytical, X'Pert Pro) rotating anode diffractometer (45 kV, 40 mA) with Cu *K*α radiation ($\lambda_{K\alpha}$ = 1.5406 Å). The Raman spectra were recorded with laser Raman spectrometer (Jasco, NRS-7200); an argon ion laser at 532 nm was used. Thermal analysis (TG-DTA) was conducted on dried powders on a TG-8120 (Rigaku). TG-DTA curves were recorded under air flow in the temperature range from 25 to 900℃.

Photocatalytic activity of TiO_2 films was evaluated by monitoring the change in the contact angle of a droplet of water under UV light irradiation using a contact angle meter (Kyowa Interface Science Co., LTD. CA-X). The 0.5 wt% oleic acid in heptane solution (1 mL) was dropped on the TiO_2 film, to make the surface hydrophobic before the evaluaction. After the films were rotated at 500 rpm for 5 seconds and then 2,000 rpm for 10 seconds by using spin-coater, the film was dried at 70℃ for 15 minutes. A high power black light (TOSHIBA FL20S/BLB-A, 10 W/m^2) was used as a light source.

1.3 Results and discussion

1.3.1 Size distribution of aqueous colloidal titania sols

Figure 1-1 shows photographs of the aqueous solutions in which TIPT (0.4 M) was dissolved under different conditions. The appearance of AA-sol prepared via adding both TIPT and acac into aqueous AcOH solution was clear yellow with high transparency (see the left one). Interestingly, this solution was found to be stable without forming any visible precipitations even after leaving under atmospheric condition for more than 1 year. Although the addition of acac into the ethanol solution containing TIPT has been reported to lower the rate of hydrolysis of TIPT effectively,[16-24] the addition of TIPT into water together with acac immediately formed yellow suspension (see the middle); producing visible precipitation. Simple addition of TIPT into aqueous solution of AcOH also resulted in rapid formation of white suspension (see the right), which then changed to precipitation.

DLS measurement revealed that the AA-sol contained colloidal particles with diameters ranging from 0.8 nm to 10 nm (average diameter d = ca. 3.7 nm, see Figure 1-2). These colloidal particles, certainly consist of amorphous titania or titanium hydrate (the XRD pattern of dried powder showed no appreciable peaks, not shown), are much more uniform and smaller than conventional titania colloids stabilized by strong acid such as HCl or HNO_3, which possess non-uniform feature with diameters ranging from 10 nm to some hundred nm.[12-15] The use of diluted HCl or HNO_3 for adjusting the pH of

aqueous solutions similar to that of AcOHaq (pH ~ 4) could not stabilize TIPT effectively even in the presence of acac; precipitations were immediately produced after adding TIPT/acac into the solution.

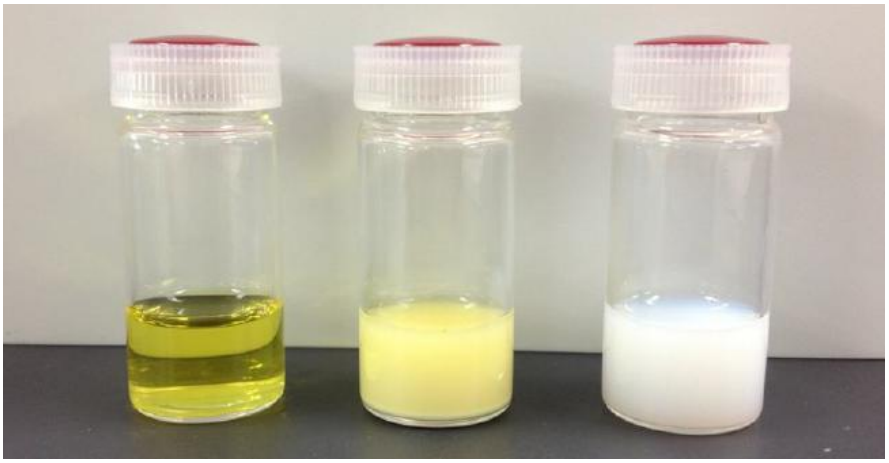

Figure 1-1. An image of AA-sol (left), TIPT/acac in water (middle), and TIPT in AcOH aq. (right).

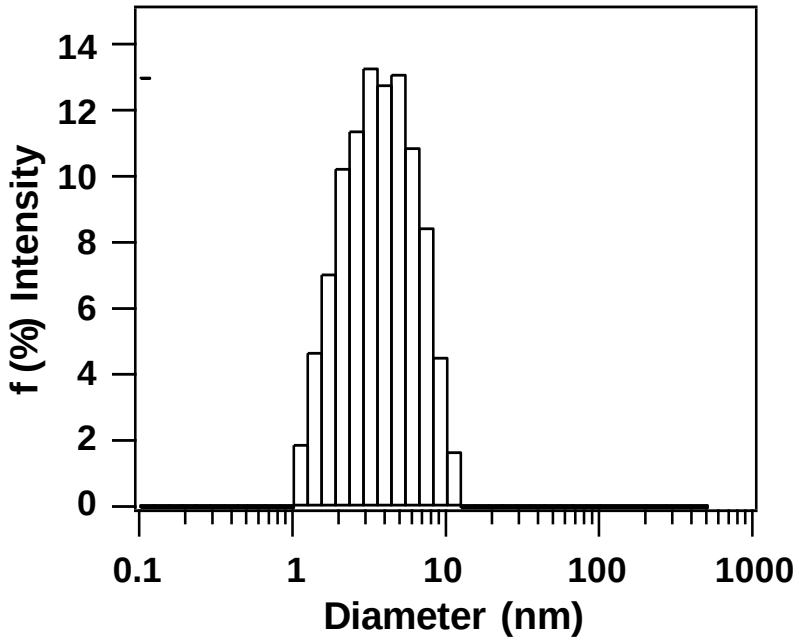

Figure 1-2. Size distribution of the titania colloidal particles in AA-sols.

1.3.2 Characterizations of titanium species in the aqueous titania sols

In order to clarify the titanium species that were stabilized as colloidal state in AA-sols, FT-IR and NMR spectroscopies were employed. Figure 1-3 shows infrared absorption spectrum of the AA-sols, along with those of aqueous acac or AcOH solutions for comparison. The AA-sols exhibited specific absorption bands at 1574, 1537, 1467, 1384, 1127, 1107 and 954 cm^{-1}, which were not observed for either acac[16,19,20,25] or AcOH[24] solutions.

The bands observed at 1467, 1384, 1127, 1107 and 954 cm^{-1} can be assigned to the absorption by 2-propanol molecules,[26] which should be formed by hydrolysis of TIPT. The bands at 1574 and 1537 cm^{-1} are assignable to the vibrational bands of ν(C-C) and ν(C=O) of the enol-form acac molecules that bounded to Ti cations, indicating the chelation of acac to the surface of titania species.[16,27] It appears that the absorption bands at around 1721 and 1297 cm^{-1} due to the existence of acetate species bound to titanium species.[28]

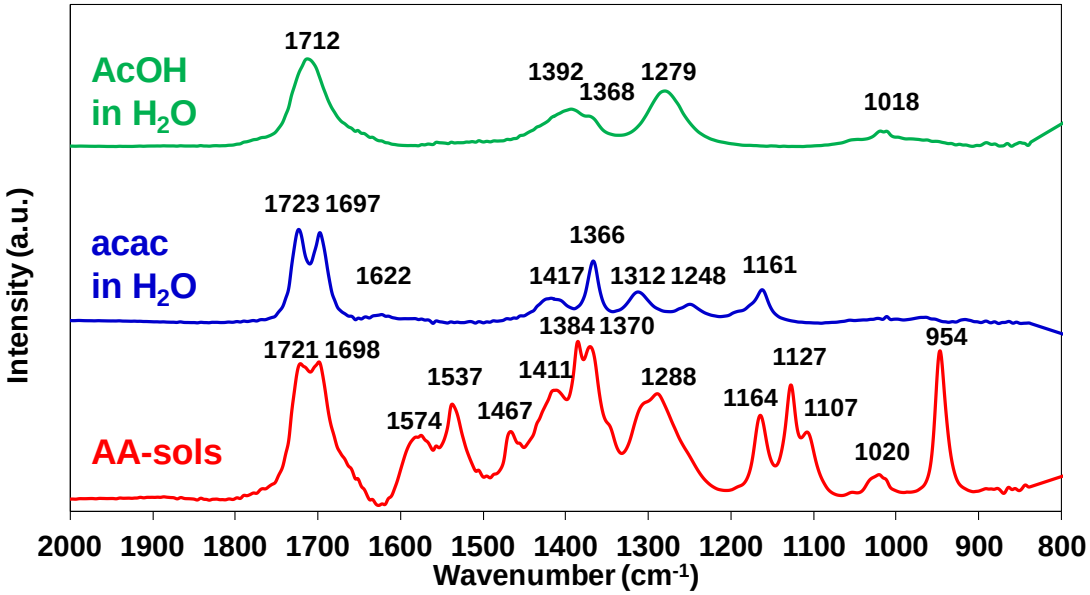

Figure 1-3. FT-IR spectra of AA-sols, acac in H_2O, and AcOH in H_2O.

The detailed structures of titanium species in the AA-sols were further estimated by mean of the liquid state ^{1}H NMR and ^{13}C NMR spectroscopies. The ^{1}H NMR spectrum of the AA-sol is shown in Figure 1-4; the assignments of the observed signals are summarized in Table 1-1. The ^{1}H NMR spectrum of AA-sol showed the characteristic broad resonance at around 2 ppm, along with the weak but sharp chemical shifts at 2.00 ppm, 2.23 ppm, and 5.87 ppm; these weak chemical signals were different from those corresponding to the free forms of AcOH, acac (keto/enol = 4:1) and 2-propanol. It

has been reported that the signals derived from the species having large molecular weight, such as products of hydrolysis or condensation, became broad or undetected in NMR because the molecules having larger weight generally shows lower mobility.[20]

Judging from the fact that the signals attributed to the methyl groups of acac and AcOH are generally observed at around 2 ppm, the board resonance observed from 1.9 to 2.3 ppm in AA-sol is certainly derived from the acac and/or AcOH molecules that terminate the surface Ti cation centers and the hydroxyl groups, as illustrated in Figure 1-5 (a). The weak chemical shifts at 2.00 ppm, 2.23 ppm, and 5.87 ppm can be assigned to a small amount of Ti-acac complex as depicted in Figure 1-5 (b), since the similar spectral pattern was obtained with the ^{1}H NMR spectrum of the Ti-acac complex in $CDCl_3$ (see Figure 1-6). All the signals observed in ^{13}C NMR spectrum of AA-sol was well assigned to the species that were indicated by the ^{1}H NMR spectrum, while the broad signal was not observed. It is known that ^{13}C NMR is generally less sensitive than ^{1}H NMR for the species having large molecular weight.

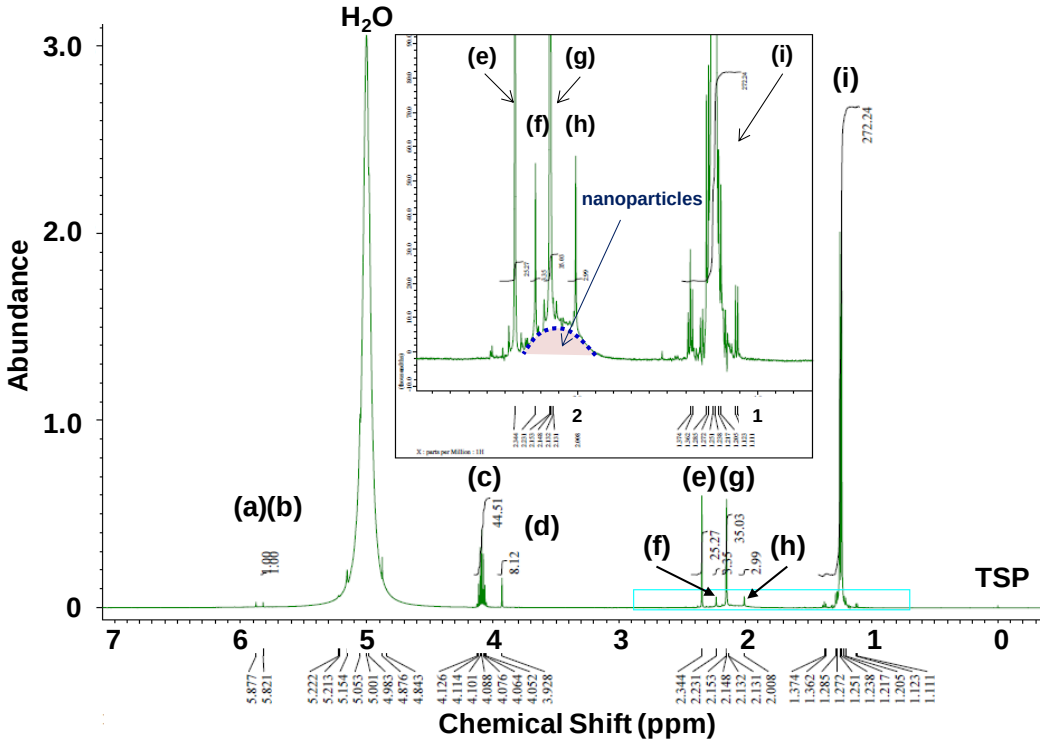

Figure 1-4. ^{1}H NMR spectrum of AA-sols.

Table 1-1. ^{1}H NMR and ^{13}C NMR chemical shifts of AA-sols and authentic samples.

Species	^{1}H NMR		^{13}C NMR	
	AA- sols [ppm]	Authentic sample [ppm]	AA-sols [ppm]	Authentic sample [ppm]
AcOH	(g) 2.15 (CH_3, 29H)	2.10 (CH_3)	21.1 (CH_3)	20.8 (CH_3)
			177.3 (CO)	177.1 (CO)
acac	(e) 2.35 (CH_3, 25H)	2.30 (CH_3)	30.9 (CH_3)	30.8 (CH_3)
(keto-form)	(d) 3.93 (CH_2, 8H)	3.89 (CH_2)	57.5 (CH_2)	57.5 (CH_2)
			208.9 (CO)	208.9 (CO)
acac	(g) 2.15 (CH_3, 6H)	2.10 (CH_3)	24.5 (CH_3)	24.4 (CH_3)
(enol-form)	(b) 5.82 (CH, 1H)	5.76 (CH)	101.4 (CH)	101.2 (CH)
			193.5 (CO)	193.4 (CO)
2-Propanol	(i) 1.24 (CH_3, 272H)	1.19 (CH_3)	24.3 (CH_3)	24.1 (CH_3)
	(c) 4.09 (CH, 44H)	4.04 (CH)	64.7 (CH)	64.7 (CH)
Ti-acac complex (depicted in Figure 2-5(b))	(h) 2.00 (CH_3, enol-form, 3H)	—	194.6 (CO)	—
			187.8 (CO)	
			104.9 (CH)	
	(f) 2.23 (CH_3, enol-form, 3H)		26.7 (CH_3)	
			25.4 (CH_3)	
	(a)5.87 (CH, enol-form, 1H)			

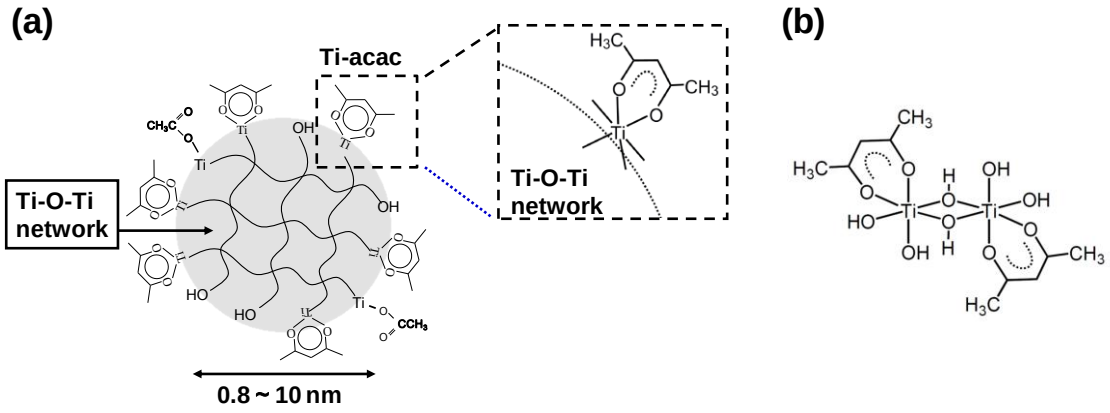

Figure 1-5. (a) Possible structure of titania particles in AA-sols. (b) Proposed structure of the Ti-acac complex of trace components contained in AA sols.

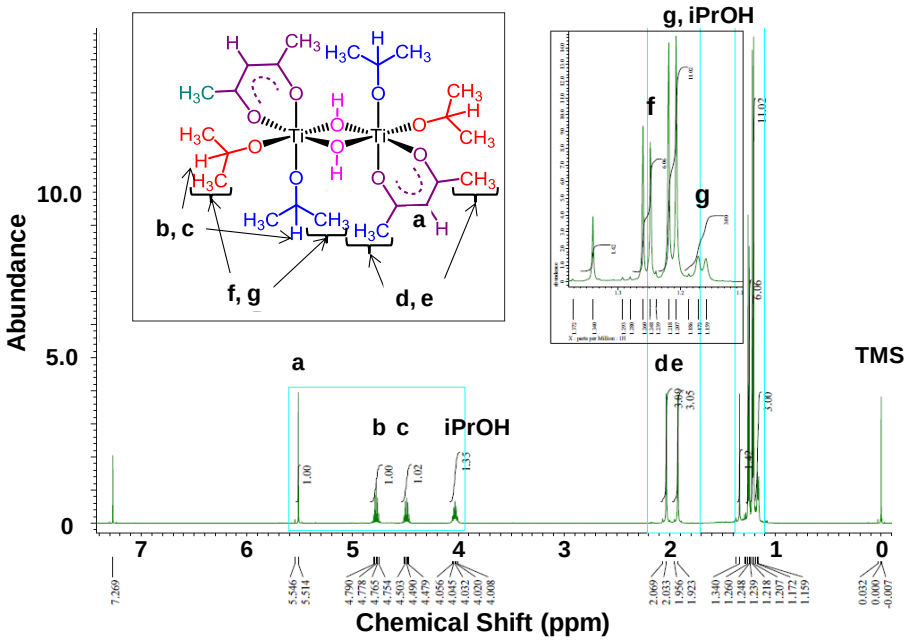

Figure 1-6. ^{1}H NMR spectrum of a Ti-acac complex in $CDCl_3$.

Based on these results, it can be concluded that the colloidal titania particles with diameters ranging from 0.8 to 10 nm are stabilized by the co-existence of acac and AcOH in the AA-sol as illustrated in Figure 1-5 (a). Although the TIPT molecules were undergone hydrolysis and condensed in the initial period into amorphous titania nano colloids with Ti-O-Ti networks, the surface Ti species were effectively protected from further hydrolysis and condensation *via* the chelation of acac molecules to Ti cations. This stabilization mechanism in aqueous system seems reasonable because it is known that the chelated acac molecules can effectively suppress the hydrolysis and further condensation of various alchoxides such as TIPT in organic solvents.[23] As for the roles of AcOH, it is likely that AcOH molecules also inhibit the condensation of titania colloids by affecting the surface Ti cations and/or hydroxyl groups.[28-31] Additionally, it has been reported that the added AcOH molecules can work as peptizer of TiO_2-sols in organic solvents.[12] Although, the sole addition of acac or AcOH is effective to suppress the hydrolysis and condensation of TIPT in organic media, neither can suppress the rapid hydrolysis of TIPT in aqueous media. The co-existence of acac and AcOH in an appropriate ratio specifically can stabilize the amorphous titania colloid even in aqueous media through a kind of concerted mechanism.

1.3.3 Characterizations of TiO_2 films prepared by simple spin-coating and following calcination

Preparation of TiO_2 thin films was attempted by coating three different water-base precursor solutions on various substrates such as quartz followed by calcinations in air at various temperatures. The AA-sol, which was stabilized by the co-exsistence of acac and AcOH, was found to readily form homogeneous and transparent films on various substrates besides quartz (e.g., Si) by simple spin-coating (see AA-film-as in Figure 1-7, for example). Although the aqueous solution of titanium-peroxo-citrate could form transparent films on hydrophilic quartz (see P-film-as), it produced inhomogeneous film on Si substrate (not shown) due to the insufficient wettability. As for the aqueous solution of titanium lactate complex, it could not be homogeneously coated even on quartz substrate, resulting in an opaque and non-uniform film (see L-film-as). Figure 1-8 shows the laser micrograph images of the films after the calcination at 900°C in air. Clearly, AA-900 and P-900 films possess much smoother surface than L-900.

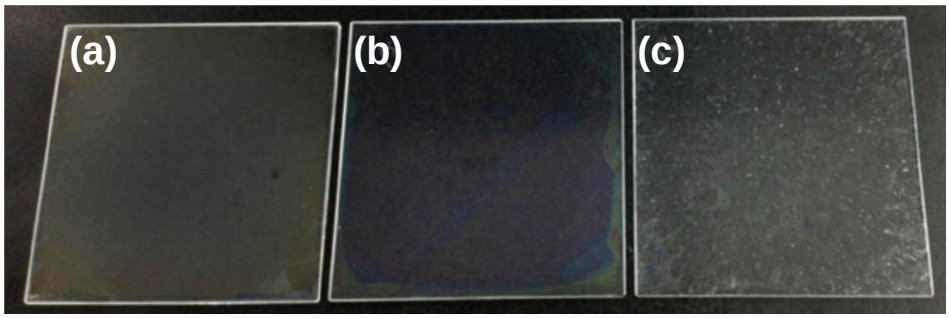

Figure 1-7. A photograph of as prepared TiO_2 films on the glass substrate (5×5 cm) by using (a) AA-sol, (b) titanium lactate complex solution, and (c) peroxo-titanium-citrate complex solution.

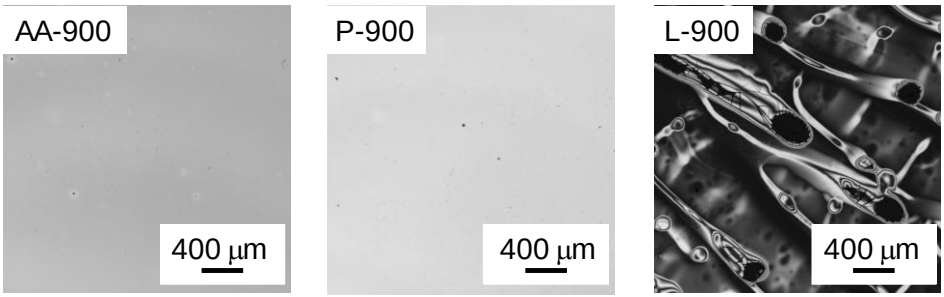

Figure 1-8. Laser micrographs of TiO_2 films prepared by using by using (a) AA-sol, (b) peroxo-titanium-citrate complex solution, and (c) titanium lactate complex solution, followed by calcinations at 900℃.

Figure 1-9 shows SEM images of TiO_2 films (AA- and P-films) calcined at different temperatures. As described later, all the films were confirmed to have anatase and/or rutile TiO_2 phase after calcination at above 600℃ (see Figure 1-10 for the XRD patterns). Although the grain sizes of TiO_2 particles gradually increased with increasing calcination temperature in both cases, the degree of increase on P-films was much more significant than on AA-films. The difference in crystal growth was also confirmed in the average sizes of TiO_2 particle calculated from the full width of half maximum intensity of the (101) diffraction peaks by the Scherrer formula (see Table 1-2). The P-films calcined at above 700℃ had coarse particles with size larger than 200 nm along with observable pores between the particles. As seen in the XRD patterns (see Figure 1-10), the peaks corresponding to rutile phase were obviously appeared along with those of anatase one after the calcination of P-films above 700℃, indicating the phase transition from anatase to rutile accompanied by the crystal growth. On the other hand, AA-films had crack free and flat surfaces consisting of density-packed nanoparticles even after the calcination at 900℃, with an average primary particle of 50 nm sizes. Interestingly, no peaks

corresponding to rutile phase was observed in the XRD pattern of AA-900. Raman spectra of these films (see Figure 1-11) also indicated that the phase transition from anatase to rutile was effectively suppressed up to 900℃ in the case of AA-films, while the presence of rutile phase was clearly observed in the Raman spectra of the P-films above 700°C. Although the peaks corresponding to rutile phase were not observed in the XRD pattern of L-700, rutile phase was appreciably observed in the Raman spectrum, indicating that phase transition partially occurred at 700℃ in the case of L-films. The thermogravimetry and differential thermal analysis (TG-DTA) was conducted to confirm the temperatures at which the phase transition from anatase to rutile occurred in each sample. Since it was difficult to analyze precisely the changes accompanied by the crystallization and/or phase transition behaviors owing to the quite small amount of TiO_2 loaded on the glass substrate, the TG-DTA analysis was conducted on the powder samples that were obtained by the simply dryness of precursor sol solutions. As shown in Figure 1-12, no clear peaks was observed for the AA-powder from 500 to 900℃, while exothermic peaks corresponding to phase transition from anatase to rutile were observed at around 800℃ for P- and L-powders. The TG-DTA results on the temperatures of phase transition to rutile were well agreed with those obtained by XRD and Raman spectra measurements, indicating the interesting nature of AA-sol for preventing the phase transition to rutile at high temperatures.

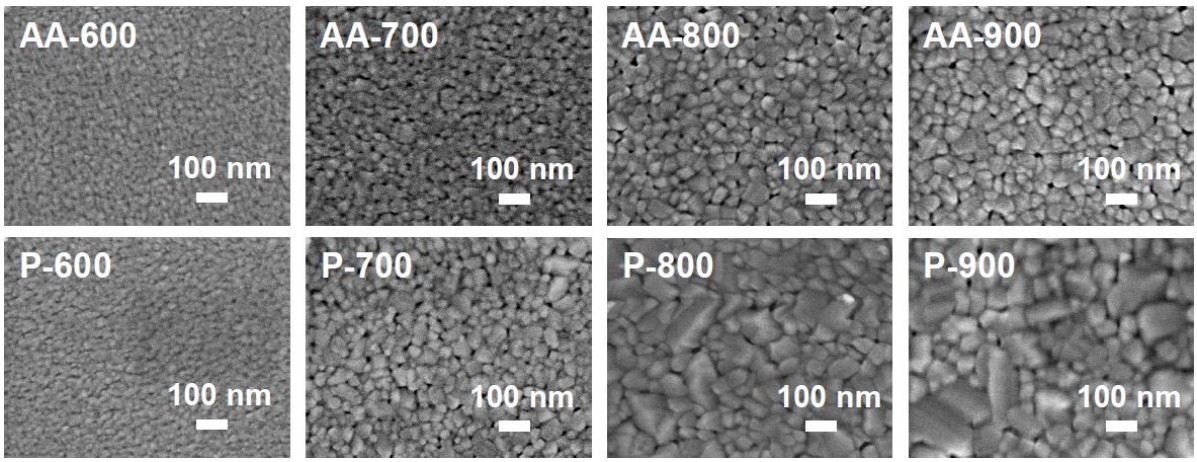

Figure 1-9. SEM images of TiO_2 films prepared by using AA-sol or peroxo-titanium-citrate complex solution (AA- or P-films) followed by calcination at different temperatures.

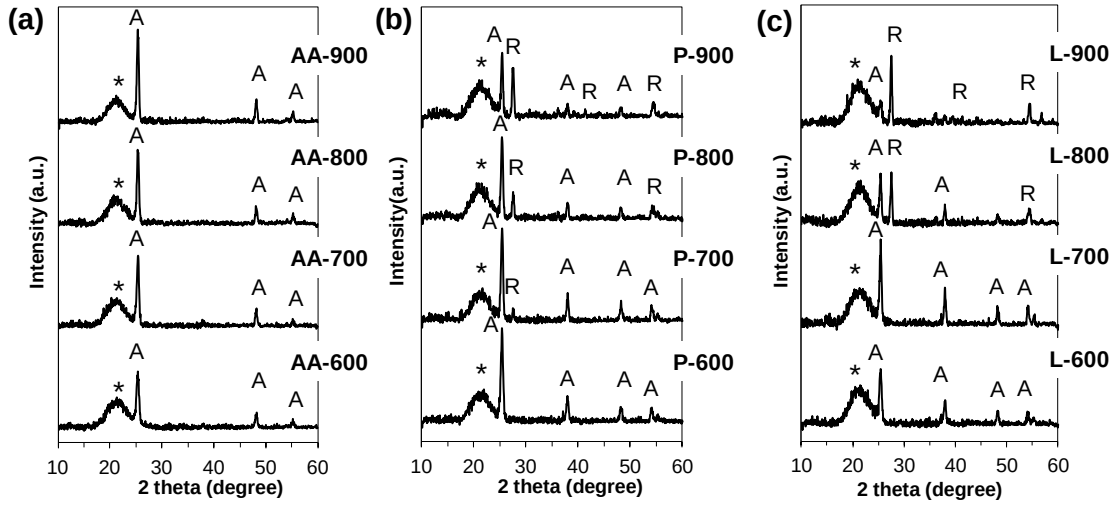

Figure 1-10. XRD patterns of TiO_2 films prepared by using (a) AA-sol, (b) peroxo-titanium-citrate complex solution, and (c) titanium lactate complex solution, followed by calcinations at different temperatures. *: quarts substrate, A: TiO_2 (anatase), R: TiO_2 (rutile)

Table 1-2. Crystalline sizes of TiO_2 films prepared by using (a) AA-sol, (b) peroxo-titanium-citrate complex solution, and (c) titanium lactate complex solution, followed by calcinations at different temperatures.

	(a) AA-films	(b) P-films	(c) L-films
600℃	23.7	32.0	25.0
700℃	31.2	35.2	37.3
800℃	35.7	36.7	40.3
900℃	33.2	36.4	46.2

Calculated from the FWHM of the (101) peak by the Scherrer formula.

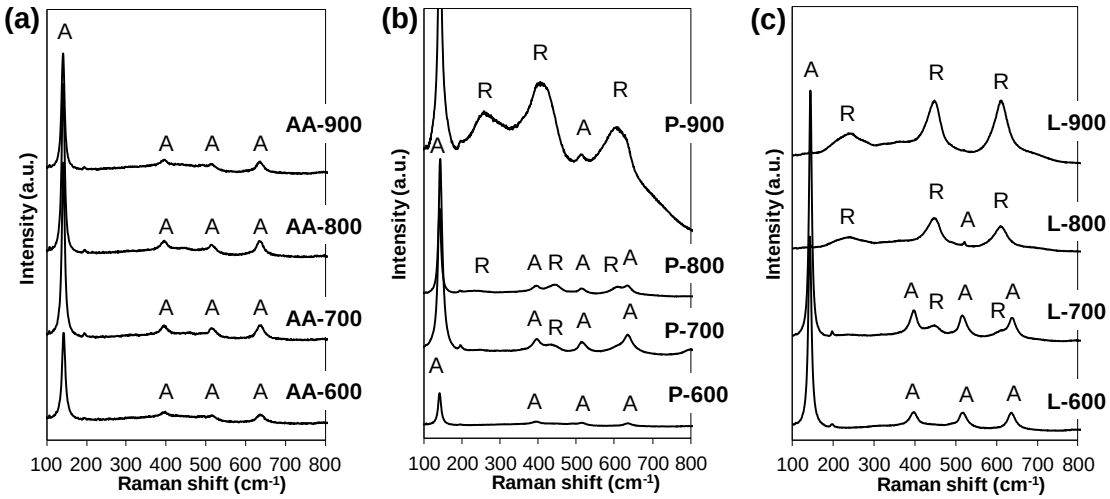

Figure 1-11. Raman spectra of TiO_2 films prepared by using (a) AA-sol, (b) peroxo-titanium-citrate complex solution, and (c) titanium lactate complex solution, followed by calcinations at different temperatures. A: TiO_2 (anatase), R: TiO_2 (rutile)

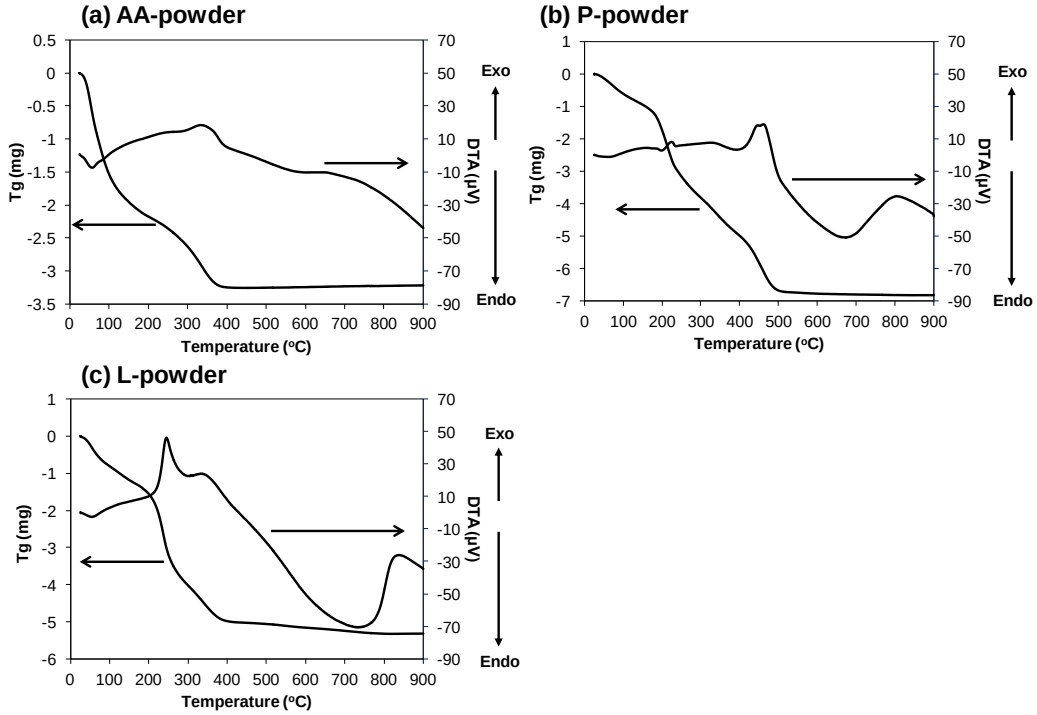

Figure 1-12. TG-DTA curves of dried powders prepared by dryness of the (a) AA-sol, (b) peroxo-titanium-citrate complex solution, and (c) titanium lactate complex solution.

It has been reported that the addition of acac and/or AcOH into the organic solvents containing titania precursor effectively suppressed the phase transition[21] and crystal growth[12,24] during the calcination. As for phase transition, it has been reported that some supporting ligands can suppress hydrolysis of titania and affect phase transition behavior from anatase to rutile phase in the case of sol-gel method using organic solvents.[32] For example, it was demonstrated that the TiO_2 films prepared by sol-gel process with methanol or 2-propanol solvent could retain the anatase phase even at temperatures as high as 800℃, after addition of acac or AcOH[21] into the precursor solution. Therefore it seems reasonable to consider that the phase transition from anatase to rutile was also suppressed at high temperatures by the co-existence of acac and AcOH in aqueous media, based on the similar mechanisms in organic solvents. Barbe et al. has been reported that anatase TiO_2 particles with small size were obtained by adding acetic acid in precursor titania sols during hydrothermal synthesis. [12] Attar et al. has also reported that small anatase TiO_2 particles were obtained by adding acetylacetone in precursor titania sols during sol-gel preparation in organic solvents. They suggested that crystallization temperature shift to higher temperature in presence of acethylacetone.[24] Considering the similar results shown in these previous reports, the acetic acid and acetylacetone added in the AA-sol also work to suppress the particle growth in water solvent, while most of the previous reports were done in organic solvents. Another possibility will be that the strong perpendicular interaction between the coated titania colloids and the quartz substrate effectively suppressed the horizontal grain growth of titania.

The surface roughness (Ra values) of TiO_2 films was estimated by means of AFM; the obtained Ra values are summarized in Table 1-3. Clearly, the AA-films showed small Ra values even after the calcination above 600℃, while those of P-films appreciably increased after the calcination. These results clearly demonstrated that the aqueous AA-sol, in which titania nano colloids are effectively stabilized by the co-existence of acac and AcOH, is quite useful to prepare homogeneous and transparent TiO_2 thin films by simple procedures such as spin coating. The smaller Ra values of AA-films than those of P-films at above 700℃ clearly revealed the smoother surfaces of AA-films.

Table 1-3. Surface roughness of TiO_2 films prepared by using (a) AA-sol and (b) peroxo-titanium-citrate complex solution followed by calcinations at different temperatures.

	AA-films	P-films
600℃	1.59	1.47
700℃	1.47	2.42
800℃	1.72	4.18
900℃	1.75	3.00

1.3.4 Photocatalytic surface cleaning of TiO_2 films

Finally, the photocatalytic activity of the prepared TiO_2 films was evaluated on the basis of photo-induced surface superhydrophilicity, by monitoring the change in water contact angle (CA) under UV light irradiation. Before evaluation, the surfaces of TiO_2 films were made hydrophobic by applying small amount of oleic acid. Figure 1-13 shows the change in CA on AA-films calcined at different temperatures. Upon irradiation, the CA on all samples gradually decreased due to the photocatalytic decomposition of residual oleic acid on the surface and the following photoinduced hydrophilicity.[2] Clearly, the AA-films calcined at lower temperatures exhibited higher activity for the photoinduced hydrophilicity. In general, the surface wettability has been known to increase as the surface roughness increases.[33] Judging from the fact that the Ra values in AA-films were similar independently on the calcination temperatures (see Table 1-3), other factors, such as change in the surface area of the TiO_2 particles dominated the activity.

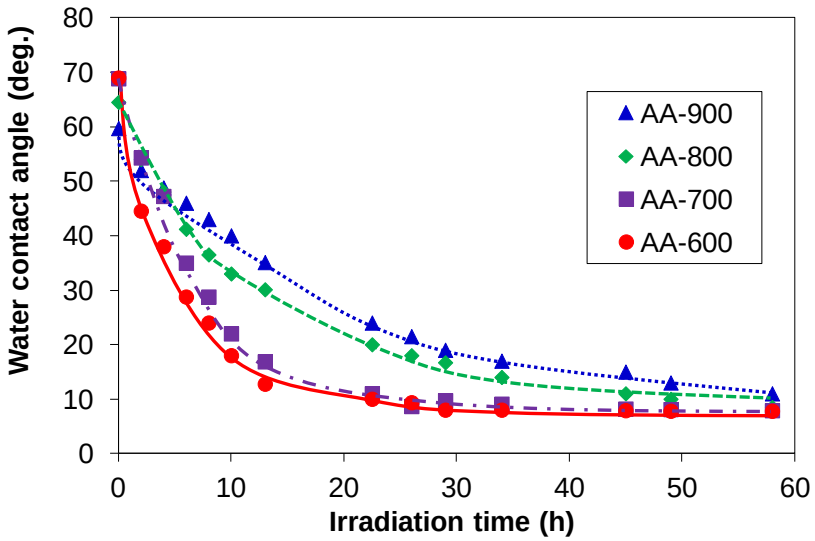

Figure 1-13. Changes in water contact angles upon AA films under UV light irradiation.

Figure 1-14 shows the CA values of AA-films and P-films before and after 10 hours under UV irradiation. Clearly, the AA-films showed higher activity, i.e., greater change in CA, than the P-films on each calcination temperature. The photocatalytic activity of AA-films was compared with those of the TiO_2 films prepared *via* one of the well-known sol-gel methods (denoted as SG-films).[34] The XRD analysis indicated that SG-film was composed of anatase phase when it was calcined at 600℃, and converted to rutile phase after calcined at 900℃. As shown in Figure 1-14, the AA-films showed higher photocatalytic activity than the SG-films at each calcination temperature, indicating high potential of AA-sol for preparing highly active TiO_2 photocatalyst films. As for the samples calcined at 600℃, the higher activity of AA-film is undoubtedly due to the higher surface areas (i.e., smaller particle size) of TiO_2 particles compared to those in P-films. As for the samples calcined above 700℃, the pure content of anatase phase in AA-films probably contributed to the higher photocatalytic activity, since in general anatase phase exhibits higher activity than rutile one for various photocatalytic reactions including the decomposition of organic contaminants of surface.[35] Thus, we demonstrated that the AA-films, which were prepared using the newly-developed AA-sols, show high photocatalytic activity for both the self-cleaning (decomposition of organic compounds on the surface and photoinduced superhydrophilicity).

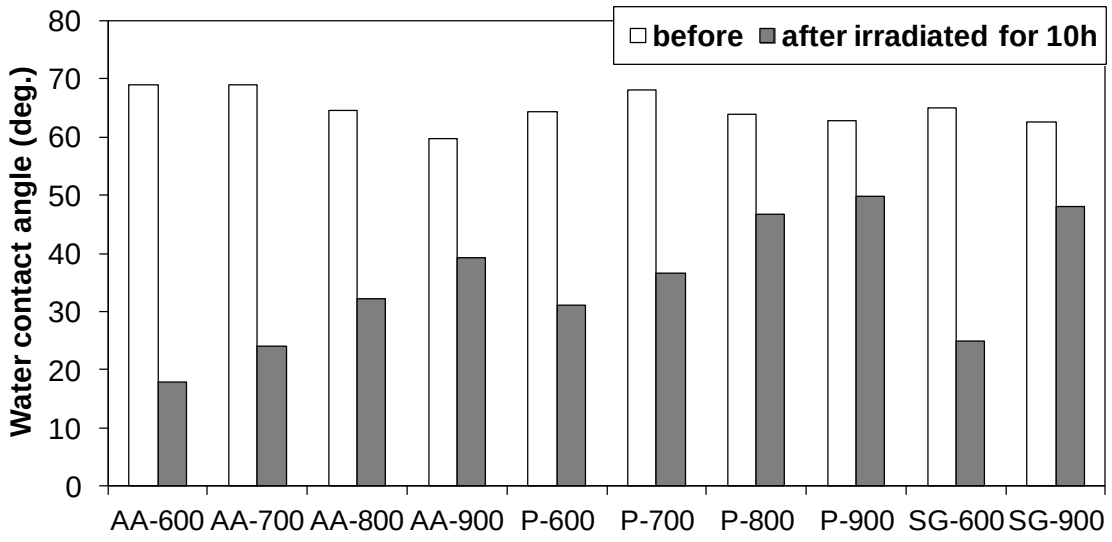

Figure 1-14. Water contact angles of TiO_2 films before and after UV irradiation for 10 hours.

1.4 Conclusions

An significantly-simple method was developed for preparing stable water-base titania sols by employing three common and cheap chemicals, TIPT, acac and AcOH, as raw materials; just mixing them with appropriate ratio and sequence. The present titania sols possess desirable properties as precursor for fabricating TiO_2 thin films, such as quite high stability (for more than one year), no use of organic solvents, mild acidity (pH ~ 4), sufficiently small sizes of titania colloids, and indeed can easily be transformed into homogeneous and transparent TiO_2 thin films on various substrates by post calcination. The TiO_2 thin films prepared from the present new water-base titania sols showed much higher photocatalytic activity for photoinduced superhydrophilicity under UV light irradiation, certainly due to the much smaller size of TiO_2 particle, and the higher content of highly active anatase phase. These superior features of newly developed aqueous titania sols will widen the application of TiO_2 thin films in the practical use on large scales.

Reference

1. A. Fujishima, K. Honda, *Nature*, 1972, 238, 37–38.

2. R. Wang, K. Hashimoto, A. Fujishima, M. Chikuni, E. Kojima, A. Kitamura, M. Shimohigoshi, T. Watanabe, *Nature*, 1997, 388, 431–432.

3. J. Livage, M. Henry, C. Sanchez, *Prog. Solid St. Chem*., 1988, 18, 259–341.

4. C. Sanchez, J. Livage, M. Henry, F. Babonneau, *J. Non-Cryst. Solids*., 1988, 100, 65–76.

5. U. Schubert, *J. Mater. Chem.*, 2005, 15, 3701–3715.

6. J. Livage, C. Sanchez, *J. Non-Cryst. Solids*., 1992, 145, 11–19.

7. T. Ohya, M. Ito, K. Yamada, T. Ban, Y. Ohya, Y. Takahashi, *J. Sol-Gel Sci. and Tech.*, 2004, 30, 71–81.

8. M. Kakihana, M. Kobayashi, K. Tomita, V. Petrykin, *Bull. Chem. Soc. Jpn*., 2010, 83, 11, 1285–1308.

9. M. Kakihana, M. Tada, M. Shiro, V. Petrykin, M. Osada,Y. Nakamura, *Inorg. Chem*., 2001, 40, 891–894.

10. N. Serpone, D. Lawless, R. Khairutdinovt, *J. Phys. Chem.*, 1995, 99, 16646–16654.

11. B. L. Bischoff, M. A. Anderson, *Chem. Mater*., 1995, 7, 1772–1778.

12. C. J. Barbe, F. Arendse, P. Comte, M. Jirousek, F. Lenzmann, V. Shkolver, M. Grätzel, *J. Am. Ceram. Soc*., 1997, 80 (12), 3157–3171.

13. N. Serpone, D. Lawless, R. Khairutdinov, *J. Phys. Chem.*, 1995, 99, 16646–16654.

14. A. V. Vinogradov. V. V. Vinogradov, *J. Am. Ceram. Soc.*, 2014, 97 (1), 290–294.

15. L. Bischoff, M. A. Anderson, *Chem. Mater*., 1995, 7, 1772–1778.

16. A. Lgaustic, F. Babonneau, J. Livage, *Chem. Mater.*, 1989, 1, 240–247.

17. A. Lgaustic, F. Babonneau, J. Livage, *Chem. Mater.*, 1989, 1, 248–252.

18. A. Yamamoto, S. Kambara, *J. Am. Chem. Soc*., 1957, 79, 4344–4348.

19. H-J. Chen, L. Wang, W-Y Chiu, *Mater. Chem. Phys*., 2007, 101, 12–19.

20. E. Scolan, C. Sanchez, *Chem. Matter.*, 1998, 10, 3217–3223.

21. Y. Djaoued, S. Badilescu, P.V. Ashrit, D. Bersani, P.P. Lottici, J. Robichaud, *J. Sol-Gel Sci. and Tech.*, 2002, 24, 255–264.

22. M. L. Calzada, R. Sirera, F. Carmona, B. Jimenez, *J. Am. Ceram. Soc*., 1995, 78 (7), 1802–1808.

23. M. W. Jung, H. J. Oh, J. C. Yang, Y. G. Shul, *Bull. Korean Chem. Soc.*, 1999, 20 (12), 1394–1398.

24. A. S. Attar, M. S. Ghamsari, F. Hajiesmaeilbaigi, S. Mirdamadi, *J Mater Sci*., 2008, 43, 1723–1729.

25. D. L. Pavia, G. M. Lampman, G. S. Kriz, *Introduction to Spectroscopy, W. B. Saunders Co., Philadelphia, London, Toronto*, 1979 (Chapter 2).

26. P. D. Moran, G. A. Bowmaker, R. P. Cooney, K. S. Finnie, J. R. Bartlett, J. L. Woolfrey, *Inorg. Chem.*, 1998, 37, 2741–2748.

27. Nakamoto. K., *Infrared and Raman Spectra of Inorganic and Coordination Compounds; Wiley-Interscience*: 1962, New York

28. S. Doeuff, M. Henry, C. Sanchez, J. Livage, *J. Non-Cryst. Solids.*, 1987, 89, 206–216.

29. R. Parra, M. S. Góes, M. S. Castro, E. Longo, P. R. Bueno, J. A. Varela, *Chem. Mater*., 2008, 20, 143–150.

30. D.P. Birnie III, N.J. Bendzko, *Mater. Chem. Phys.*, 1999, 59, 26–35.

31. S. Doeuff, M. Henry, C. Sanchez, *Mat. Res. Bull.*, 1990, 25, 1519–1529.

32. D. Bersani, G. Antonioli, P. P. Lottici, T. Lopez, *J. Non-Cryst. Solids.*, 1998, 232–234, 175–181.

33. R N. Wentzel, *Ind. Eng. Chem.*, 1936, 28 (8), 988–994.

34. Y. Ohya, J. Mishina, T. Matsuda, T. Ban, Y. Takahashi, *J. Am. Ceram. Soc.*, 1999, 82(10), 2601–2606.

35. T. Shibata, H. Irie, M. Ohmori, A. Nakajima, T. Watanabe, K. Hashimoto, *Phys. Chem. Chem. Phys.*, 2004, 6, 1359–1362.

Chapter 2

Facile Water-based Preparation of Rh-doped $SrTiO_3$ Nanoparticles for Efficient Photocatalytic H_2 Evolution under Visible-light Irradiation

2.1 Introduction

Photocatalytic water splitting using semiconductors[1] has attracted much attention as one of the technologies that can produce hydrogen (H_2) cleanly and directly from water by utilizing abundant solar light; especially the effective utilization of visible light has become one of the most important challenges for achieving desired efficiency in practical application.[2-4] Visible-light-induced water splitting has so far been demonstrated based on two different systems, one-step[5-7] or two-steps systems.[8-22] The latter system, which is so-called Z-scheme, basically consists of two different semiconductor photocatalysts and a redox couple (e.g., IO_3^-/I^-, Fe^{3+}/Fe^{2+}, $[Co(bpy)_3]^{3+/2+}$, $[Co(phen)_3]^{3+/2+}$) that transfer electrons between the two photocatalysts,[8-18] while some systems can work even without such a redox couple.[20-23] Among the various visible-light-responsive photocatalysts developed so far, strontium titanate ($SrTiO_3$) doped with Rh species has been regarded as one of the most promising candidates of H_2-evolving photocatalyst workable under visible light for two-step system,[8-24] as well as for one-step one.[7] The apparent quantum efficiency for H_2 production on the $SrTiO_3$:Rh systems, however, is relatively low[24] and their improvement is still of significant challenge. Both high crystallinity and high specific surface area of semiconductor particles are generally required for achieving efficient photocatalysis. However, it is basically hard to satisfy these two prerequisites simultaneously by using conventional preparation processes such as solid-state (SS) reaction, because grain growth cannot be avoided during the calcination at high temperatures. Thus, the development of new synthesis process that can produce semiconductor particles having both small particle size and high crystallinity have been highly desired and extensively explored.

In Chapter 1, highly-active anatase-TiO_2 photocatalyst films, consisting homogeneous TiO_2 particle smaller than 50 nm even after calcination at high temperatures (900℃) were prepared by employing a newly-developed stable aqueous titania sol. The aqueous titania sol is effectively stabilized *via* simultaneous chelating of acetylacetone and acetic acid to the surface of titania colloids.[25] These findings have motivated to use the stable aqueous titania sol as a precursor in the synthesis of fine particles of various mixed titanates, such as $SrTiO_3$ or its derivatives, as highly active photocatalysts. In this chapter, highly efficient H_2 evolution under visible light irradiation (ca. 13.3% of quantum efficiency at 420 nm) from aqueous methanol solution is demonstrated on the $SrTiO_3$:Rh particles having homogeneous and small particle size (< 50 nm), which were prepared *via* facile aqueous procedure employing the stable aqueous titania sol as Ti-precursor with other metal salts.

2.2 Experimental

2.2.1 Materials

Titanium(IV) tetraisopropoxide (TIPT, 95.0%), acetylacetone (acac, 99.0%), acetic acid (AcOH, 99.7%), strontium acetate hemihydrate ($Sr(OAc)_2 \cdot 0.5H_2O$), rhodium(III) chloride trihydrate ($RhCl_3 \cdot 3H_2O$), lactic acid (85.5-94.5%) and Rh_2O_3 were purchased from Wako Pure Chemical Industries, Ltd., Osaka, Japan. TiO_2 (99.9%) was purchased from Soekawa chemical. $SrCO_3$ (99.9%) was purchased from Kanto chemical. Titanium(IV)-peroxo-citrate complex ($(NH_4)_4[Ti_2(C_6H_4O_7)_2(O_2)_2] \cdot 4H_2O$) was purchased from Furuuchi Chemical Corporation. Acrylic emulsion (VONCOAT(EC-905EF), particle size: 100~150 nm) was purchased from DIC Corporation. All reagents were used as received, and all the experiments were carried out under ambient condition without eliminating moisture from the atmosphere.

2.2.2 Preparation of $SrTiO_3$:Rh(2%) particles

The stable aqueous titania sol (AA-sol) was prepared as follows.[25] TIPT (20.0 mmol) was added to acac (20.0 mmol) slowly under continuous stirring at room temperature and stirred for 10 minutes. The resulting yellow solution of TIPT/acac precursor was added dropwise to an aqueous solution of AcOH (0.40 mol/L, 50.0 mL) under continuous stirring for 1 hour at room temperature. The co-existence of acac and AcOH effectively suppressed the hydrolysis and condensation reaction of TIPT even in water, retaining the diameter of titania colloidal particles lower than 10 nm (average diameter ca. 4 nm) as shown in Figure 1-2. The particles of $SrTiO_3$:Rh(2%) were prepared as follows. An aqueous solution of $Sr(OAc)_2$ (1.08 mol/L) containing lactic acid (2.16 mol/L), AA-sol and an aqueous solution of $RhCl_3$ (0.24 mol/L) were mixed basically at the ratio of Sr : Ti : Rh = 1.02 : 0.98 : 0.02, and stirred for 1 hour at room temperature, yielding orange transparent sols. In some cases, the samples were prepared with different ratio of Sr/(Ti+Rh) (1–1.03) or Rh/(Ti+Rh) (0.01–0.03). The sols were added by the acrylic emulsion and stirred for 15 minutes at room temperature, then dried at 80℃ for 3 hours, and finally calcined at 900–1050℃ for 10 hours, yielding $SrTiO_3$:Rh(Rh:2%) powdered samples. The $SrTiO_3$:Rh samples prepared *via* the above method (water-based hetero-chelate method, WH-method) will be denoted by WH-*T* (*T* = 900–1050) hereafter). The five kinds of $SrTiO_3$:Rh(2%) samples were also prepared from different water based titania precursors (titanium lactate[26] and titanium-peroxo-citrate[27,28]) with the acrylic emulsion, from AA-sol with the different polymers

(polymethyl methacrylate latex particles (PMMA) and polyethylene glycol (PEG)), or from AA-sol without emulsion. These precursor solutions were dried and calcined at 1000℃ for 10 hours, which will be denoted as L-1000, P-1000, WH''-1000(PMMA), WH''-1000(PEG) and WH'-1000 (without emulsion) respectively. In addition, $SrTiO_3$:Rh particles were synthesized by solid state reaction method (SS-method) from TiO_2, $SrCO_3$ and Rh_2O_3 as raw materials. These materials were mixed basically at the ratio of Sr:Ti:Rh = 1.00 : 0.98 : 0.02 and calcined at 900–1050℃ for 10 hours, while these ratio were changed as required. These particles will be denoted SS-*T* (*T* = 900–1050) hereafter.

2.2.3 Characterization of $SrTiO_3$:Rh(2%) particles

The obtained $SrTiO_3$:Rh2% particles were characterized by mean of an X-ray diffraction (XRD, PANalytical, X'Pert Pro, rotating anode diffractometer, 45 kV, 40 mA) with Cu *K*α radiation (K_α = 1.5406Å), a UV-vis-NIR spectrometer (UV-vis. DRS, Jasco, V-670), a scanning electron microscope (SEM, HITACHI, S-4100) and a transmission electron microscope (TEM, JEOL, JEM-2100F). Thermal analysis (TG-DTA) was conducted on dried powders on a TG-8120 (Rigaku). TG-DTA curves were recorded under air flow in the temperature range from 25 to 1000℃.

The photocatalytic activity was evaluated using a gas-closed circulation system with a 300W Xe-arc lamp (Perkin-Elmer, Cermax PE300BF) attached with a cut-off filter (Hoya; L42). The amounts of gas produced were analyzed and quantified by using an on-line gas chromatograph (GL Science; GC-3200, TCD, Ar carrier, MS-5A column). The apparent quantum yields were determined using a 150W Xe lamp (BUNKOUKEIKI, SM-25F) attached with various bandpass filters as monochromatic light sources; the number of incident photons at each wavelength were measured using a spectroradiometer (Ushio, USR-45VA). The apparent quantum yields were calculated by the following equation:

apparent quantum yield (%) in H_2 production

= [number of H_2 molecules evolved × 2] / [number of incident photons] × 100

2.3 Results and discussion

2.3.1 Characterizations of $SrTiO_3$:Rh(2%) particles prepared from stable titania sol (AA-sol)

All the XRD patterns of the WH- and SS-samples calcined at above 1000℃ exhibited pure perovskite phase of $SrTiO_3$; no appreciable peak attributed to impurity phases was observed for the samples (see Figure 2-1). On the other hand, small amount of impurity peaks were observed for WH- and SS-samples calcined at below 950℃, along with the peaks corresponding to $SrTiO_3$ phase. Some of them in WH-samples could be assigned to $SrRh_2O_4$ but the others could not be assigned to any possible mixed oxides from the precursors (Sr, Ti, Rh), thus shown as "unknown". The impurity phases observed in SS-900 samples were assigned to Sr_2TiO_4, RhO_2, and rutile-TiO_2.

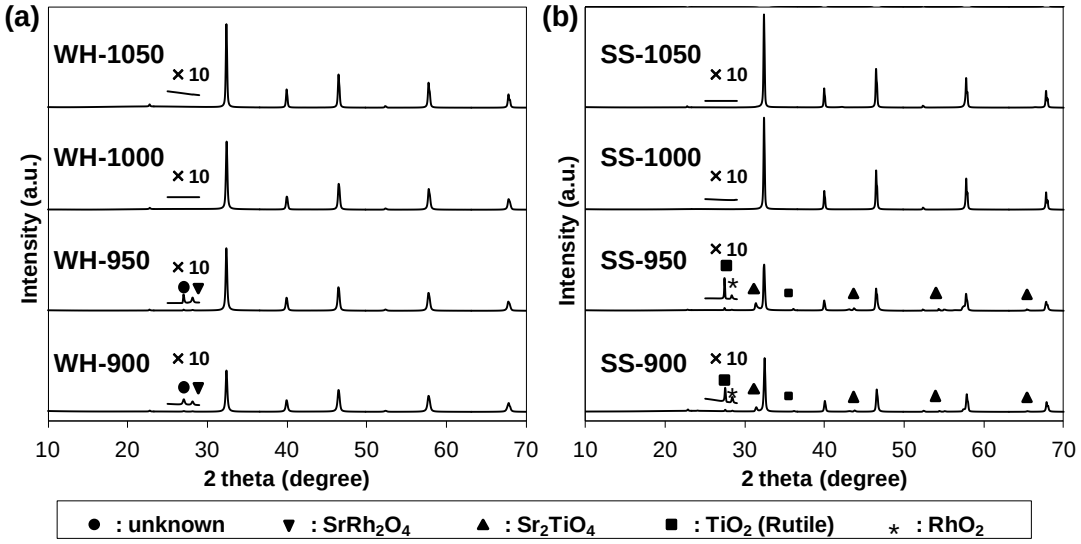

Figure 2-1. XRD patterns of $SrTiO_3$:Rh particles prepared at different calcination temperatures.

The diffuse reflectance spectra of all WH-powders are shown in Figure 2-2 (a), in which two absorption bands were observed in visible region along with the band gap transition of $SrTiO_3$ host (shorter than 400 nm). The absorption at around 420 nm and 580 nm in $SrTiO_3$:Rh materials have been assigned to the transitions from the donor levels formed by Rh^{3+} to the conduction band (ca. 2.3 eV) and that from the valence band to the acceptor levels formed by Rh^{4+} (ca. 1.7 eV), respectively, based on the results of both the detailed characterization and first principle calculation on $SrTiO_3$:Rh samples prepared by SS or CVD method.[29] The absorption at around 580 nm for the present WH-powders were weaker than those observed for SS-powders (see Figure 2-2 (b)) in spite of the same amount of Rh species doped (2 mol% to Ti site). The lower absorption at around 580 nm might indicate that the Rh

cations were doped into the WH-particles preferentially in the form of Rh^{3+} instead of Rh^{4+}, while it is difficult to analyze the amount of each species precisely due to the overlap of the absorptions corresponding to Rh^{3+} and Rh^{4+}. Another possibility will be that a part of Rh cations was doped into other sites, not to Ti^{4+} site, such as interstitial site and/or Sr^{2+} site.

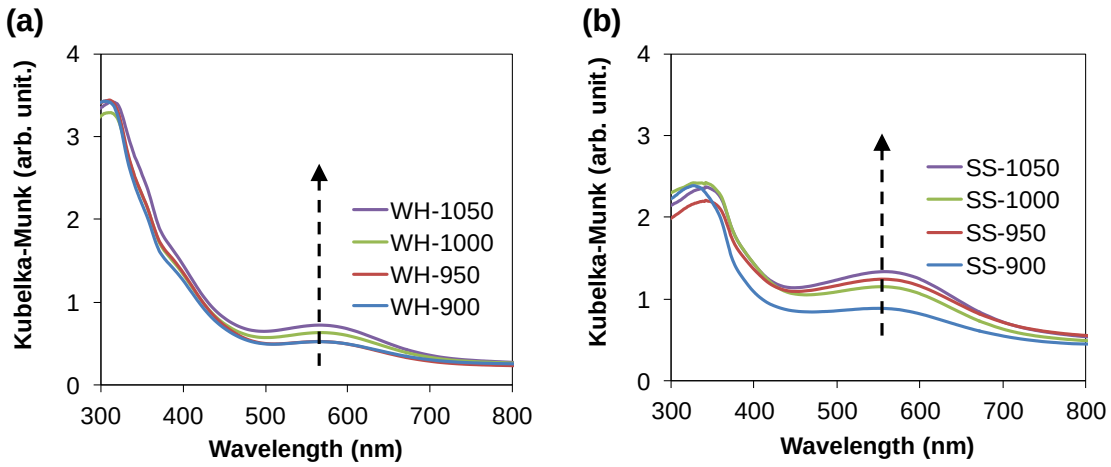

Figure 2-2. UV-vis spectra of (a) WH-particles and (b) SS-particles ($SrTiO_3$:Rh(2%)) prepared at different calcination temperatures.

Figure 2-3 show SEM (or TEM) images of the $SrTiO_3$:Rh(2%) samples prepared *via* WH- or SS-method at different calcination temperatures. The $SrTiO_3$:Rh samples prepared *via* WH-method up to 1000℃ (see Figure 2-3 (a)–(c)) consisted of relatively uniform primary particles smaller than 50 nm, while the calcinations at 1050℃ (Figure 2-3 (d)) resulted in appreciable increase in the particle size up to ca. 80 nm. A considerable number of the particles in the WH-1000 sample was found to exhibit cubic shapes with average particle size of ca. 50 nm (see the TEM image shown in Figure 2-3 (e) for example), undoubtedly due to the cubic perovskite structure of $SrTiO_3$. In addition, the crystalline sizes of WH-1000 were estimated to be 46.8 nm by the Scherrer formula, suggesting that the WH-1000 sample was dominantly consisted of single crystalline particles. So far as known, there is no report on the preparation of $SrTiO_3$:Rh particles smaller than 50 nm *via* conventional SS- or other methods, which require high temperatures (at least 1000℃) to produce pure perovskite structure. Indeed the primary particle sizes of all SS-samples prepared at higher than 900℃ were larger than 300 nm (see Figure 2-3 (f)–(i)), basically agreeing with the previous reports on the synthesis of $SrTiO_3$-based particles *via* solid-state reaction.[24]

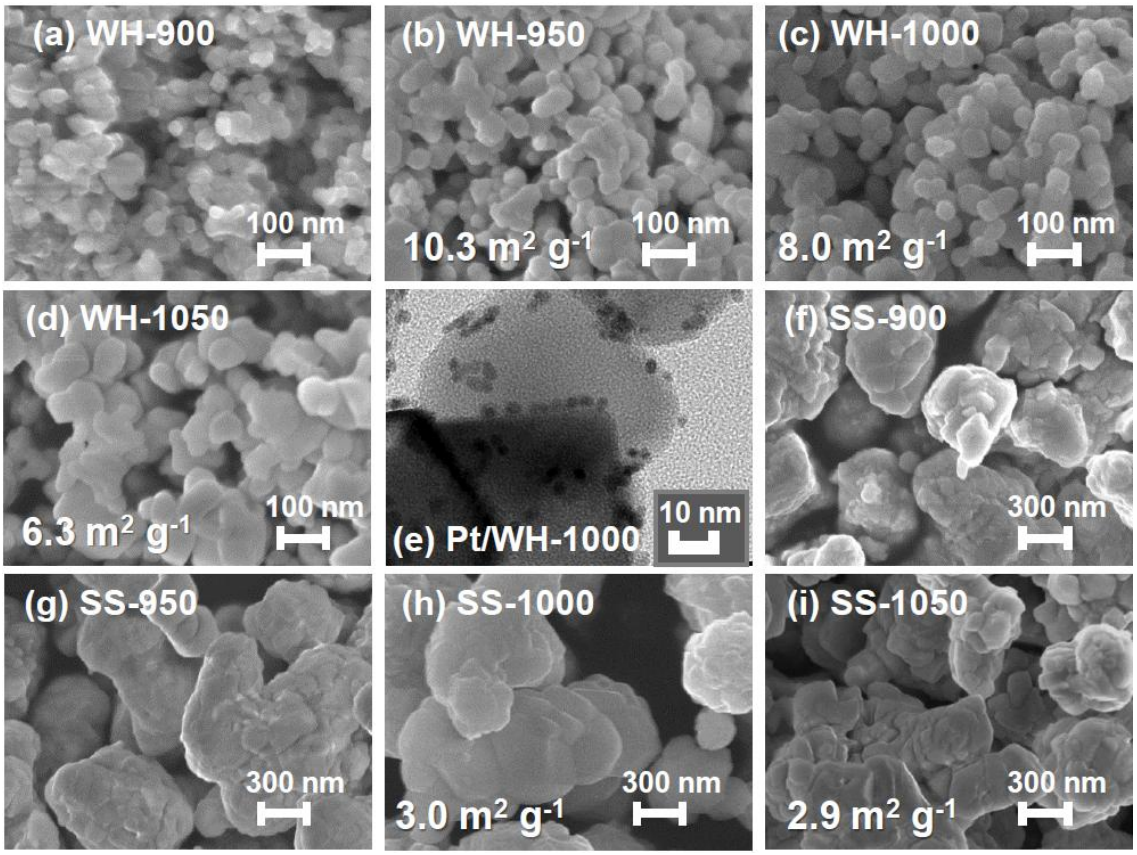

Figure 2-3. SEM images of the $SrTiO_3$:Rh(2%) samples prepared *via* WH and SS method and followed by calcination at different temperatures (a–d, f–i) and TEM images of the Pt-loaded WH-1000 (e). Numerical values at the bottom left indicate specific surface areas of the samples.

2.3.2 Influence of titanium precursors and additives on the particle size of $SrTiO_3$:Rh

In the conventional sol-gel method using active titanium precursors such as titanium tetraisopropoxide (TIPT), the precise control in particle size is basically difficult due to the rapid condensation and polymerization reaction of active alkoxides with water.[30] On the other hand, the present WH-method successfully produced $SrTiO_3$:Rh particles having homogeneously small size (~ 50 nm) after calcination at appropriate temperatures (~ 1000℃). As described in the experimental section, the present AA-sol was prepared *via* quite facial process, just mixing TIPT, acac and AcOH in aqueous solution with appropriate procedure.[25] However, it was confirmed that the co-existence of acac and AcOH efficiently suppressed the hydrolysis and condensation reaction of TIPT even in water, retaining the diameter of titania colloidal particles lower than 10 nm (average diameter ca. 4 nm) as shown in Figure 1-2. It therefore appears that the use of the stable and small titania colloidal particles as

Ti-precursor is one of the key factors of the yielding of such small and homogeneous $SrTiO_3$:Rh particles. To clarify this, $SrTiO_3$:Rh samples were prepared using other water-based Ti-precusors.

There are several reports on the preparation of $ATiO_3$ (A=Ba, Sr) particles using water-soluble titanium-complex precursors such as titanium lactate and titanium-peroxo-citrate.[31-33] Figure 2-4 (a) and (b) shows SEM images of $SrTiO_3$:Rh(2%) samples prepared from titanium lactate (denoted as L-1000) and titanium-peroxo-citrate (P-1000), respectively, instead of AA-sol, in the presence of the acrylic emulsion, which were finally calcined at 1000℃. The primary particle sizes in both the samples were inhomogeneous and larger than 100 nm. These findings strongly suggested that the thermal polymerization reaction between the functional group (i.e., -COOH, -OH) of these water-soluble titania precursors could not completely be suppressed and consequently produced large crystal nuclei that incorporate Sr and Rh cations. The generation of such large crystal nuclei certainly results in the production of large $SrTiO_3$:Rh particles. In general, the crystalline partciles of mixed oxides such as perovskite are produced through the nucleation and particle growth process. As for the nucleation process, it was reported that the primary particle size of $SrTiO_3$ prepared through a hydrothermal method can be controlled by changing the structure of precursor titania colloids (i.e., $TiO_2 \cdot nH_2O$ gel, Ti cluster).[34-37] Dang et al. reported that the use of small TiO_2 clusters, which were generated from titanium lactate complex, produced $SrTiO_3$ nanoparticles.[36] It was suggested that Sr species such as Sr^{2+} and $SrOH^+$ can be easily incorporated into the Ti-O structure to generate many crystal nuclei.[36] It is therefore likely that the present small titania colloids in AA-sol produce a number of small nuclei that contain all the precursors (Ti, Sr and Rh) with nearly the desired stoichiometic ratio during their mixing in aqueous solution, because the core amorphous titania were effectively protected from condensation by the chelating of acac and AcOH to the outer Ti species. The formation of such a large numbers of small and stable nuclei certainly enable the production of $SrTiO_3$:Rh particles having homogeneously small size after drying and final calcination (see Figure 2-5).

However, the sole use of AA-sol was proven inadequate for the production of such homogeneously small particles. Figure 2-4 (c) shows SEM image of $SrTiO_3$:Rh(2%) particles prepared from the AA-sol without acrylic emulsion; in which particles larger than 100 nm were observed. It has been reported that the addition of inhibitors such as latex particles or linear polymers to the precursor solution effectively suppressed the growth of crystals and aggregation during calcinations at high temperature.[38-40] Indeed, the primary particle sizes of $SrTiO_3$:Rh(2%) samples from the AA-sol with

different polymer (polymethyl methacrylate latex particles and polyethylene glycol) instead of the acrylic emulsion were 60–80 nm and 50–100 nm, respectively (see Figure 2-4 (c) and (d)), smaller than that of $SrTiO_3$:Rh particles prepared without any polymers (100–150 nm, see Figure 2-4 (e)). These findings indicate that the use of present acrylic emulsion worked more effectively as inhibitor and consequently produced the $SrTiO_3$:Rh particles with much smaller size (~50 nm). TG-DTA analysis indicated that the acrylic emulsions were decomposed at temperatures below 500℃ (Figure 2-6), suggesting that the residue components produced from the emulsions after calcinations did not affect the particle size. Based on these results, it can be concluded that the combination of the stable aqueous titania sol and the acrylic emulsion is necessary and useful to prepare metal oxide particles such as $SrTiO_3$:Rh with uniform and small particle sizes.

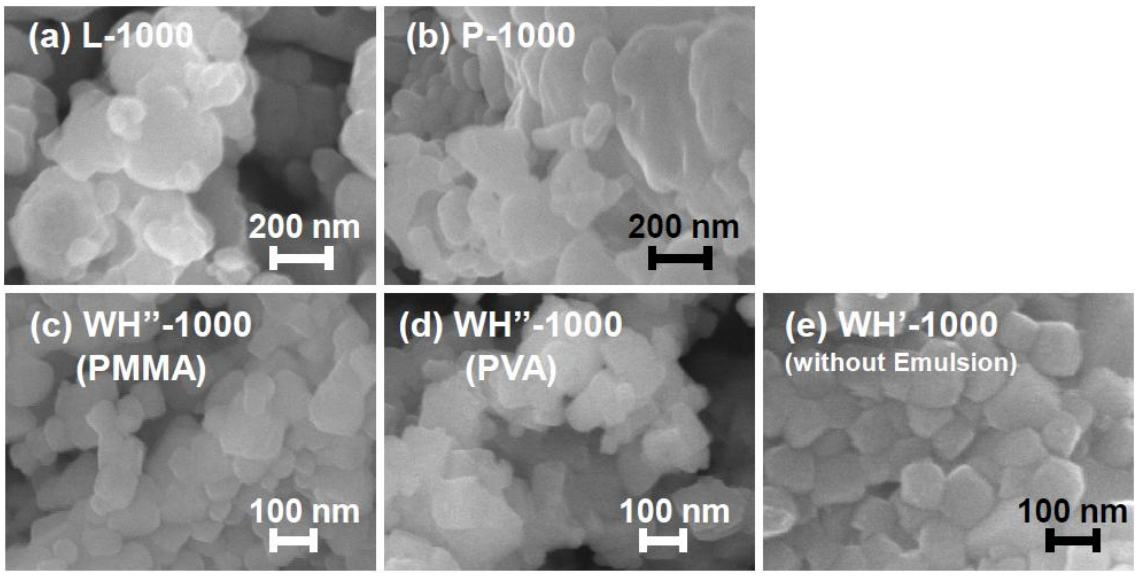

Figure 2-4. SEM images of the $SrTiO_3$:Rh(2%) samples prepared *via* different method and followed by calcination at 1000℃.

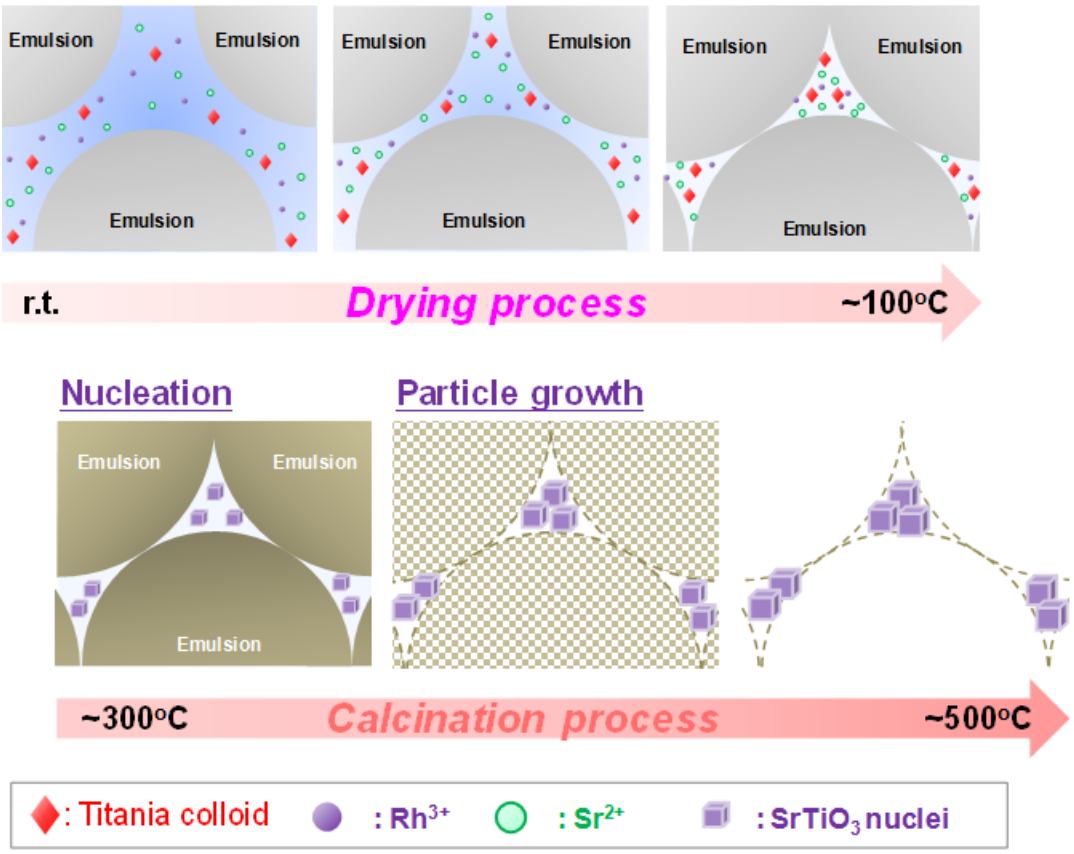

Figure 2-5. Proposed mechanism of the nucleation and particle growth on $SrTiO_3$:Rh particles synthesized by WH-method.

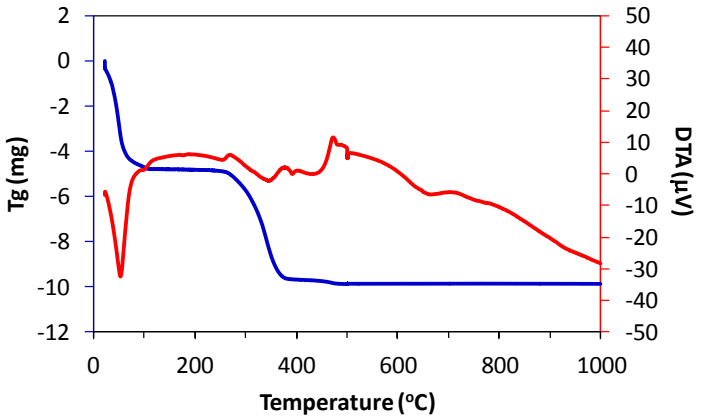

Figure 2-6. TG-DTA curves of acrylic emulsion.

2.3.3 Photocatalytic activity of $SrTiO_3$:Rh particles for H_2 production from aqueous methanol solution

The photocatalytic activity of these $SrTiO_3$:Rh(2%) samples was evaluated for the H_2 evolution from aqueous methanol solution under visible light irradiation ($\lambda > 410$ nm). As an effective cocatalyst for water reduction, small amount (0.5 wt%) of platinum particles were loaded on all the samples by mean of in-situ photodeposition method,[24] by which fine Pt particles with diameters of ca. 2 nm were loaded on the surface of $SrTiO_3$:Rh as shown in Figure 2-3 (d), for example. All the samples were confirmed to show the activity for H_2 evolution with almost steady rate (see Figure 2-7 for example). In the all cases, the color of sample was changed from grey to pale yellow after the H_2 evolution under visible light (see inset of Figure 2-8 for example), certainly due to the photocatalytic reduction of Rh^{4+} species to Rh^{3+} by the photoexcited electrons as previously suggested by Kudo et al.[24] Figure 2-8 shows the action spectrum (apparent quantum efficiency at each wavelength) for the H_2 evolution on WH-1000 sample, which were obtained by the irradiation of monochromatic light at each wavelength. As for the determination of apparent quantum efficiency, the sample was irradiated beforehand under continuous visible light to reduce the Rh^{4+} species in the sample and also the $PtCl_4^{2-}$ precursor to Pt nanoparticles by photoexcited electrons.

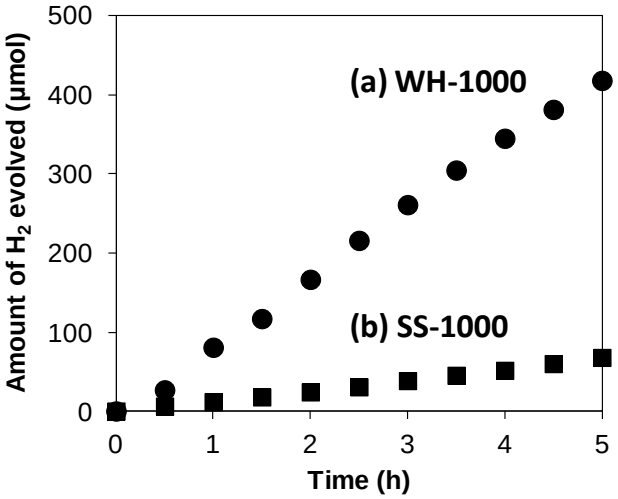

Figure 2-7. H_2 evolution from an aqueous methanol solution under visible light irradiation over a Pt (0.5 wt %)/$SrTiO_3$:Rh(2%) photocatalyst prepared *via* (a)WH- and (b)SS-method followed by calcination at 1000°C for 10 h. *Catalyst, 0.1 g; reactant solution, 200 mL of 10 vol % aqueous methanol solution; light source, 300 W Xe lamp with cut-off filters ($\lambda > 410$ nm).

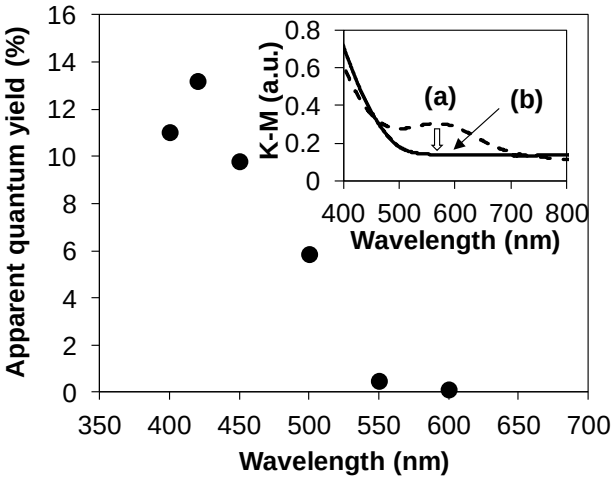

Figure 2-8. Action spectrum for H_2 evolution from an aqueous methanol solution of photocatalytic reaction over Pt loaded WH-1000 ($SrTiO_3$:Rh(2%), Sr/(Ti+Rh) = 1.02). The inset shows diffuse reflectance spectra of (a) before and (b) after photocatalytic reaction. Catalyst, 0.1 g; cocatalyst, Pt (0.5 wt %); reactant solution, 200 mL of 10 vol % aqueous methanol solution; light source, 150 W Xe lamp.

The inset of Figure 2-8 shows the absorption spectra of Pt-loaded WH-1000 sample before and after the reaction under continuous visible light for 10 h. The shape of action spectrum was similar to the absorption spectrum of the WH-1000 sample after reaction, in which the onset of the action spectrum was observed at around 550 nm, almost agreeing with the absorption edge. This result indicates that the H_2 evolution on the present $SrTiO_3$:Rh sample proceeded photocatalytically through the photoexcitation of electrons from the Rh^{3+} donor level to empty conduction band under the irradiation of light with wavelength shorter than 550 nm, as previously reported on the $SrTiO_3$:Rh prepared by SS-method.[24] The apparent quantum efficiencies at 420 nm on the $SrTiO_3$:Rh(2%) samples prepared *via* different method (WH or SS) and different calcination temperatures are summarized in Table 2-1, along with the rates of H_2 evolution at steady state in each reaction under visible light irradiation ($\lambda > 410$ nm). The amount of Pt cocatalyst was optimized for each system (WH-1000 and SS-1000 samples); 0.5 wt% was confirmed to result in nearly best rate of H_2 evolution on WH and SS systems (see Table 2-2). Thus all other samples were loaded with 0.5 wt% of Pt cocatalyst *via* photodeposition method for fair comparison. As for the Pt-loaded WH-samples, both the amount of H_2 generated under visible light irradiation and the quantum efficiency at 420 nm increased with the elevated calcinations temperature up to 1000℃, while they decreased at a higher temperature (1050℃).

Table 2-1. H_2 evolution from an aqueous methanol solution under visible light irradiation on WH and SS samples ($SrTiO_3$:Rh(2%)) prepared under different conditions

	Sr/(Ti+Rh)	Calcined temperature (℃)	H_2 evolution (μmol h^{-1}) *1	Apparent quantum yield at 420 nm (%)
WH	1.00	1000	63	9.8
	1.01	1000	79	-
	1.02	900	35	7.6
	1.02	950	44	-
	1.02	1000	87	13.3
	1.02	1050	59	9.4
	1.03	1000	67	10.1
SS	1.00	1000	15	2.4
	1.02	1000	14	2.4
	1.03	1000	12	2.2
	1.00	1050	10	1.8
	1.03	1050	14	1.9
L	1.00	1000	41	-
P	1.00	1000	47	-
WH	1.00	1000	124*2	-
SS	1.00	1000	34*2	-

*1 Catalyst, 0.1 g; cocatalyst, Pt (0.5 wt %); reactant solution, 200 mL of 10 vol % aqueous methanol solution; light source, 300W Xe lamp with a L-42 cut-off filter ($\lambda > 410$ nm).

*2 light source, 300W Xe lamp without cut-off filters ($\lambda > 300$ nm).

The enhanced efficiency for H_2 evolution up to 1000℃ is dominantly due to the improved crystallinity of particles, in other words, the decreased amount of crystal defects that generally work as recombination sites between photogenerated electrons and holes. Although the surface area was slightly decreased at the present temprature range (see Figure 2-3), the primary particle size was appreciably increased by the calcinations at 1050℃. The average crystalline sizes of WH-1000 and WH-1050,

which were calculated by the Scherrer formula, were estimated to be 46.8 and 54.1 nm, respectively. The appreciable decrease in efficiency for WH-1050 sample can probably be explained by the obvious increase in the particle size, which elongates the migration length of carriers generated in the bulk and consequently increases the possibility of recombination of them before reaching the surface. The SS-samples, which were prepared *via* conventional solid-state reaction for comparison, indeed showed lower H_2 evolution rates than WH-samples; slightly decreased with the increasing calcination temperature from 1000 to 1050℃ as shown in Table 2-1. It seems reasonable to consider that the much larger particle size of SS-samples is one of the dominant reasons for the significantly lower efficiencies for H_2 evolution compared to those of WH-samples, while the influence of other factors such as density of crystal defects cannot be excluded. Additionally, the $SrTiO_3$:Rh(2%) samples prepared *via* WH-method showed higher activity for H_2 evolution than those prepared *via* SS-method (see Table 2-1) under the irradiation of light containing both UV and visible light ($300 < \lambda < 800$ nm), in which direct excitation of $SrTiO_3$ host is also occurred. The higher activity of WH-sample under this condition (UV irradiation) strongly suggested the low density of crystal defect in the material prepared *via* the present WH-method. It is therefore can be concluded that the present WH-method is useful to prepare highly crystallized mixed metal oxide particles. The WH-1000 sample exhibited significantly high quantum efficiency (ca. 13.3 %) for H_2 evolution at 420 nm, compared to the previously reported values on the $SrTiO_3$:Rh samples prepared *via* SS-method.[24] Kudo et al. have previously reported the highest apparent quantum efficiency (ca. 5.3 % at 420 nm) for H_2 evolution on Pt-loaded $SrTiO_3$:Rh(1%) sample, which was prepared *via* SS-method at 1000℃, under similar reaction conditions, while the rate of H_2 evolution decreased to be almost half by increasing amount of doped Rh species from 1 to 2 mol% to Ti site in $SrTiO_3$.[24] Therefore the quantum efficiency (2.4 %) of our $SrTiO_3$:Rh(2%) sample (SS-1000) prepared *via* SS method seems reasonable and comparable to the values reported previously by other groups. However, it has been reported that the activity of $SrTiO_3$:Rh photocatalysts was significantly affected by the ratio of Sr to Ti, not only that of Rh to Ti, in the preparation; slightly higher ratio of Sr to Ti than the stoichiometric one (1:1) generally resulted in higher activity.[17] From this point of view, WH- and SS-samples with different ratio of Sr/(Ti+Rh) (1–1.03) were prepared and evaluated their activity under visible light ($\lambda > 410$ nm) or monochromatic light (420 nm) in some case; the results are summarized in Table 2-1 along with Table 2-3. Cleary, all the $SrTiO_3$:Rh samples prepared *via*

WH-method exhibited higher efficiency than those prepared *via* SS-method regardless to the ratio of Sr/(Ti+Rh), while the ratio actually affected the efficiency.

Table 2-2. H_2 evolution activity of $SrTiO_3$:Rh2% prepared *via* WH- and SS-method loaded with different amount of Pt cocatalyst.

	Amount of loaded Pt (wt%)	H_2 evolution ($\mu mol\ h^{-1}$)
WH-1000 (Sr/Ti = 1.02)	0.1	32
	0.25	53
	0.5	87
	0.75	75
	1	66
	2	56
SS-1000 (Sr/Ti = 1.00)	0.1	1
	0.25	5
	0.5	11
	0.75	12

*Catalyst, 0.1 g; reactant solution, 200 mL of 10 vol % aqueous methanol solution; light source, 300 W Xe lamp with cut-off filters ($\lambda > 410$ nm).

Table 2-3. H_2 evolution from an aqueous methanol solution under visible light irradiation of $SrTiO_3$:Rh(2%) photocatalyst prepared upon different doping amount.

	Amount of doped Rh ion (%)	H_2 evolution ($\mu mol\ h^{-1}$)
WH-1000 (Sr/Ti = 1.02)	1	50
	2	87
	3	77
SS-1000 (Sr/Ti = 1.03)	1	15
	2	12

*Catalyst, 0.1 g; reactant solution, 200 mL of 10 vol % aqueous methanol solution; light source, 300 W Xe lamp with cut-off filters ($\lambda > 410$ nm).

2.4 Conclusions

In conclusion, fine particles of Rh-doped $SrTiO_3$ ($SrTiO_3$:Rh) were successfully synthesized *via* newly developed water-based process, in which stable aqueous titania sol was used as Ti source together with other water soluble metal salts, followed by calcination in air. This method enabled the facile synthesis of $SrTiO_3$:Rh particles smaller than 50 nm even after calcination at 1000℃ and afforded significantly high efficiency for H_2 evolution under visible light, probably due to the small particle size and high crystallinity. The present water-based method was confirmed to have versatility for preparing various mixed titanate semiconductors having both high crystallinity and small particle size, providing environmentally-benign process that can be used for synthesis of highly active photocatalyst materials in large scale without using toxic organic solvent.

Reference

1. A. Fujishima and K. Honda, *Nature*, 1972, **238**, 37–38.
2. K. Maeda and K. Domen, *J. Phys. Chem. Lett.*, 2010, **1**, 2655–2661.
3. A. Kudo and Y. Miseki, *Chem. Soc. Rev.*, 2009, **38**, 253–278.
4. F. E. Osterloh, *Chem. Mater.* 2008, **20**, 35–54.
5. K. Maeda, K. Teramura, D. L. Lu, T. Takata, N. Saito, Y. Inoue and K. Domen, *Nature*, 2006, **440**, 295.
6. Y. Lee, H. Terashima, Y. Shimodaira, K. Teramura, M. Hara, H. Kobayashi, K.Domen, M. Yashima, *J. Phys. Chem. C*, 2007, **111**, 1042.
7. R. Asai, H. Nemoto, Q. Jia, K. Saito, A. Iwase and A. Kudo, *Chem. Commun.*, 2014, **50**, 2543–2546
8. A. Kudo, *Mater. Res. Bull.*, 2011, 36, 32–38.
9. R. Abe, *Bull. Chem. Soc. Jpn.*, 2011, 84, 1000–1030.
10. K. Maeda, *ACS Catal.*, 2013, 3, 1486–1503.
11. K. Sayama, K. Mukasa, R. Abe, Y. Abe and H. Arakawa, *Chem. Commun.*, 2001, 2416–2417.
12. K. Sayama, K. Mukasa, R. Abe, Y. Abe and H. Arakawa, *J. Photochem. Photobiol., A*, 2002, 148, 71–77.
13. R. Abe, K. Sayama, K. Domen, H. Arakawa, *Chem. Phys. Lett.*, 2001, **344**, 339–344.
14. H. Kato, M. Hori, R. Konta, Y. Shimodaira and A. Kudo, *Chem. Lett.*, 2004, **33**, 1348–1349.
15. H. Kato, Y. Sasaki, A. Iwase and A. Kudo, *Bull. Chem. Soc. Jpn.*, 2007, **80**, 2457–2464.
16. Y. Sasaki, A. Iwase, H. Kato and A. Kudo, *J. Catal.*, 2008, **259**, 133–137.
17. H. Kato, Y. Sasaki, N. Shirakura and A. Kudo, *J. Mater. Chem. A*, 2013, **1**, 12327–12333.
18. Y. Sasaki, H. Kato and A. Kudo, *J. Am. Chem. Soc.*, 2013, **135**, 5441.
19. A. Iwase, Y. H. Ng, Y. Ishiguro, A. Kudo and R. Amal, *J. Am. Chem. Soc.*, 2011, 133, 11054–11057.
20. Y. Sasaki, H. Nemoto, K. Saito and A. Kudo, *J. Phys. Chem. C*, 2009, **113**, 17536–17542.
21. S. S. K. Ma, K. Maeda, T. Hisatomi, M. Tabata, A. Kudo and K. Domen, *Chem.–Eur. J.*, 2013, **19**, 7480–7486.
22. Q. Jia, A. Iwase, A. Kudo, *Chem. Sci.*, 2014, **5**, 1513–1519.
23. Q. Wang, T. Hisatomi, S. S. K. Ma, Y. Li, K. Domen, *Chem. Mater.*, 2014, **26**, 4144–4150.

24. R. Konta, T. Ishii, H. Kato and A. Kudo, *J. Phys. Chem. B*, 2004, **108**, 8992–8995.
25. S. Okunaka, H. Tokudome, Y. Hitomi and R. Abe, *J. Mater. Chem. A*, 2015, **3**, 1688–1695.
26. T. Ohya, M. Ito, K. Yamada, T. Ban, Y. Ohya, Y. Takahashi, *J. Sol-Gel Sci. and Tech.* 2004, **30**, 71–81.
27. M. Kakihana, M. Kobayashi, K. Tomita, V. Petrykin, *Bull. Chem. Soc. Jpn.*, 2010, **83**, 11, 1285–1308.
28. M. Kakihana, M. Tada, M. Shiro, V. Petrykin, M. Osada,Y. Nakamura, *Inorg. Chem.*, 2001, **40**, 891–894.
29. S. Kawasaki, K. Akagi, K. Nakatsuji, S. Yamamoto, I. Matsuda, Y. Harada, J. Yoshinobu, F. Komori, R. Takahashi, M. Lippmaa, C. Sakai, H. Niwa, M. Oshima, K. Iwashina and A. Kudo, *J. Phys. Chem. C*, 2012, **116**, 24445–24448.
30. C. D. Chandler, C. Roger, M. J. Hampden-Smith, *Chem. Rev.*, 1993, **93**, 1205–1241.
31. K. Fujinami, K. Katagiri, J. Kamiya, T. Hamanaka, K. Koumoto, *Nanoscale*, 2010, **2**, 2080–2083.
32. K. Yamamoto, S. Matsushima, K. Tomita, Y. Miura, M. Kakihana, J. Ceram. Soc. Jpn., 2011, **119**, 494–497.
33. M. Tada, K. Tomita, V. Petrykin, M. Kakihana, *Solid State Ionics*., 2002, **151**, 293.
34. S. Zhang, J. Liu, Y. Han, B. Chen, X. Li, *Mater. Sci. Eng. B.*, 2004, **110**, 11–17.
35. S. Zhang, Y. Han, B. Chen, X. Song, *Mater. Lett.*, 2001, 368–370.
36. F. Dang, K. Mimura, K. Kato, H. Imai, S. Wada, H. Haneda, M. Kuwabara, *CrystEngComm.*, 2011, **13**, 3878–3883.
37. K. H. Ahn, Y-H. Lee, M. Kim, H. Lee, Y-S. Youn, J. Kim, Y-W. Lee, *Ind. Eng. Chem. Res.*, 2013, **52**, 13370–13376.
38. E. R. Leite, M. A. L. Nobre, M. Cerqueira, E. Longo, *J. Am. Ceram. Soc*., 1997, **80**, 2649–2657.
39. M. Sadakane, K. Sasaki, H. Kunioku, B. Ohtani, W. Ueda, R. Abe, *Chem. Commun.*, 2008, 6552–6554.
40. M. Abdullah, K. Okuyama, I. W. Lenggoro, S. Taya, *J. Non-Cryst Sol.* 2005, **8-9**, 697–704.

Chapter 3

Structure-controlled Porous Films of Nanoparticulate Rh-doped $SrTiO_3$ Photocatalyst toward Efficient H_2 Evolution under Visible-light Irradiation

3.1 Introduction

Photocatalytic water splitting using semiconductors has attracted much attentions as technology that can produce hydrogen (H_2) directly from water by harvesting abundant solar light.[1] The design of photocatalytic systems that enable efficient utilization of wide range of solar light spectrum, especially in visible region has become one of the cutting-edge research areas for achieving practically sufficient efficiency in solar hydrogen production, as well as the development of semiconductor materials employed.[2-4] So far, two types of semiconductor-based systems have been extensively studied for photo-induced water splitting; one is heterogeneous system[5-8] with suspended semiconductor particles and the other is photoelectrochemical system[8-10] with semiconductor photoelectrodes. The former suspended system has, however, some disadvantages in large-scale applications.[11] Such heterogeneous system undoubtedly require the energy for keeping the semiconductor particles suspended in the solution, by mean of mechanical stirring or gas-bubbling, and also required separation of particles for recycling or replacing the used photocatalysts. Although these problems can be solved in the latter photoelectrochemical systems, in which semiconductor materials are generally fixed on substrates, other cost disadvantages come up to the surface, i.e., the costs for the conductive substrates (such as conductive glass or metals) and for the external circuit including power source.

Photocatalyst panels, wherein semiconductor particles are fixed on an inexpensive substrate such as glass, will be another candidate of cost-effective and efficient water splitting system, if they exhibit comparable (or higher) efficiency to those in conventional systems.[11,12] Although Domen et al. recent demonstrated simultaneous evolution of H_2 and O_2 under UV-vis irradiation using photocatalyst panels of GaN-ZnO solid solution semiconductor prepared *via* drop-casting or squeegee method,[11] there is only a few report on the water splitting using such kinds of photocatalyst panels.[11-13] Thus, detailed and systematic studies on photocatalyst panels are highly desired to evaluate their feasibility by examining the influences of various factors such as types of semiconductor and structure of films on the performance. It is expected that high performance photocatalyst panels should have both the controlled structures for efficient light absorption and the controlled pores allowing efficient reaction and transportation of substances. However, such well-designed panels are generally difficult to be fabricated by using the semiconductor particles prepared *via* conventional synthesis processes such as solid-state (SS) reaction, in which large and inhomogeneous particles are generally produced.[14] The use of semiconductor particles having well-controlled particle sizes, specifically in nano~submicron

regions, is highly desirable to fabricate such well-designed photocatalyst panels; the use of such fine particles will be also beneficial to ensure the mechanical strength of panels by forming good adhesion.[15]

A facile synthesis of fine particles of Rh doped $SrTiO_3$ ($SrTiO_3$:Rh) semiconductor, which is well known as one of the promising materials of visible light responsive photocatalyst for H_2 production[16-26], was developed in Chapter 2 *via* a newly-developed water-based hetero-chelate method using a stable aqueous titania sol[27] as a precursor with other metal salts .[28] The prepared $SrTiO_3$:Rh particles possessed homogeneous and small particle size (ca. 50 nm) and exhibited significantly high efficiency for H_2 evolution from aqueous methanol solution under visible light irradiation (ca. 13.3% of quantum efficiency at 420 nm).[28] These findings have motivated to apply the $SrTiO_3$:Rh fine particles as a model photocatalyst to the fabrication of photocatalyst panels that can efficiently generate H_2 under visible light. In this chapter, the nanoparticulate $SrTiO_3$:Rh were employed to prepare the porous $SrTiO_3$:Rh films having both the controlled thickness and pores from the nanoparticulate $SrTiO_3$:Rh by means of simple screen-printing and applied them for photocatalytic H_2 production under visible light.

3.2 Experimental

3.2.1 Materials

Titanium(IV) tetraisopropoxide (TIPT) (95.0%), acetylacetone (acac) (99.0%), acetic acid (AcOH) (99.7%), strontium acetate hemihydrate ($Sr(OAc)_2 \cdot 0.5H_2O$), rhodium(III) chloride trihydrate ($RhCl_3 \cdot 3H_2O$), lactic acid (85.5–94.5%), Rh_2O_3, α-terpineol, 2-(2-butoxyethoxy)ethanol and poly(vinyl butyral) were purchased from Wako Pure Chemical Industries, Ltd., Osaka, Japan. Acrylic emulsion (VONCOAT (EC-905EF), particle size: 100–150 nm) was purchased from DIC Corporation. TiO_2 (99.9%) was purchased from Soekawa chemical. $SrCO_3$ (99.9%) was purchased from Kanto chemical. All reagents were used as received, and all the experiments were carried out under ambient condition without eliminating the moisture from the atmosphere.

3.2.2 Preparation of $SrTiO_3$:Rh films

The particles of $SrTiO_3$:Rh(2%) were prepared *via* the water-based hetero-chelate method (WH-method), which was recently developed by our group,[28] using a stable titania sol[27] as a precursor. The aqueous titania sol (AA-sol) was prepared by mixing TIPT, an aqueous solution of acac, and an

aqueous solution of AcOH.[27] The AA-sol was mixed with an aqueous solution containing both $Sr(OAc)_2$ (1.08 mol/L) and lactic acid (2.16 mol/L) and an aqueous solution of $RhCl_3$ (0.24 mol/L) at the ratio of Sr:Ti:Rh = 1.02:0.98:0.02, and stirred for 1 hour at room temperature, yielding an orange transparent sol. The sol was added by an acrylic emulsion and stirred for 15 minutes at room temperature, then dried at 80℃ for 3 hours, and finally calcined at 1000℃ for 10 hours, yielding $SrTiO_3$:Rh(Rh: 2%) powdered samples (these samples will be denoted by WH-particles). For comparison, $SrTiO_3$:Rh(2%) particles were also prepared *via* the solid state reaction method (SS-method) using from TiO_2, $SrCO_3$ and Rh_2O_3 as raw materials, and following calcination at 1000℃ for 10 hours (these samples will be denoted by SS-particles). Although some reports have suggested that the addition of excess Sr in the preparation of $SrTiO_3$-based particles *via* the SS-method is effective to obtain more active photocatalyst samples, we confirmed that the $SrTiO_3$:Rh particles prepared *via* the SS-method with excess amount of Sr (Sr/(Ti+Rh) =1.03, for example) showed almost same rate of H_2 evolution as that on the sample prepared with the stoichiometric ratio.[28] Thus in the present study, the $SrTiO_3$:Rh particles prepared *via* the SS-method with stoichiometric ratio (Sr:(Ti+Rh) = 1) was employed as the almost best SS-sample for fabricating $SrTiO_3$:Rh films for comparison. As an effective cocatalyst for water reduction, small amount (0.5 wt%) of platinum particles were loaded on all the samples by mean of in-situ photodeposition method.[16,17,28]

The $SrTiO_3$:Rh(2%) films were prepared *via* a conventional screen printing method as follows. The WH- or SS-particles were first dispersed in methanol solution and then dried at 80℃ for 5 min. After dispersion process, the particles were mixed with organic compounds (α-terpineol: 2-(2-butoxyethoxy)ethanol: poly(vinyl butyral) = 60:15:25) as vehicles, yielding the paste of WH- or SS-particles (ca. 20 wt%) having an appropriate viscosity for screen-printing. Films were then prepared by screen-printing using the prepared pastes, followed by calcination in air at 500℃ for 30 min. To control the thickness, the screen-printing procedure was repeated (1–10 times) before calcination; the obtained films will be denoted as WH- or SS-x where x (x = 1–10) indicates the times of print repitation. To obtain the thicker film having same thickness as to WH-10 and SS-10 without repeating the printing process, another setup of screen-printing with a thicker screen was used. The obtained films will be named WH-10’ and SS-10’.

3.2.3 Preparation of $SrTiO_3$ films

An aqueous solution containing both of $Sr(OAc)_2$ (1.08 mol/L) and lactic acid (2.16 mol/L) and the AA-sol were mixed at the ratio of Sr:Ti = 1.02:1.00, and stirred for 1 hour at room temperature, yielding an yellow transparent sol. The sol was added by an acrylic emulsion and stirred for 15 minutes at room temperature, then dried at 80℃ for 3 hours, and finally calcined at 1000℃ for 10 hours, yielding $SrTiO_3$ powders samples. As an effective cocatalyst for water reduction, small amount (0.5 wt%) of platinum particles were loaded on all the samples by mean of in-situ photodeposition method.

The $SrTiO_3$ films were prepared by following process. The $SrTiO_3$-particles were first dispersed in methanol solution and then mixed with organic compounds (α-terpineol: 2-(2-butoxyethoxy)ethanol: poly(vinyl butyral) = 60:15:25) as vehicles, yielding the paste of $SrTiO_3$-particles (ca. 20 wt%) having an appropriate viscosity for printing. The films were prepared by screen-printing using pastes of $SrTiO_3$-particles, followed by calcinations at 500℃ for 30 min.

3.2.4 Characterization of $SrTiO_3$:Rh films

The obtained $SrTiO_3$:Rh films were characterized by mean of a scanning electron microscope (SEM, HITACHI, S-4100), an X-ray diffraction (XRD, PANalytical, X'Pert Pro, rotating anode diffractometer, 45 kV, 40 mA, Cu Kα radiation), and , a UV-vis-NIR spectrometer (UV-vis. DRS, Jasco, V-670). The photocatalytic activity of $SrTiO_3$:Rh(2%) films was evaluated for the H_2 evolution from aqueous methanol solution under visible light irradiation, using a gas-closed circulation system equipped with a top-irradiation type reaction cell (Pyrex-made), in which the photocatalyst film was fixed horizontally in the solution. The light irradiation was carried out from the top of reactor by a 300W Xe-arc lamp (Perkin-Elmer, Cermax PE300BF) attached with a cut-off filter (Hoya; L42) to eliminate the UV light. The amounts of gas produced were analyzed and quantified by means of an on-line gas chromatograph (GL Science; GC-3200, TCD, Ar carrier, MS-5A column).

3.3 Results and discussion

3.3.1 Characterizations of $SrTiO_3$:Rh films prepared *via* screen-printing method

Figure 3-1, 3-2 and 3-3 show the SEM images of the films that were prepared *via* screen-printing with the pastes of $SrTiO_3$:Rh(2%) particles followed by calcination at 500℃ for 30 min. The thickness of the films was controlled by changing the repeated numbers of the screen-printing before calcination or by using another setup. The SEM images of WH-x films ("x" represent the repeated numbers) revealed that the film thickness increased by ca. 1 μm with increasing numbers of the screen-printing repetition (see Figure 3-1). For example, the film thickness of WH-1, 3, 5 and 10' were about 1, 3, 5 and 10 μm, respectively (Figure 3-1 (a), (c), (d), (f)). In addition, all the WH-films exhibit flat surfaces. It was also confirmed that the WH-10' film, which was prepared by using a thicker screen, possessed almost same thickness (ca. 10 μm) as to that of WH-10 (see Figure 3-1 (g)), indicating the availability of such thicker screen for fabricating thicker films without repetition of screen printing. The flat surface morphology and uniform increment in thickness are certainly due to the homogeneously small size of WH-particles (ca. 50 nm, see Figure 3-4 (a)), which were prepared *via* newly developed water-based procedure. On the other hand, the surfaces of SS-films, especially in the case of thinner ones (e.g., SS-3), were not smooth as seen in Figure 3-1 (i), while the thickness actually increased roughly in proportion with the increasing numbers of the screen-printing. The inhomogeneous and large size of SS-particles (ca. 200–500 nm, see Figure 3-4 (b)) is undoubtedly one of the causes for the rough surfaces of SS-films. The magnified views of the cross-section revealed that both the WH-10' and SS-10' films have densely-packed porous structures (Figure 3-2). Figure 3-3 shows the top-view SEM images of WH- and SS-films (x = 1, 3, 5, 10'). All the WH-films were exhibits smooth surfaces without exposing the glass substrates, even in the case of thinner one (see Figure 3-3 (a)–(d)). On the other hand, uncovered parts of substrate were clearly observed for thinner SS-1 and SS-3 samples (see Figure 3-3 (e) and (f)), while the repeated printing improved the homogeneity to some extent (see SS-5, 10' in Figure 3-3 (g) and (h)). These findings indicated the difficulty in preparing thin films with well-controlled structures from the SS-particles.

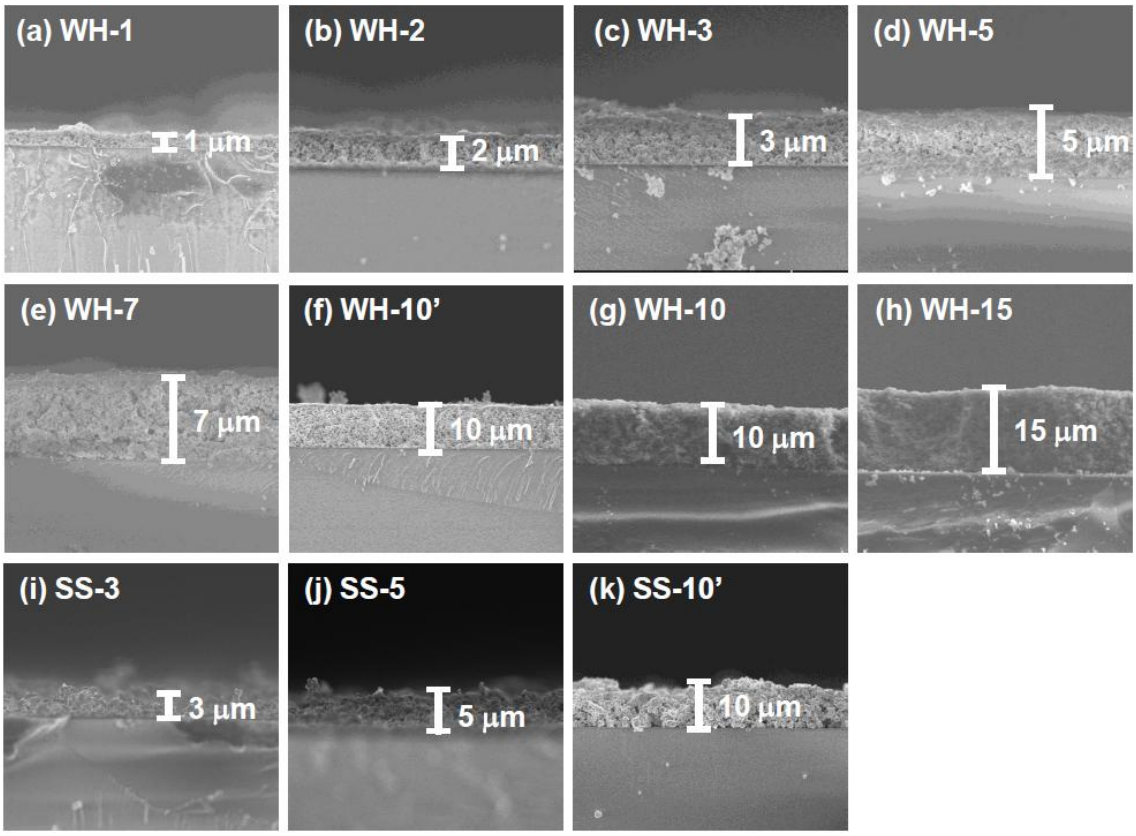

Figure 3-1. Cross-sectional SEM images of $SrTiO_3$:Rh films prepared by using WH- or SS-particles (WH- or SS-films) with different thicknesses.

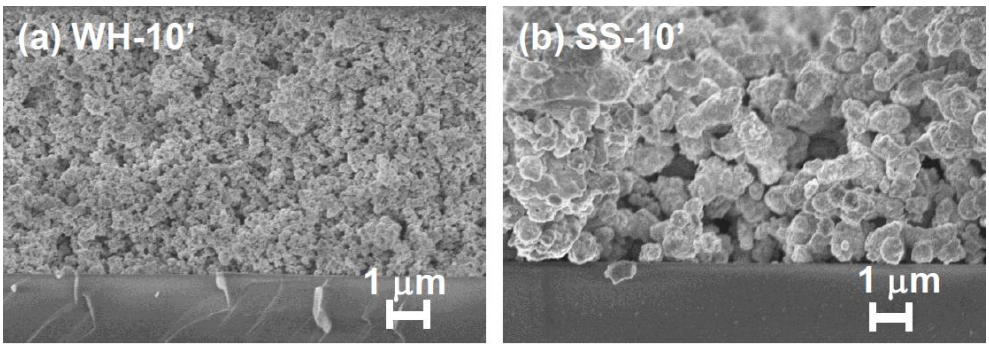

Figure 3-2. Magnified cross-sectional views of $SrTiO_3$:Rh films prepared by using WH- or SS-particles (WH- or SS-film) with 10 μm thickness.

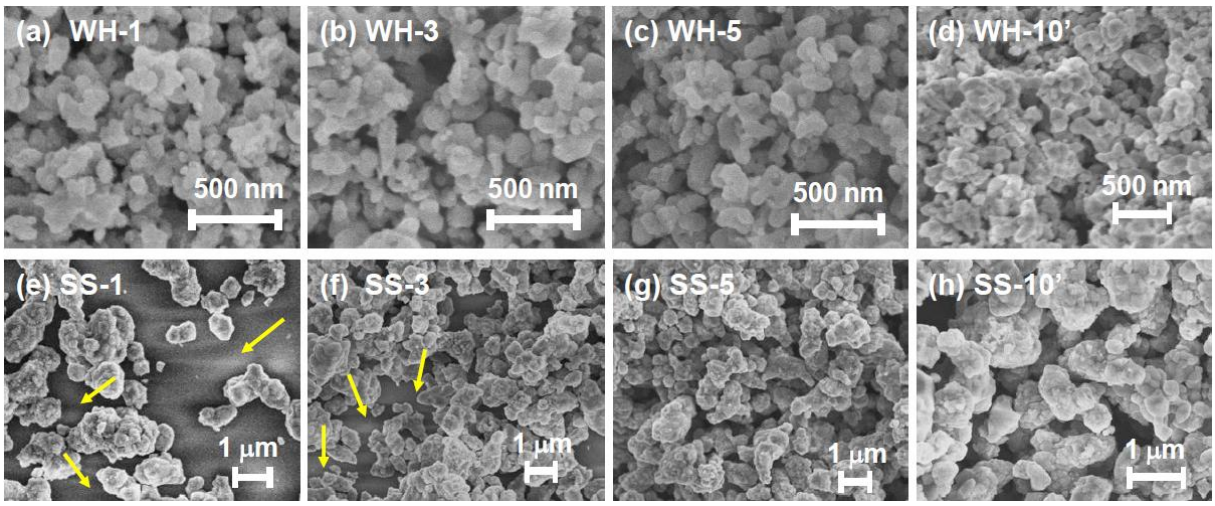

Figure 3-3. Surface SEM images of $SrTiO_3$:Rh films prepared by using WH- or SS-particles (WH- or SS-films) with different thicknesses. Yellow arrowed lines show the uncovered parts of substrate.

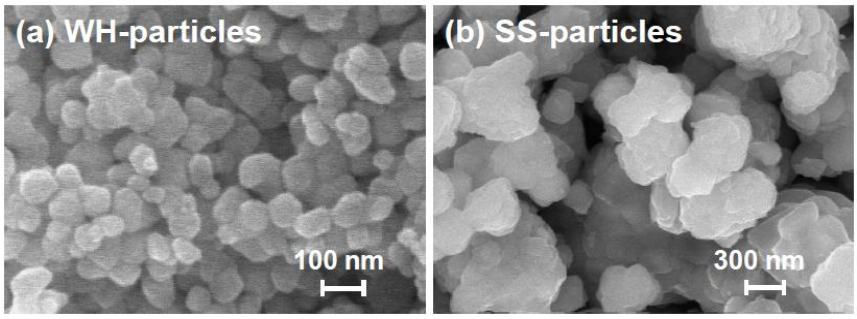

Figure 3-4. SEM images of $SrTiO_3$:Rh particles ((a) WH-particles, (b) SS-particles)).

As clearly seen in the SEM images, the WH- and SS-films were composed of the $SrTiO_3$:Rh particles whose primary particle sizes were almost same as those of WH- or SS-particles (see Figure 3-4). The XRD patterns of WH- and SS-films showed a single phase of $SrTiO_3$; no appreciable peaks attributed to impurity phase was observed (Figure 3-5). The diffuse reflectance spectra of WH- and SS-films (Figure 3-6) were similar to those reported for $SrTiO_3$:Rh particles.[28] The two absorption bands were observed at around 420 nm and 580 nm, which are attributed to the transitions from the donor levels formed by the Rh^{3+} species to the conduction band (2.3 eV), and from the valence band to the acceptor levels formed by the Rh^{4+} species (1.7 eV), respectively. These results indicated that the particles contained in WH- and SS-films retained the physicochemical properties of the original WH- and SS-particles, even after the preparation process accompanied by final calcinations at 500℃. As demonstrated above, the screen printing of appropriate pastes of WH-particles, which possess uniformly small size (ca. 50 nm), was proven as an effective way for fabricating porous films of

$SrTiO_3$:Rh with homogenous and controllable thickness ranging from 1 to 10 μm.

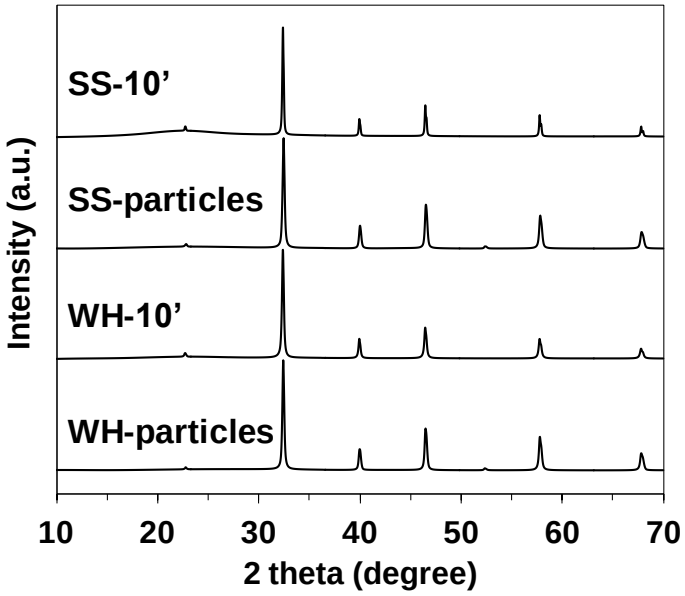

Figure 3-5. XRD patterns of $SrTiO_3$:Rh films (WH- and SS-films) and particles (WH- and SS-particles).

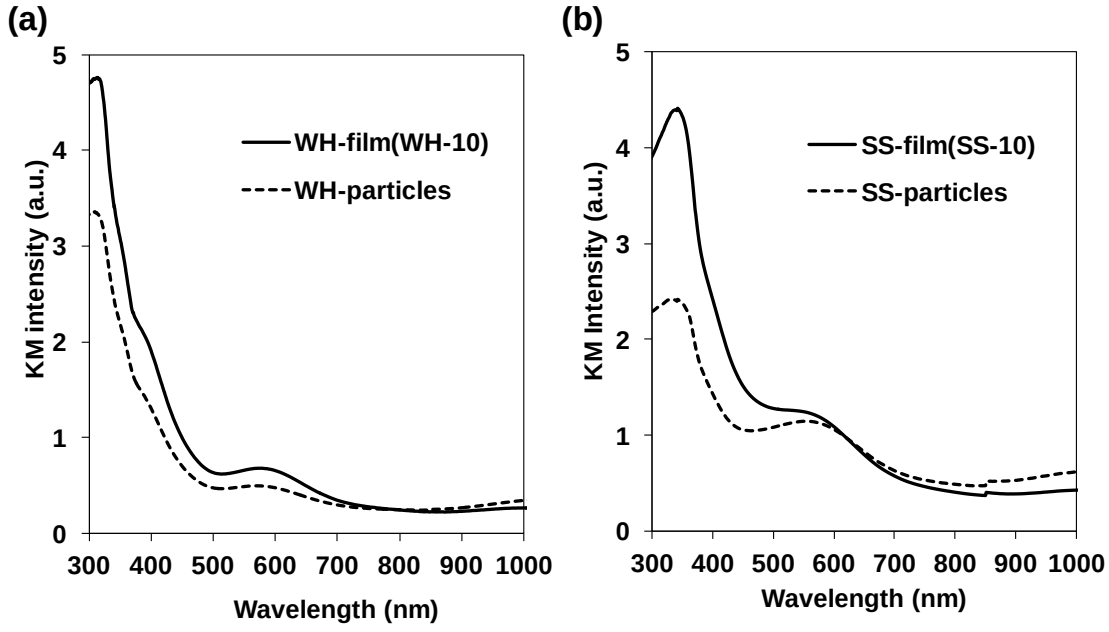

Figure 3-6. UV-vis spectra of $SrTiO_3$:Rh films with 10 μm thickness (WH-10' and SS-10') and $SrTiO_3$:Rh particles (WH- and SS-particles).

3.3.2 Photocatalytic H_2 evolution from aqueous methanol solution under visible light on $SrTiO_3$:Rh films

The photocatalytic activity of these $SrTiO_3$:Rh(2%) films was evaluated for the H_2 evolution from aqueous methanol solution under visible light irradiation ($\lambda > 410$ nm). As an effective co-catalyst for water reduction, 0.5 wt% of platinum particles were loaded on the WH-1000 or SS-1000 samples by means of in-situ photodeposition method[28] prior to the preparation of paste. All the WH- and SS-films showed the photocatalytic activity for H_2 evolution from aqueous methanol solution under visible light irradiation ($\lambda > 410$ nm) with almost steady rate. The time courses of H_2 evolution on WH-10' and SS-10' are shown in Figure 3-7, for example, in which the H_2 evolution rate on WH-film was about 4 times higher than that on SS-film.

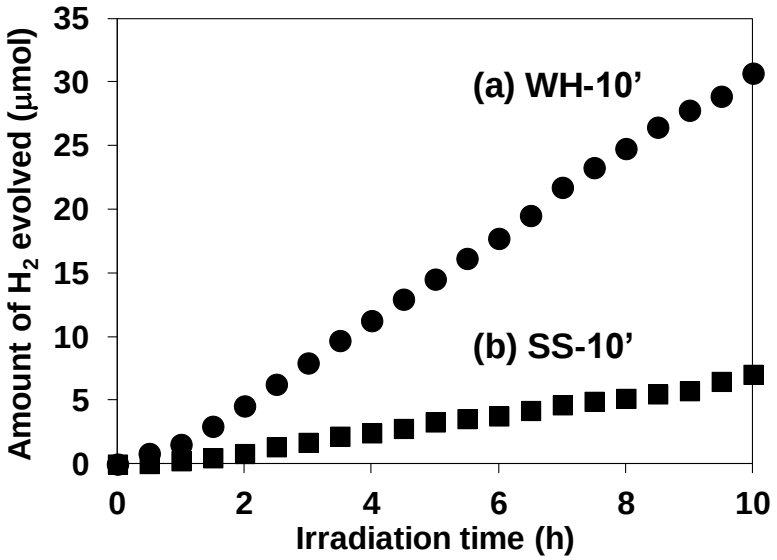

Figure 3-7. H_2 evolution from an aqueous methanol solution under visible light irradiation over a $SrTiO_3$:Rh film ((a) WH-10' or (b) SS-10'). Conditions: 3×3 cm film; reactant solution, 100 mL of 10 vol% aqueous methanol solution; light source, 300 W Xe lamp with cut-off filters ($\lambda > 410$ nm).

During the reaction, the color of WH-film changed from gray to pale yellow (see Figure 3-8), indicating the photocatalytic reduction of Rh^{4+} species to Rh^{3+} by photo-excited electrons, as previously reported for $SrTiO_3$:Rh particles.[16,28] No appreciable release of particles from the substrate was observed for WH-10' film after the reaction. On the other hand, the fraction of expose surface of substrate was appreciably increased in the SS-10' film after the reaction, indicating that a part of

particles was detached from the substrate during the H_2 evolution reaction (see Figure 3-9). Even the stirring the solution in dark resulted in particle release from the SS-10' film (not shown). These results indicated that the WH-films were mechanically more robust than the SS-films. The small particle sizes of WH-particles certainly allowed the sufficient contact among the particles in WH-film as well as the sufficient adhesion between particles and substrate.

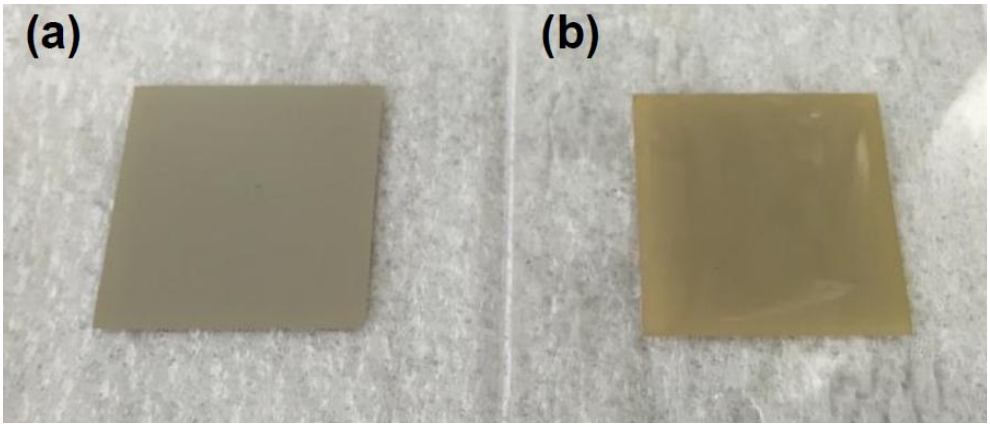

Figure 3-8. Picture of WH-10' (a) before and (b) after photocatalytic reaction.

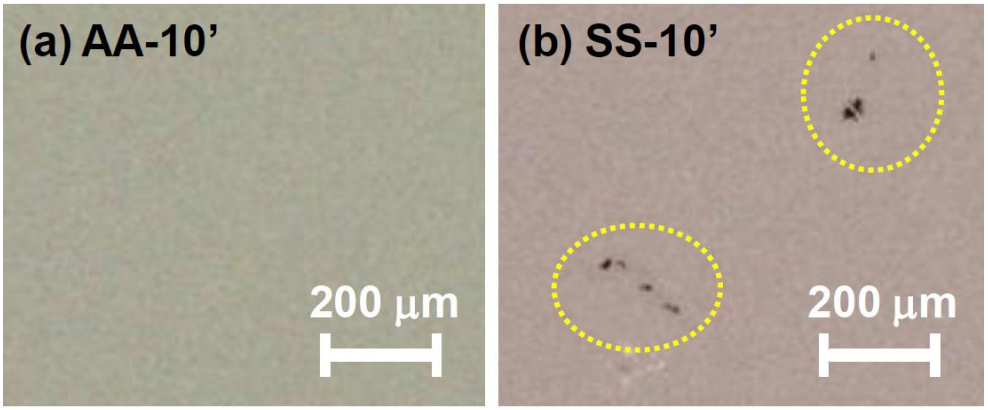

Figure 3-9. Optical microscope images of $SrTiO_3$:Rh films ((a) WH-10' or (b) SS-10') after photocatalytic reaction. Yellow dashed lines show the uncovered parts of substrate.

Figure 3-10 shows the dependence of film thickness on the H_2 evolution rates. The rates of H_2 evolution on the WH-films increased linearly with increasing thickness up to 5 μm and gradually increased to reach maximum value at 10 μm (3.2 μmol/h). The rates of H_2 evolution on SS-films increased with increasing film thickness, however, saturated at a thinner thickness of 5 μm. Up to 5 μm, each WH-film showed nearly 4 times higher H_2 evolution rates than the corresponding SS-films with

same thicknesses. As reported in Chapter 2, $SrTiO_3$:Rh particles prepared by the present WH-method showed higher photocatalytic activity for H_2 evolution than the $SrTiO_3$:Rh particles prepared by the SS-method. Indeed, the present WH-particles, which were prepared at 1000℃, showed ca. 4 times higher H_2 evolution rates than SS-particles prepared at the same temperature.[28] This finding strongly suggested that the higher photocatalytic activity of WH-particles dominantly contributed to the higher performance of WH-films for H_2 production. It also should be noted that the H_2 evolution rates of WH-films increased as the film thickness increased up to 10 μm, while those of SS-films saturated as the film thickness at 5 μm. In the case of SS-film, large SS-particles (> 300 nm) existing in the upper side certainly scattered back the incident photons partially, as well as absorbed, and consequently inhibited the light penetration into the bottom part, resulting in the saturated rate of H_2 evolution in the thicker films. In other word, a part of the particles in SS-films, especially those in bottom side, is unable to absorb the incident photons. On the other hand, in the case of WH-films, which consist of small WH-particles (ca. 50 nm), most of the particles effectively absorbed the light and functioned as photocatalyst due to the much less scattering of the incident light, consequently afforded the enhanced H_2 evolution with the increasing thickness up to 10 μm, while further increase in thickness resulted in the saturation because nearly all of the incident photons were absorbed within the films.

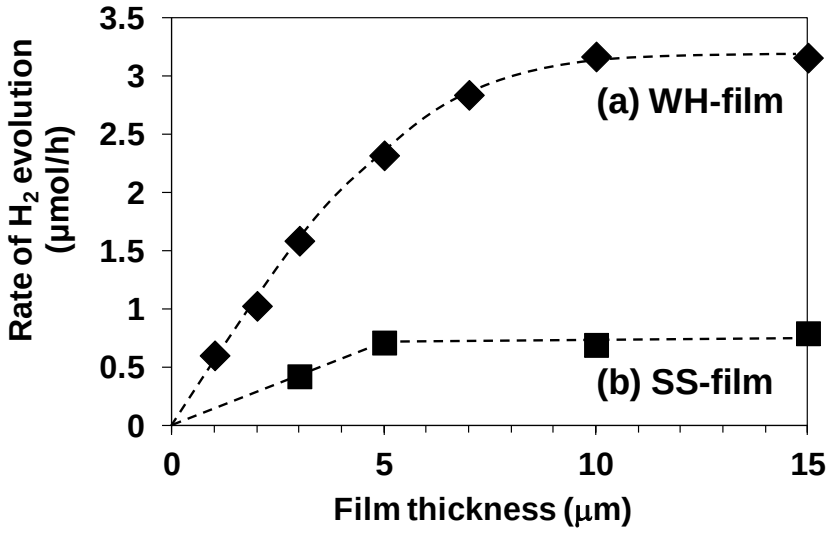

Figure 3-10. Rate of H_2 evolution from an aqueous methanol solution under visible light irradiation over a $SrTiO_3$:Rh film ((a) WH-film and (b) SS-film) having different thickness. Conditions: 3×3 cm film; reactant solution, 100 mL of 10 vol% aqueous methanol solution; light source, 300 W Xe lamp with cut-off filters (λ > 410 nm).

3.3.3 Influence of immobilization on the photocatalytic performance

To evaluate the influence of immobilization on the performance, the H_2 evolution rates on the films were compared with those on the suspended particles. For example, the immobilization of the particles on substrates may lower diffusion of the substances (e.g., water) and/or the products (e.g., H_2 gas) inside the pores of film and therefore may decrease the H_2 evolution rate. The rates of H_2 evolution using suspended WH- or SS-particles or fixed WH- or SS-*T* (*T* = 5, 10') films are summarized in Figure 3-11. The amounts of particles loaded on each film with thickness of 5 and 10 μm were measured to be ca. 8 mg and 16 mg, respectively, regardless to the kind of particles (WH or SS). Thus, the same amounts of particles were used in suspended system for comparison. Except for SS-10', the films showed higher activity than the corresponding suspended systems employing the same amounts of photocatalyst particles. These results indicated that the $SrTiO_3$:Rh particles immobilized on the films, especially in the case of WH-films, could absorb the light more efficiently than the suspended particles. The higher efficiency in the films were probably due to the more effective absorption of the photons by the neighboring particles in the densely packed film even if a part of incident photons was scattered on the surface of particles. On the other hand, in the suspended systems, a portion of photons is scattered on the surface of particles and then uselessly passed through the diluted suspension, resulting in the lower efficiency than in the film systems. As for SS-10', the light can be used only on the upper side because of significant light scattering due to the large particle size, resulting in the similar rate of H_2 evolution to that on suspension system. The higher H_2 evolution rates in other films also implied that the diffusion of substances was not significantly lowered in the pores in the WH- and SS-films. However, the rates of gas evolution on the present $SrTiO_3$:Rh films were still lower than those on general suspension systems for water splitting under visible light. The low evolution rates make it difficult to evaluate objectively the efficiency in the diffusion of substances and/or products in the present porous films. Thus, non-doped-$SrTiO_3$ porous films (10 μm) were prepared. Non-doped $SrTiO_3$ porous films are expected to evolve H_2 with much higher rates than the Rh-doped one, while the former required the irradiation of UV light. The non-doped-$SrTiO_3$ particles were prepared *via* same preparation procedure to that for Rh-doped-$SrTiO_3$ (WH-) particles, except for the absence of Rh-salt, producing the non-doped-$SrTiO_3$ having the same particles size (ca. 50 nm) to that of Rh-doped one. As shown in Figure 3-12, the H_2 evolution rate on the $SrTiO_3$ porous film showed much higher rate (78 μmol/h) than that on Rh-doped one (3.2 μmol/h, under visible light). The

H_2 evolution rate on the $SrTiO_3$ porous film was almost same with that on the corresponding suspended particles, strongly suggesting that the diffusion of substances and/or products was not significantly lowered in the pores in the present $SrTiO_3$ film systems, including Rh-doped one, prepared *via* screen-printing.

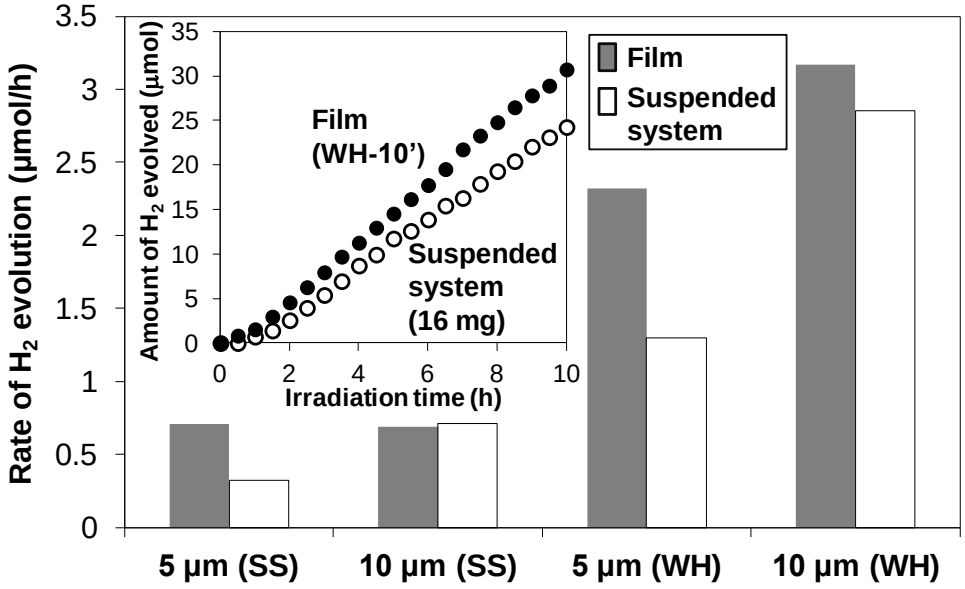

Figure 3-11. Rate of H_2 evolution from an aqueous methanol solution under visible light irradiation on a WH/SS-x film (x = 5 or 10') and from a $SrTiO_3$:Rh-suspended system containing $SrTiO_3$:Rh particles with the same amount as the film contains. Inset shows the H_2 evolution from an aqueous methanol solution under visible light irradiation over a $SrTiO_3$:Rh film (WH-10') and $SrTiO_3$:Rh particles. *Conditions: 3×3 cm film, 8 mg (5 μm) or 16 mg (10 μm) particles; reactant cell, top-irradiation-type separable cell, reactant solution, 100 mL of 10 vol% aqueous methanol solution; light source, 300 W Xe lamp with cut-off filters (λ > 410 nm).

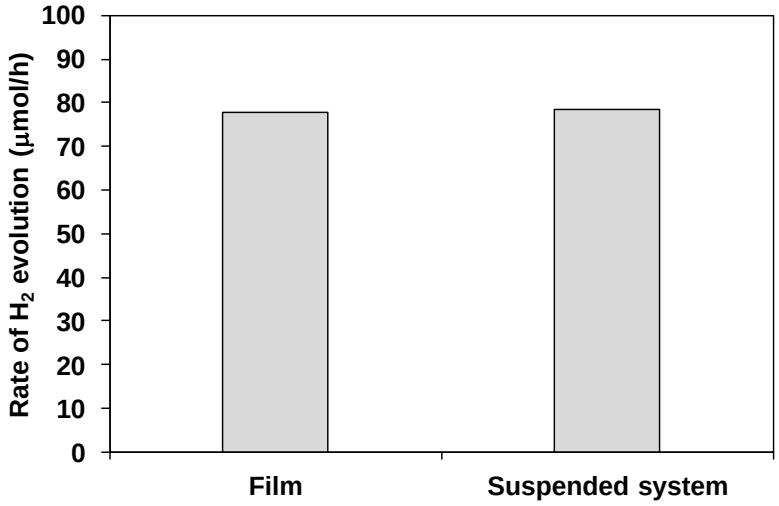

Figure 3-12. Rate of H_2 evolution from an aqueous methanol solution under visible light irradiation on a $SrTiO_3$ film and from a $SrTiO_3$-suspended system containing $SrTiO_3$ particles with the same amount as the film contains. *Conditions: 3×3 cm film with 10 μm thickness, 16 mg particles; reactant solution, 100 mL of 10 vol% aqueous methanol solution; light source, 300 W Xe lamp without cut-off filters.

3.3.4 Effect of adding the light scattering centers on the photocatalytic performance

As shown above, the combination of the screen-printing method with $SrTiO_3$:Rh particles prepared *via* the WH-method enable the fabrication of porous $SrTiO_3$:Rh film that possess capability of evolving H_2 efficiently from aqueous methanol solution under visible light irradiation, in which the use of small WH-particle probably minimize the light scattering and enable the most of $SrTiO_3$:Rh particles to absorb the incident light. However, too low scattering may result in the transmittance of a part of incident light without absorption in the WH-film. To solve the discrepancy between the light absorbance and scattering in the WH-film, small amounts of SS-particles, which have larger diameters and significantly scatter the light, were attempted to add into WH-particles that shows higher activity of H_2 evolution. For example, for the improvement of the photon-to-current efficiency in the dye-sensitized solar cell (DSSC), small amount of large TiO_2 particles (> 200 nm) that scatter the visible light are often added into the nano-sized TiO_2 particles which absorb large amount of dye molecules and conduct electrons efficiently.[29-33] Thus, a part of incident visible light is expected to be scattered by the large SS-particles and subsequently absorbed by small WH-particles, resulting in more efficient utilization of incident light. The films were prepared by screen-printing using the paste composed of various ratios of WH- and SS-particles. The fractions of SS-particles X were 0, 10, 20,

and 30 wt%. The resulting films are denoted as (WH+X-SS) hereafter. As shown in the SEM image of (WH+20-SS), for example, SS-particles were dispersed in the film homogeneously (see Figure 3-13). Figure 3-14 shows the relationship between the ratios of SS-particles added and the H_2-evolution rate on the films with different thickness. The rate of H_2 evolution in every thickness increased with the increasing amounts of SS-particles up to 20 wt%, but decreased with further addition. If the WH- and SS-particles act independently as photocatalysts, the H_2 evolution rates should be simple sum of each contribution of WH- and SS-particles, as shown in Figure 3-14 as dotted lines. However, the H_2 evolution rates on composite films were higher than the estimated values, also higher than those on pure WH-films. The composite films (10 μm) in which SS-particles (10 wt%) exist only bottom side were also prepared, for comparison. The H_2 evolution rate of this film was higher than that of the estimated value (see Figure 3-14, open triangle), but lower than the composite film in which the SS-particles dispersed homogeneously. These results strongly suggested that the composite films could use incident light more efficiently due to the light scattering by large SS-particles added into the films. The large SS-particles might also improved the diffusion of the substrates by forming larger pores in the film, as suggested in the previous report on photocatalyst panel of GaN-ZnO particles added by large SiO_2 particles (a few μm size).[11]

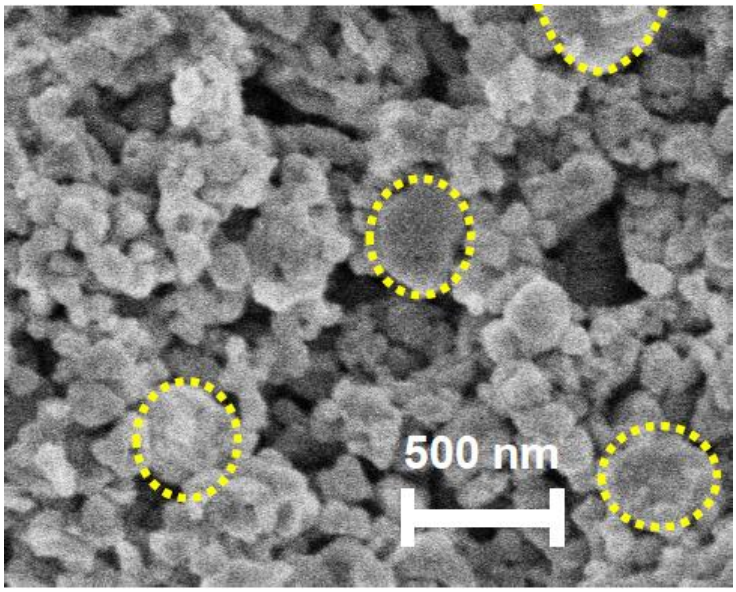

Figure 3-13. SEM images of $SrTiO_3$:Rh film (WH+20-SS) prepared with a mixture of WH- and SS-particles (SS/(WH+SS) = 20 (wt%)) Yellow dashed lines show the SS-particles.

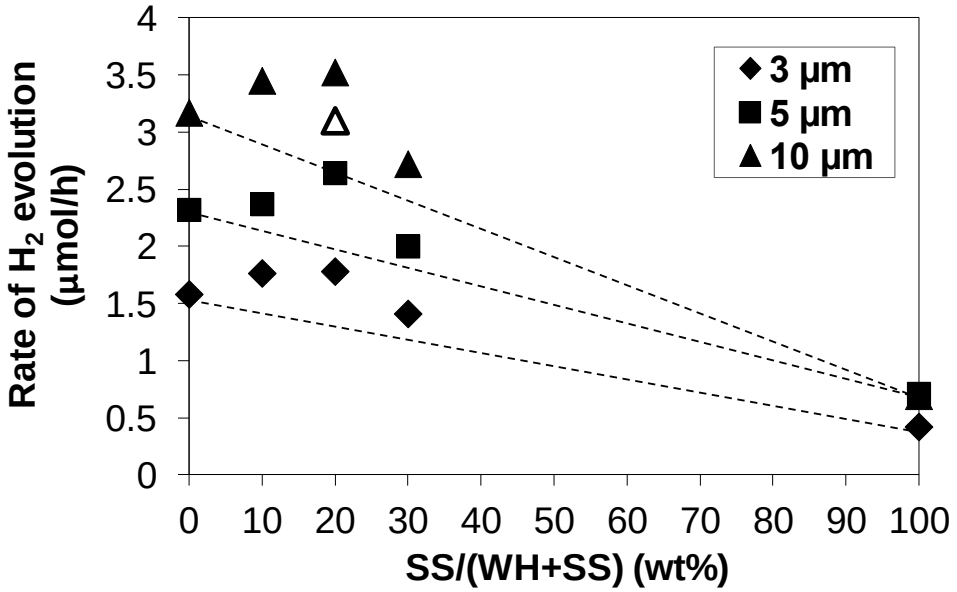

Figure 3-14. Plots of the H_2 evolution rate from an aqueous methanol solution on films prepared with a mixture of WH and SS-particles under visible light irradiation against the ratio of SS-particles over the sum of WH and SS-particles (weight %). Filled triangle, filled square, and filled diamond show films with 3, 5, and 10 μm-thickness. Open triangle shows a layered film consisted of WH-particles (80 wt%) over SS-film (20 wt%). The dashed lines indicate the expected rate based on the rates with pure WH- and SS-films. *Conditions: 3×3 cm film; reactant solution, 100 mL of 10 vol% aqueous methanol solution; light source, 300 W Xe lamp with cut-off filters ($\lambda > 410$ nm).

3.4 Conclusion

In this chapter, the photocatalyst panels that can efficiently generate H_2 under visible light were fabricated by employing highly active $SrTiO_3$:Rh fine particles prepared *via* a water-based hetero-chelate method. The combination of the fine particles with screen-printing method enabled precise controlling of the thickness (1 to 10 μm) of the porous films with enough mechanical strength after calcination (500°C) in air, whereas the use of large particle prepared *via* a conventional solid state reaction method resulted in inhomogeneous and uncontrollable thickness. The porous $SrTiO_3$:Rh films prepared with fine particles exhibited almost linear increase in H_2 evolution rate with increasing film thickness up to 5 μm and gradually increased to reach a maximum value at 10 μm; the H_2 evolution rates on the films (5 and 10 μm) were higher than those on the suspended system using the same amounts of photocatalyst particles. These results indicate that the present photocatalyst panels, as assembled 2-D structure, can effectively utilize the incident light comparable to the conventional suspension systems. Efficient H_2 production on these panels also suggested that the transfer of substance and products was not significantly inhibited within the porous films. Moreover, the improved of H_2 evolution rate by adding light scattering media (large $SrTiO_3$:Rh particles) will provide an effective strategy for achieving highly efficient photocatalysis in fixed panels. The concept of constructing highly active porous structures with fine photocatalyst particles *via* simple screen-printing method is useful for large-scale application of photocatalyst panels for practical splitting of water under solar light.

Reference

1. A. Fujishima and K. Honda, *Nature*, 1972, **238**, 37–38.
2. K. Maeda and K. Domen, *J. Phys. Chem. C*, 2007, **111**, 7851.
3. A. Kudo and Y. Miseki, *Chem. Soc. Rev.*, 2009, **38**, 253–278.
4. F. E. Osterloh, *Chem. Mater.* 2008, **20**, 35–54.
5. A. Kudo, *Mater. Res. Bull.*, 2011, **36**, 32–38.
6. R. Abe, *Bull. Chem. Soc. Jpn.*, 2011, **84**, 1000–1030.
7. K. Maeda, *ACS Catal.*, 2013, **3**, 1486–1503.
8. R. Abe, *J. Photochem. Photobiol. C. Photochem. C.*, 2010, **11**, 179–209.
9. T. Hisatomi, J. Kubota, K. Domen, *Chem. Soc. Rev.*,2014, **43**, 7520.
10. F. E. Osterloh, *Chem. Soc. Rev.*,2013, **42**, 2294.
11. A. Xiong, G. Ma, K. Maeda, T. Takata, T. Hisatomi, T. Setoyama, J. Kubota, K. Domen, *Catal Sci Technol.*, 2014, **4**, 325–328.
12. B.Pinaud, J. Benck, L.Seitz, A. Forman, Z. Chen, T. Deutsch, B. James, K. Baum, G. Baum, S. Ardo, H. Wang, E. Miller and T. Jaramillo, *Energy Environ. Sci.*, 2013, **6**, 1983.
13. Q. Wang, Y. Li, T. Hisatomi, M. Nakabayashi, N. Shibata, J. Kubota, K. Domen, *J. Catal.*, 2015, **328**, 308–315.
14. K. Takanabe, K. Domen, *Chem Cat Chem*, 2012, **4**, 1485.
15. C. Agrafiotis, A. Tsetsekou, *J. Eur. Ceram. Soc.*, 2000, **20**, 815–824.
16. R. Konta, T. Ishii, H. Kato and A. Kudo, *J. Phys. Chem. B*, 2004, **108**, 8992–8995.
17. H. Kato, M. Hori, R. Konta, Y. Shimodaira and A. Kudo, *Chem. Lett.*, 2004, **33**, 1348–1349.
18. H. Kato, Y. Sasaki, A. Iwase and A. Kudo, *Bull. Chem. Soc. Jpn.*, 2007, **80**, 2457–2464.
19. Y. Sasaki, A. Iwase, H. Kato and A. Kudo, *J. Catal.*, 2008, **259**, 133–137.
20. Y. Sasaki, H. Nemoto, K. Saito and A. Kudo, *J. Phys. Chem. C*, 2009, **113**, 17536–17542.
21. A. Iwase, Y. H. Ng, Y. Ishiguro, A. Kudo and R. Amal, *J. Am. Chem. Soc.*, 2011, **133**, 11054–11057.
22. H. Kato, Y. Sasaki, N. Shirakura and A. Kudo, *J. Mater. Chem. A*, 2013, **1**, 12327–12333.
23. Y. Sasaki, H. Kato and A. Kudo, *J. Am. Chem. Soc.*, 2013, **135**, 5441.
24. S. S. K. Ma, K. Maeda, T. Hisatomi, M. Tabata, A. Kudo and K. Domen, *Chem.–Eur. J.*, 2013, **19**, 7480–7486.

25. Q. Jia, A. Iwase, A. Kudo, *Chem. Sci.*, 2014, **5**, 1513–1519.
26. Q. Wang, T. Hisatomi, S. S. K. Ma, Y. Li, K. Domen, *Chem. Mater.*, 2014, **26**, 4144–4150.
27. S. Okunaka, H. Tokudome, Y. Hitomi and R. Abe, *J. Mater. Chem. A*, 2015, **3**, 1688–1695.
28. S. Okunaka, H. Tokudome and R. Abe, *J. Mater. Chem. A*, 2015, **3**, 14794–14800.
29. C. J. Barbè, F. Arendse, P. Comte, M. Jirousek, F. Lenzmann, V. Shkolver, M. Grätzel, *J. Am. Ceram. Soc.* 1997, **80** (12), 3157–3171.
30. T. G. Deepak, G. S. Anjusree, S. Thomas, T. A. Arun, S. V. Nair and A. S. Nair, *RSC Adv.*, 2014, **4**, 17615–17638.
31. A. Usami, *Chem. Phys. Lett.*, 1997, **277**, 105.
32. S. Hore, C. Vatter, R. Kern, H. Smit and A. Hinsch, *Sol. Energy mater. Sol. Cells*, 2006, **90**, 1176.
33. J.-K. Lee, B.-H. Jeong, S. J. Y.-G. Kim, Y.-W. Jang, S.-B. Lee and M.-R. Lim, *J. Ind. Eng. Chem.*, 2009, **15**, 724.

Chapter 4

Preparation of Fine Particles of Sheelite-Monoclinic Phase $BiVO_4$ via an Aqueous Chelating Method for Efficient Photocatalytic Oxygen Evolution under Visible-light Irradiation

4-1. Introduction

Photocatalytic splitting of water is a promising technology for the clean and direct production of H_2 from water, and thus is expected to contribute to the realization of a sustainable society based on clean energy cycles involving H_2 carriers. Great progress has been made on photocatalytic (and photoelectrochemical) water splitting[1-6] since the pioneering work on photoelectrochemical water splitting using TiO_2 anodes first reported in 1972.[7] Development of photocatalysis systems that efficiently split water by harvesting a wide range of visible light is crucial to demonstrate the feasibility of photocatalytic solar H_2 production. Photocatalytic water splitting under visible light has been demonstrated on two different systems, i.e., one-step[8-11] and two-steps systems.[12,13] The latter system (so-called Z-scheme) basically consists of two different photocatalysts and a redox couple (e.g., IO_3^-/I^-) that mediates the electron transfer between them.[14,15] Among the various visible-light-responsive photocatalysts developed so far, bismuth vanadate ($BiVO_4$) has attracted much attention as an efficient photocatalyst for O_2 evolution under visible-light irradiation in the presence of various reversible electron acceptors, such as Fe^{3+}/Fe^{2+}, $[Co(bpy)_3]^{3+/2+}$, and $[Co(phen)_3]^{3+/2+}$.[16-20] The main crystal forms of $BiVO_4$ are zircon-tetragonal (z-t), scheelite-monoclinic (s-m) and scheelite-tetragonal (s-t).[21] A number of reports have demonstrated that s-m phase $BiVO_4$ particles exhibit higher photocatalytic activity for O_2 evolution than that of other crystal phases.[22,23] The higher activity of s-m $BiVO_4$ is primarily because of narrower bandgap (2.4 eV), which is due to a greater contribution of Bi-6s orbitals mixed with O-2p orbitals in its valence band. However, it is widely recognized that the activity of photocatalysts is determined not only by the band structure but also by other physicochemical properties of the semiconductor particles.[24] Among these physicochemical properties, the particle size often influences the photocatalytic activity significantly, because it dictates the distance of charge transport from the bulk material to its surface, and the number of active sites on the surface. This influence differs depending on the reaction systems.[24] Various methods, such as solid-state reactions,[25-27] liquid-phase reactions,[28,29] hydrothermal processes,[30-33] and co-precipitation techniques,[34] have been employed to control the crystal phase and particle size of $BiVO_4$ photocatalysts in order to achieve highly efficient O_2 evolution. However, the synthesis of small s-m phase $BiVO_4$ particles is basically difficult because the s-m phase is formed at high temperatures. For example, it has been reported that the phase transition from z-t to s-m phase occurs above 500°C in conventional solid-state reactions. Such high temperatures usually cause crystal growth and aggregation. Although

the application of liquid-base methods, such as hydrothermal processes and co-precipitation methods, allows the formation of s-m phase $BiVO_4$ at low temperatures, there is still a limited number of reports on the preparation of fine s-m $BiVO_4$ particles smaller than 100 nm in diameter.[33,34] In addition, the low crystallinity of s-m $BiVO_4$ particles prepared *via* such methods generally necessitates post-calcination in order to improve their activity by reducing crystal defects where the recombination of photoexcited electrons and holes is often accelerated. However, such post-calcination inevitably leads to particle growth.

The synthesis of fine particles (ca. 50 nm) of Rh-doped $SrTiO_3$ ($SrTiO_3$:Rh) *via* an environmentally friendly water-based process, and their high activity for photocatalytic H_2 evolution under visible light, were demonstrated in Chapter 2.[35] One of the key features of this process is the use of an appropriate combination of chelating agents, which effectively stabilize the titania nanocolloid (ca. 4 nm) precursor, even in water.[36] The calcination of the precursor sols produce highly crystallized $SrTiO_3$:Rh with particles sizes of ca. 50 nm, even after calcination above 900°C. These results suggested that appropriate chelators not only stabilize precursor cations in water but also suppressed particle growth during calcination, affording highly crystallized and small particles of mixed metal oxides.

In this chapter, fine particles of s-m phase $BiVO_4$ were attempted to synthesize in aqueous solution through a similar chelating process. Various chelating ligands with different numbers of carboxyl groups are used to stabilize the Bi^{3+} and V^{5+} ions in aqueous solution. The influence of these ligands on the size and photocatalytic activity of the obtained s-m $BiVO_4$ particles is evaluated.

4.2 Experimental

4.2.1 Materials

Ammonium vanadate(V) (99%, NH_4VO_3), bismuth(III) nitrate pentahydrate (99.9%, $Bi(NO_3)_3 \cdot 5H_2O$), glycolic acid (gly), L(+)-tartalic acid (tart), citric acid (cit), ethylenediamine tetraacetic acid (edta), silver nitrate (99.5%, $AgNO_3$) and iron(III) chloride (99.9%, $FeCl_3 \cdot 6H_2O$) were purchased from Wako Pure Chemical Industries Ltd., Japan. Aqueous ammonia (28.0–30.0%) was purchased from Kanto Chemical Ltd., Japan. All reagents were used as received, and all the experiments were carried out under ambient conditions without eliminating the moisture from the atmosphere.

4.2.2 Preparation of fine $BiVO_4$ particles *via* an aqueous chelating method

$BiVO_4$ particles were prepared *via* a newly developed aqueous chelating method (hereafter denoted by AC-method). $Bi(NO_3)_3 \cdot 5H_2O$ (0.17 mol/L, 0.82 g) was added to an aqueous solution (10 mL) containing edta (0.34 mol/L, 0.73 g) and aqueous ammonia (ca. 1.0 mL) to adjust the pH of the solution to 8, producing a clear solution (hereafter denoted by Bi(edta)-sol.). For the chelation of V^{5+} species, four kinds of ligands (gly, tart, cit, or edta) were tested. NH_4VO_3 (0.17 mol/L, 0.20 g) was added to an aqueous solution (10 mL) containing one of the ligands (0.17 mol/L). Then, aqueous ammonia (ca. 0.5 mL) was added, resulting in a transparent solution of pH 7–8, depending on the ligand (hereafter denoted by V(*L*)-sol., where *L* = gly, tart, cit, or edta). The Bi(edta)-sol. and one of the V(*L*)-sol. were mixed at a molar ratio of Bi:V = 1:1 with stirring (30–60 min) at room temperature to prepare the precursor solutions for $BiVO_4$ synthesis (hereafter denoted by Bi(edta)+V(*L*)-sol., where *L* = gly, tart, cit, or edta). The precursor solution was evaporated at ca. 80℃ to complete dryness, followed by calcination in air. To determine the appropriate calcination temperature, thermal analysis (TG-DTA, TG-8120, Rigaku) was carried out for the precursor gels obtained by the drying of the Bi(edta)+V(*L*)-sol.. No significant weight loss was observed above 430℃ for all samples (see Figure 4-1), strongly suggesting that almost all ligands were combusted at ca. 430℃.

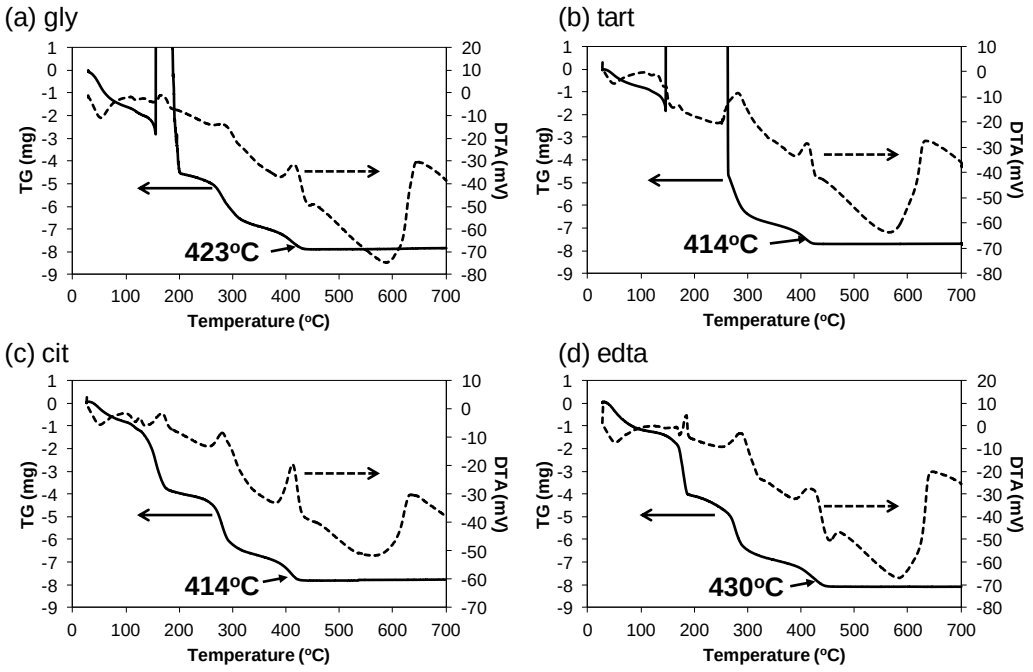

Figure 4-1. TG-DTA curves of dried gels obtained by dryness of Bi(edta)+V(*L*)-sol.

Thus, we set the basic calcination temperature as 500℃, while other temperatures (e.g., 450 and 550℃) were applied in some cases. The samples calcined at 500℃ are denoted by AC-*L* (where *L* = gly, tart, cit, or edta), unless otherwise stated. For comparison, $BiVO_4$ particles were prepared *via* the conventional solid-solution reaction method (SS-method) using NH_4VO_3 and $Bi(NO_3)_3 \cdot 5H_2O$ as metal sources. These materials were mixed at a molar ratio of Bi:V = 1:1 and calcined in air at 500–700℃ for 6 h, yielding $BiVO_4$ particles, hereafter denoted by SS-*T* (where *T* is the calcination temperature).

4.2.3 Characterization

^{1}H NMR spectra of the precursor solutions were recorded in 10% D_2O on a JMN-ECA 500 spectrometer (JEOL). For ^{1}H NMR measurements, sodium 3-(trimethylsilyl)propionate-2,2,3,3-d_4 in D_2O was used as an external reference in a capillary tube. Thermogravimetry and differential thermal analysis (TG-DTA) of dried powders was conducted on a TG-8120 (Rigaku).

The obtained powdered samples were characterized by X-ray diffraction (XRD, PANalytical, X'Pert Pro, rotating anode diffractometer, 45 kV, 40 mA) with Cu *K*α radiation ($\lambda_{K\alpha}$ = 1.5406Å), ultraviolet-visible-near infrared spectrometry (UV-Vis-NIR. DRS, Jasco, V-670), and scanning electron microscopy (SEM, HITACHI, S-4100). Specific surface areas of the powdered samples were determined by N_2 adsorption at 77 K (BET, MicrotracBEL, BELSORP mini).

4.2.4 Photocatalytic reactions

The photocatalytic activity of the $BiVO_4$ particles was evaluated by monitoring O_2 evolution from an aqueous solution containing an electron acceptor (Ag^+ or Fe^{3+}) under visible-light irradiation, using a gas-closed circulation system equipped with a top-irradiation type reaction cell (Pyrex-made). The catalyst powder (50 mg) was suspended in 120 mL of an aqueous $AgNO_3$ solution (10 mM, pH 5.2) or an aqueous $FeCl_3$ solution (10 mM, pH 2.2). The suspension was thoroughly degassed *via* repeated evacuation with a vacuum pump, and subsequently introduction of Ar gas (80 Torr). Light irradiation was introduced from the top of the reactor with a 300 W Xe-arc lamp (Perkin-Elmer, Cermax PE300BF) attached with a cut-off filter (Hoya; L42) to eliminate the UV light. The gases in the circulation system were analyzed and quantified by means of an on-line gas chromatograph (GL Science; GC-3200, TCD, Ar carrier, MS-5A column).

4.3 Results and discussion

4.3.1 Preparation of stable $BiVO_4$ precursor solutions with different ligands

The present study attempted to stabilize V^{5+} and Bi^{3+} cations in water using four different ligands (gly, tart, cit, or edta), and the results are summarized in Table 4-1. A simple addition of $Bi(NO_3)_3 \cdot 5H_2O$ or NH_4VO_3 to water results in a precipitation due to rapid hydrolysis (Figure 4-2 (a)–(b)). In contrast, the combination of $Bi(NO_3)_3 \cdot 5H_2O$ with two equivalents of edta produces a transparent solution without any precipitation (see Figure 4-2 (c)), whereas the use of other lignads, even two equivalents, results in precipitation. The solution prepared with two equivalents of edta will be denoted as Bi(edta)-sol., hereafter. For NH_4VO_3, all the ligands (*L* = gly, tart, cit, or edta) were effective in stabilizing V^{5+}, even at just one equivalent (see Figure 4-2 (d)). These solutions prepared with one equivalent of ligand will be denoted hereafter as V(*L*)-sol. (where *L* = gly, tart, cit, or edta). Although the formation of stable complexes of V^{5+} and Bi^{3+} in aqueous solution have been reported previously,[37-47] excess amounts of ligand were used in most cases. In the present case, it is confirmed that one and two equivalents of the appropriate ligand are effective for stabilizing V and Bi cations, respectively. As for the stabilization of Bi^{3+} cation, less amounts (e.g., one and a half equivalents) of edta results in precipitation (as summarized in Table 4-1). In addition, NMR spectrum of Bi(edta)-sol. indicates no signals corresponding to free edta species in the solution (see Figure 4-4). These results strongly suggest that more than one edta ligands contribute to the stabilization of one Bi^{3+} cation. It is also confirmed that a simple mixing of Bi(edta)-sol. with V(*L*)-sol. (*L* = tart, cit, or edta) produces clear yellow solutions (see Figure 4-3). Although the combination of Bi(edta)-sol. and V(gly)-sol. readily produces a clear yellow solution immediately after mixing, precipitates are gradually generated. The other mixed solutions show high stability and do not produce any appreciable precipitations, even after leaving under atmospheric conditions for more than one year.

Table 4-1. Summary of synthesis of aqueous solution containing Bi^{3+} or V^{5+} species after stirred for ca. 3 hours.

Entry No.	Metal	Ligands	ligands/metal (molar ratio)	Appearance T:transparent, P:precipitated
1	$Bi(NO_3)_3 \cdot 5H_2O$	-	0	P (white, see Fig. 4-2(a))
2		gly	1	P (white)
3			2	P (white)
4		tart	1	P (white)
5			2	P (white)
6		cit	1	P (white)
7			2	P (white)
8		edta	1	P (white)
9			1.5	P (white)
10			2	T (see Fig. 4-2(c))
11	NH_4VO_3	-	0	P (yellow, see Fig. 4-2(b))
12		gly	1	T
13		tart	1	T (see Fig. 4-2(d))
14		cit	1	T
15		edta	1	T

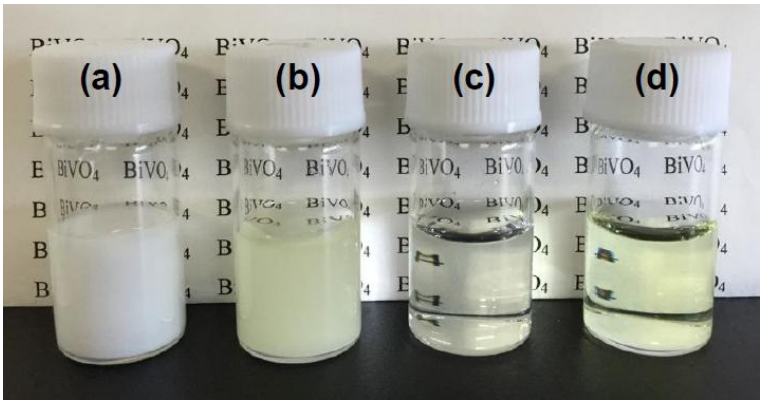

Figure 4-2. Photograph of the solutions of (a) H_2O+ $Bi(NO_3)_3 \cdot 5H_2O$, (b) H_2O+ NH_4VO_3, (c) edta-sol.+ $Bi(NO_3)_3 \cdot 5H_2O$, (d) tart-sol.+ NH_4VO_3.

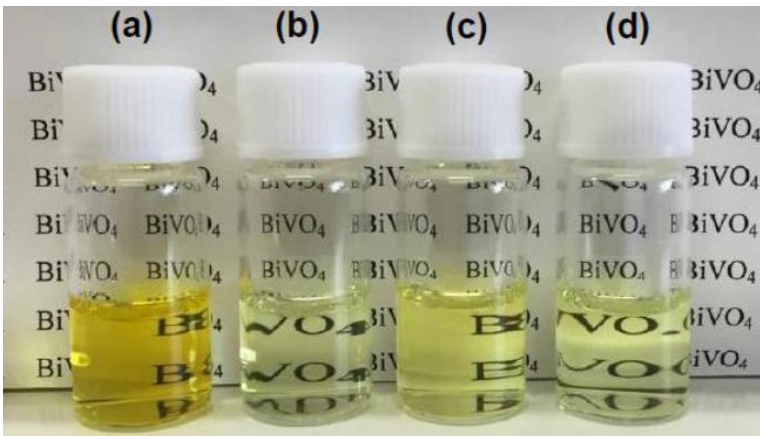

Figure 4-3. A photograph of aqueous solutions obtained by mixing Bi(edta)-sol. and V(*L*)-sol (*L* = (a) gly, (b) tart, (c) cit, and (d) edta).

As will be discussed later, the kind of ligands used for V^{5+} stabilization significantly influences the size and activity of the $BiVO_4$ particles produced after calcination of the mixed solutions (Bi(edta)+V(*L*)-sol.). Particularly, the use of tart ligands with V^{5+} (V(tart)-sol.) produces significantly smaller $BiVO_4$ particles, suggesting that the presence of the V^{5+} species coordinated by tart ligands (V(tart) species) in the mixed solution plays a significant role in reducing the particle size. However, the possibility of replacement of the tart that originally coordinated to V^{5+} by the edta that originally coordinated to Bi^{3+}, possibly by the residual free edta, in the mixed solution cannot be excluded. Thus, liquid state ^{1}H NMR measurements were conducted to obtain detailed information on the species in Bi(edta)+V(tart)-sol., and the spectrum is shown in Figure 4-4. The assignments of the observed signals estimated from comparison with authentic samples are summarized in Table 4-2. The spectrum exhibits signals assignable to both the edta that coordinates to Bi^{3+} at 3.90 and 3.25 ppm (Figure 4-4 (i) a–b) and the edta that coordinates to V^{5+} at 4.15, 3.90, 3.60, 3.20, and 2.85 ppm (Figure 4-4 (i) c–g). These results indicate that a some of the tart ligands that originally coordinated to the V^{5+} cation are replaced by edta ligands in the mixed solution. However, it is difficult to confirm the presence of tart ligands that still coordinate to V^{5+} cation (V-tart) after mixing due to the overlap of the V-tart and free tart signals (at 4.3 ppm, Figure 4-4 (i) f). The line width of the singlet signal at 4.3 ppm (a) is broader (5.6 Hz) than that of the free tart molecules (0.7 Hz) but narrower than that of the pure V(tart) complex (7.3 Hz). These findings strongly suggest that some of the tart ligands originally coordinated to V^{5+} are replaced by the excess edta ligands after mixing. However, titration experiments with excess of edta (up to three equivalents, see the detail in Table 4-3) indicate that the V-tart complex can exist to some

extent in the solution even when it contains two equivalents of free edta, strongly suggesting that complete replacement of the original tart ligands by edta does not occur under the present conditions. Based on these results, it is concluded that Bi(edta)+V(tart)-sol. contains mainly V(tart) and Bi(edta), along with free tart, and V(edta) to some extent.

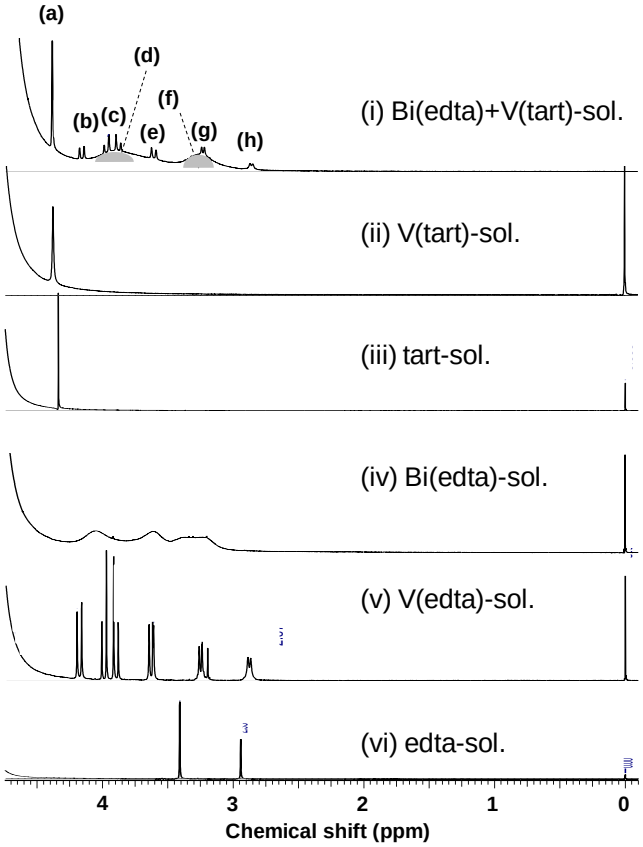

Figure 4-4 ^{1}H NMR spectrum of (i) aqueous $BiVO_4$ precursor solution (Bi(edta)+V(tart)-sol.), (ii) aqueous solutions obtained by mixing NH_4VO_3 and tart (V(tart)-sol.), (iii) aqueous tart solution (tart-sol.), (iv) aqueous solutions obtained by mixing $Bi(NO_3)_3 \cdot 5H_2O$ and edta (Bi(edta)-sol.), (v) aqueous solutions obtained by mixing NH_4VO_3 and edta (V(edta)-sol.) and (vi) aqueous edta solution (edta-sol.).

Table 4-2. ^{1}H NMR chemical sifts of aqueous $BiVO_4$ precursor solution (Bi(edta)+V(tart)-sol.) and authentic samples.

Species	Authentic samples [ppm]	Bi(edta)+V(tart)-sol. [ppm]
V(tart)	4.35 (*s*, FHWM = 7.3 Hz)	(a) 4.4 (*s*, FHWM = 5.6 Hz)
tart	4.4 (*s*, FHWM = 0.7 Hz)	
Bi(edta)	3.2 (*br*)	
	3.4 (*br*)	(f) 3.25 (*br*)
	3.6 (*br*)	(d) 3.9 (*br*)
	4.0 (*br*)	
V(edta)	2.9 (*d*)	(h) 2.85 (*d*)
	3.3 (*d*)	(g) 3.2 (*d*)
	3.6 (*d*)	(e) 3.6 (*d*)
	3.9 (*q*)	(c) 3.9 (*q*)
	4.19 (*d*)	(b) 4.16 (*d*)
edta	2.95 (*s*)	-
	3.4 (*s*)	-

Table 4-3. ^{1}H NMR chemical sifts of aqueous solution of V(tart)-sol. mixed with edta-sol.(1–3 eq.) and authentic samples.

Species	V(tart)-sol. +edta(1 eq.)-sol. [ppm]	V(tart)sol. +edta(2 eq.)-sol. [ppm]	V(tart)sol. +edta(3 eq.)-sol. [ppm]
tart / V-tart	4.4 (*s*, 1H)	4.4 (*s*, 1H)	4.4 (*s*, 1H)
edta	2.95 (*s*)	2.95 (*s*)	2.95 (*s*)
	3.4 (*s*)	3.4 (*s*)	3.4 (*s*)
V(edta)	2.9 (*d*)	2.9 (*d*)	2.9 (*d*)
	3.3 (*d*)	3.3 (*d*)	3.3 (*d*)
	3.6 (*d*)	3.6 (*d*)	3.6 (*d*)
	3.9 (*q*)	3.9 (*q*)	3.9 (*q*)
	4.19 (*d*, 0.67H)	**4.19 (*d*, 0.78H)**	**4.19 (*d*, 0.97H)**

4.3.2 Characterization of the $BiVO_4$ fine particles prepared *via* the aqueous chelating method

Figure 4-5 shows a photograph of the AC-*L* samples, which were obtained by drying the precursor solution (Bi(edta)+V(*L*)-sol.) followed by calcination at 500℃ in air. The volumes of the samples increase after calcination, regardless of the stabilizing ligands. In particular, the AC-tart sample shows the most significant increase in volume compared with the other AC-*L* samples.

Figure 4-5. Photographs of the dried gel obtained by dryness of the Bi(edta)+V(tart)-sol. and the AC-*L* samples obtained by dryness of the precursor solution Bi(edta)+V(*L*)-sol. (*L* = (a) gly, (b) tart, (c) cit or (d) edta) followed by calcination at 500℃ in air.

The XRD patterns of $BiVO_4$ particles prepared *via* the AC-method are shown in Figure 4-6. Doublet peaks at ca. 18.5° and 35° are observed for the $BiVO_4$ particles prepared with three ligands (tart, cit, and edta), indicating the production of single-phase s-m $BiVO_4$.[22,29] Conversely, the $BiVO_4$ particles prepared with gly ligands (AC-gly) show a single broad peak at ca. 18.5°, implying the formation of s-m $BiVO_4$ with low crystallinity and/or the co-existence of s-t $BiVO_4$.[29,48] The band gap of the AC-gly sample (see Table 4-4) estimated from the UV-spectrum (see Figure 4-7 (a)) is ca. 2.4 eV, which is characteristic of s-m phase $BiVO_4$.[22,23] The same value (2.4 eV) is obtained with other preparations, i.e., AC-tart, AC-cit, and AC-edta. The V−O bond length (ca. 1.69 Å), calculated from the corresponding Raman stretching signal at around 830 cm^{-1} for the AC-gly samples(see Figure 4-7 (b)), is almost the same as the values for other samples, such as AC- tart, as seen in Table 4-4. This value agrees well with the reported value for s-m $BiVO_4$ (1.69 Å) but is appreciably different from that for s-t $BiVO_4$ (1.72 Å).[26,49] From these results, it can be concluded that the AC-gly sample predominantly consists of s-m $BiVO_4$ with low crystallinity. The XRD patterns of the $BiVO_4$ particles prepared *via* the

SS-method with calcination in air at 600 and 700℃ (SS-600 and 700) also indicate single-phase s-m $BiVO_4$, whereas an unknown peak is observed in the sample calcined at 500℃ (SS-500, see Figure 4-8).

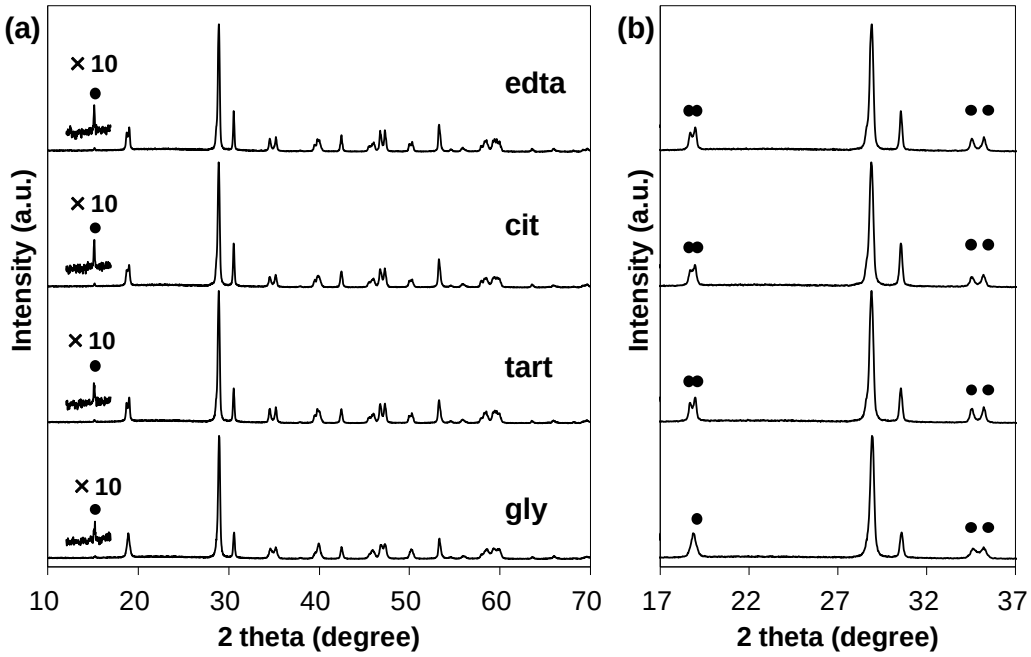

Figure 4-6. XRD patterns of $BiVO_4$ particles prepared *via* AC-method with different ligands (gly, tart, cit or edta) followed by calcination at 500℃ in air.

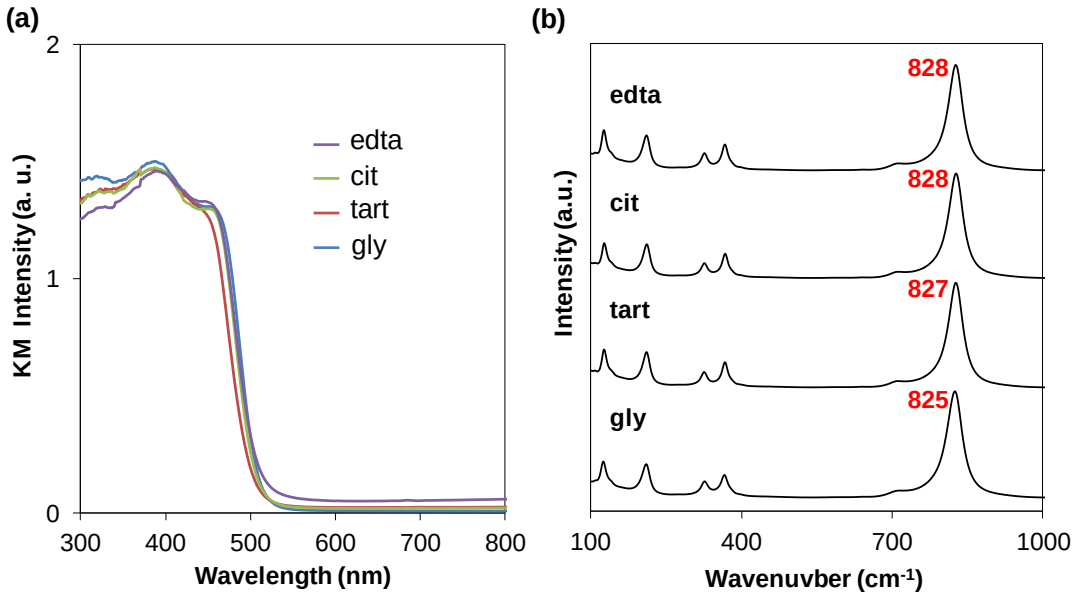

Figure 4-7. (a) UV-vis spectra and (b) Raman spectra of $BiVO_4$ particles prepared *via* AC-method with different ligands (gly, tart, cit or edta) followed by calcination at 500℃ in air.

Table 4-4. Band gap energy, Stretching Raman shift of V-O bond and bond length of V-O on $BiVO_4$ particles prepared *via* AC method with different ligands (gly, tart, cit or edta).

	B.G. [eV]	Stretching Raman shift V-O bond [cm^{-1}]	Bond length V-O [Å] *
gly	2.4	825	1.697
tart	2.4	827	1.695
cit	2.4	828	1.695
edta	2.4	828	1.695

*calculated using the empirical expression: ν (cm^{-1}) = 21349 exp[-1.9176 R(Å)]

* V-O bond length of $BiVO_4$: sheelite tetragonal structure, 1.72 Å, sheelite monoclinic structure, 1.69 Å

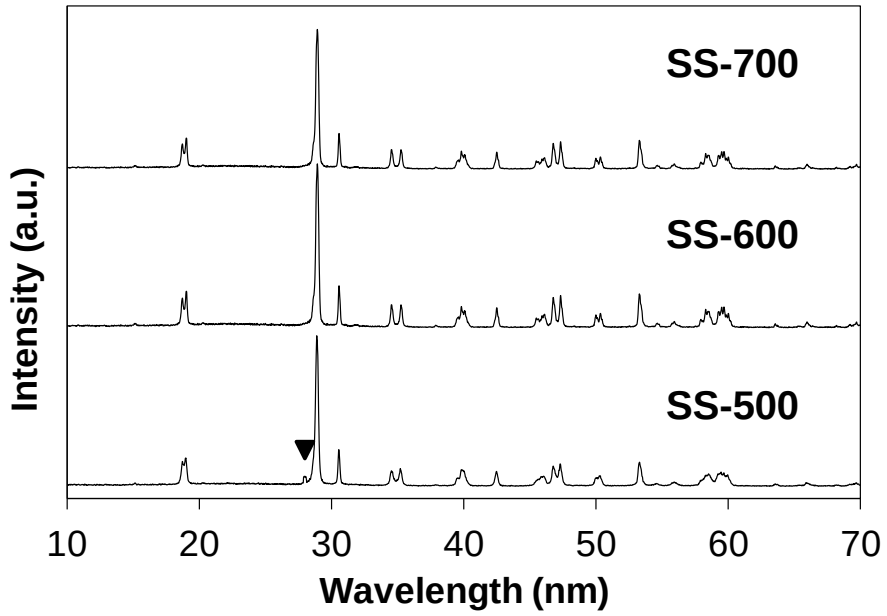

Figure 4-8. XRD patterns of $BiVO_4$ particles prepared *via* SS-method with calcinations at different temperatures. (▼: unknown)

Figure 4-9 shows SEM images of the $BiVO_4$ samples. The primary particle sizes in the AC-samples calcined at 500℃ range from 80 to 300 nm, which are much smaller than those of the SS-samples (1–10 μm) containing single-phase s-m material (SS-600, SS-700). Specifically, the sample prepared with the tart ligand (AC-tart) contains the smallest particles (ca. 80 nm) with relatively

homogeneous distribution. In addition, the specific surface area of AC-tart (5.2 m^2 g^{-1}) is larger than those of other samples (see the bottom left in Figure 4-9 for each sample). Since all the AC-samples were prepared under the same conditions (i.e., pH of precursor solution, concentration of metal ions, calcination temperature, etc.) except for the ligands used, the significant difference in the particle size strongly suggests that the ligand used for stabilizing the V^+ ions is the key factor in determining the particle size after calcination. During the drying and calcination of the Bi(edta)+V(*L*)-sol. in the AC-method, the polymerization reaction first proceeds between the functional groups (i.e., -COOH and -OH) of the ligands, followed by nuclei generation (i.e., crystallization) and further crystal growth. The TG-DTA data (see Figure 4-1) strongly suggest that the organic compounds in the dried gels are completely combusted at ca. 430℃, regardless of the type of ligands used for stabilizing the V^{5+} ion. As shown in Figure 4-9, the particle size of AC-tart calcined at 450 ℃ is slightly smaller than that when it is calcined at 500℃. Similarly, the particle size of the AC-samples prepared using other ligands and calcination at 450℃ is slightly smaller than that of those prepared at 500℃. These findings indicate that the particle size of each AC-sample is predominantly determined by the processes occurring below ca. 450℃, not those above 450℃. At temperatures lower than 430℃, at which organic species still remain, processes such as polymerization, nuclei generation, and crystal growth occur. In general, the number of carboxyl groups in the ligands considerably influences nuclei generation. A higher number of carboxyl groups in the ligands generally cause the formation of larger nuclei due to the increased probability of polymerization. Therefore, the AC-samples prepared with cit and edta, which have three and four carboxyl groups, respectively, formed larger nuclei in the precursor during polymerization, thereby resulting in the production of $BiVO_4$ particles with large sizes (> 100 nm) after calcination. Although the number of carboxyl groups in gly is lower than that in tart, the size of $BiVO_4$ particles prepared with gly (AC-gly) is larger (100–300 nm) than that prepared with tart (ca. 80 nm). This contradicting phenomenon is explained by the instability of the precursor solution. As described in the previous section, the precursor solution prepared using the gly ligand for V^{5+} stabilization (Bi(edta)+V(gly)-sol.) is unstable and gradually produces precipitations, indicating that the hydrolysis of V^{5+} species proceeds *via* replacement of gly ligands with water molecules. Thereby, larger and inhomogeneous nuclei are produced during the drying of Bi(edta)+V(gly)-sol., affording larger particles after calcination.

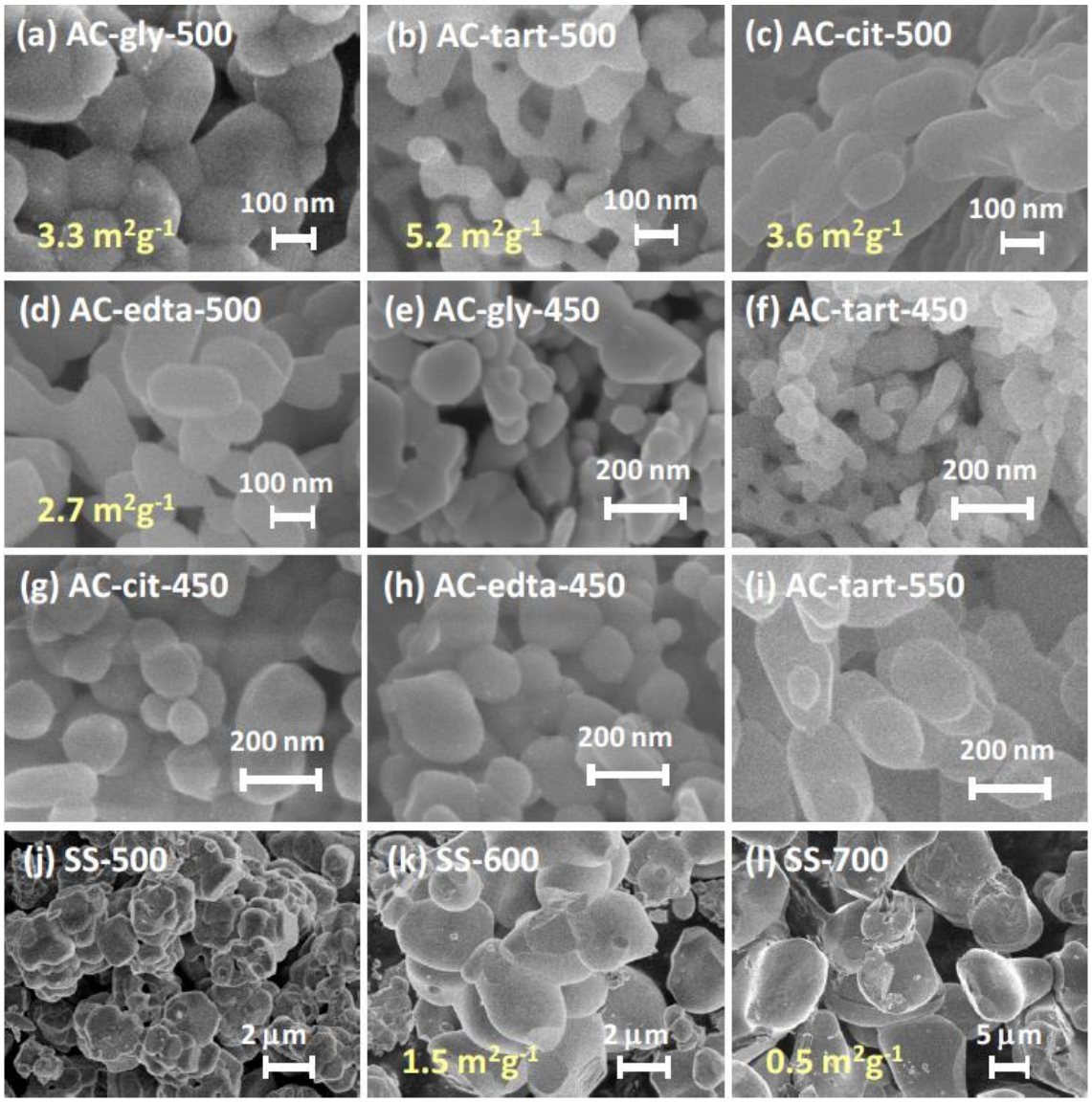

Figure 4-9. SEM images of $BiVO_4$ particles prepared *via* (a–i) AC- and (j–l) SS-methods after calcination at different temperatures.

4.3.3 Photocatalytic O_2 evolution on $BiVO_4$ prepared *via* aqueous chelating method

The photocatalytic activity of the $BiVO_4$ samples was evaluated for O_2 evolution from an aqueous solution containing an electron acceptor (Ag^+ or Fe^{3+}) under visible-light irradiation ($\lambda > 410$ nm). The initial rates of O_2 evolution over AC- and SS-samples are summarized in Table 4-5. The rate of O_2 evolution over the AC-samples was dependent on the calcination temperature during the preparation process. The highest rate is observed for AC-sample calcined at 500℃. For the SS-samples, the optimum calcination temperature is 600℃.

Table 4-5. Photocatalytic O_2 evolution from an aqueous methanol solution under visible light irradiation on WH and SS samples ($BiVO_4$) prepared under different conditions.

	Calcination temperature [℃]	O_2 evolution rate [μmol h^{-1}]	
		Ag^+	Fe^{3+}
(a) AC(gly)	500	8	39.6
(b) AC(tart)	450	13	59.4
(c) AC(tart)	500	16	89.5
(d) AC(tart)	550	15	80.8
(e) AC(cit)	500	11	44.4
(f) AC(edta)	500	10	41.2
(g) SS	500	4	16
(h) SS	600	6	19
(i) SS	700	3	15.8

* Catalyst, 0.05 g; reactant solution, 120 mL of 10 mM aqueous solution containing an electron acceptor (Ag^+ or Fe^{3+}).; light source, 300 W Xe lamp with cut-off filters ($\lambda > 410$ nm).

Figure 4-10 shows the time course of O_2 evolution from aqueous solution over these samples under visible-light irradiation in the presence of an electron acceptor (Ag^+ or Fe^{3+}). Although largely steady rates of O_2 evolution are observed for all the cases in the initial period of photo-irradiation, the rates gradually decrease due to the occurrence of the backward reaction (i.e., re-oxidation of Fe^{2+} by holes) or deposition of Ag metal particles on the surface. The higher activity over the AC-tart sample calcined at 500℃ than that prepared at 450℃ is certainly due to the improved crystallinity of the particles, which leads to a decreased amount of crystal defects that function as recombination sites between photogenerated electrons and holes. The appreciable decrease in efficiency of the AC-samples calcined above 550℃ can be explained by the increase in particle size (see Figure 4-9), which increases the migration distance for charge carriers generated in the bulk material, and consequently increases the possibility of their recombination before reaching the surface. The rate of O_2 evolution over the AC-samples also changes depending on the type of ligand used for V^{5+} stabilization in the precursor solution, with the rate increasing in the order AC-gly < AC-edta < AC-cit < AC-tart, when compared at the same calcination temperature (500℃). The primary particle size of AC-tart (80 nm) is

much smaller than that of the AC-samples prepared with other ligands (gly, cit, and edta) (100–300 nm) (see Figure 4-9). The O_2 evolution rate over AC-gly is lower than that over AC-edta, despite the larger specific surface area of AC-gly. This lower activity may be explained by the lower crystallinity of the AC-gly particles, as confirmed by XRD measurements. Thus, the highest O_2 evolution rate for AC-tart can be explained by it having the smallest particle size with similar crystallinity among the samples, except for AC-gly. It is also confirmed that the $BiVO_4$ particles prepared *via* the AC-method show higher activity for O_2 generation than the $BiVO_4$ samples prepared *via* the conventional SS-method. The O_2 evolution rate with AC-tart is ca. three times higher than that with SS-600. These results indicate that the present AC-method is extremely useful for the preparation of fine s-m $BiVO_4$ particles that exhibit high activity for photocatalytic O_2 evolution from water under visible-light irradiation.

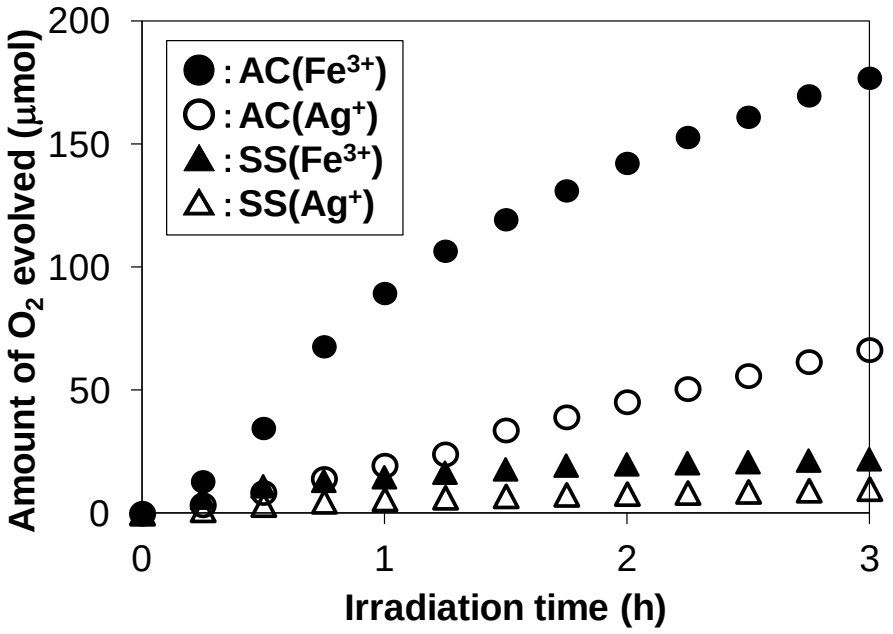

Figure 4-10. O_2 evolution from an aqueous solution containing an electron acceptor (Ag^+ or Fe^{3+}) under visible-light irradiation over $BiVO_4$ photocatalyst prepared *via* AC- or SS-method followed by calcination (AC-tart and SS-600). Conditions: Catalyst, 0.05 g; reactant solution, 120 mL of 10 mM aqueous solution containing an electron acceptor (Ag^+ or Fe^{3+}); light source, 300 W Xe lamp with cut-off filters ($\lambda > 410$ nm).

4.4 Conclusions

In this chapter, fine particles of s-m $BiVO_4$ (80–300 nm) with a particle size smaller than those produced with conventional solid-state reactions (1–10 μm) were successfully synthesized *via* a newly developed aqueous chelating method. The kind of ligands used for the stabilization of V^{5+} ions in the precursor solution was found to significantly influence the particle size of the obtained $BiVO_4$. Among the ligands examined, the use of the tart ligand produced s-m $BiVO_4$ with the smallest particles (ca. 80 nm), even after calcination at 500℃. The present method afforded catalysts capable of a significantly higher rate of O_2 evolution under visible light than that of $BiVO_4$ catalysts prepared *via* conventional solid-state reactions, probably due to their smaller particle size and higher crystallinity. The present aqueous chelating method provides an environmentally benign process that can be used for the synthesis of highly active photocatalyst materials on a large scale without the use of toxic organic solvents.

References

1. K. Maeda and K. Domen, *J. Phys. Chem. C*, 2007, **111**, 7851.
2. F. E. Osterloh, *Chem. Mater.*, 2008, **20**, 35–54.
3. A. Kudo and Y. Miseki, *Chem. Soc. Rev.*, 2009, **38**, 253–278
4. K. Maeda and K. Domen, *J. Phys. Chem. Lett.*, 2010, **1**, 2655–2661.
5. R. Abe, *J. Photochem. Photobiol. C: Photochem. Rev.*, 2010, **11**, 179–209.
6. A. Kudo, *Mater. Res. Bull.*, 2011, **36**, 32–38.
7. A. Fujishima and K. Honda, *Nature*, 1972, **238**, 37–38.
8. K. Maeda, K. Teramura, D. L. Lu, T. Takata, N. Saito, Y. Inoue and K. Domen, *Nature*, 2006, **440**, 295.
9. Y. Lee, H. Terashima, Y. Shimodaira, K. Teramura, M. Hara, H. Kobayashi, K.Domen, M. Yashima, *J. Phys. Chem. C*, 2007, **111**, 1042.
10. R. Asai, H. Nemoto, Q. Jia, K. Saito, A. Iwase and A. Kudo, *Chem. Commun.*, 2014, **50**, 2543–2546.
11. C. Pan, T. Takata, M. Nakabayashi, T. Matsumoto, N. Shibata, Y. Ikuhara and K. Domen, *Angew. Chem.*, 2015, **127**, 2998–3002.
12. R. Abe, *Bull. Chem. Soc. Jpn.*, 2011, **84**, 1000–1030.
13. K. Maeda, *ACS Catal.*, 2013, **3**, 1486–1503.
14. K. Sayama, K. Mukasa, R. Abe, Y. Abe and H. Arakawa, *Chem. Commun.*, 2001, 2416–2417.
15. R. Abe, K. Sayama, K. Domen, H. Arakawa, *Chem. Phys. Lett.*, 2001, **344**, 339-344.
16. H. Kato, M. Hori, R. Konta, Y. Shimodaira and A. Kudo, *Chem. Lett.*, 2004, **33**, 1348–1349.
17. H. Kato, Y. Sasaki, A. Iwase and A. Kudo, *Bull. Chem. Soc. Jpn.*, 2007, **80**, 2457–2464.
18. Y. Sasaki, A. Iwase, H. Kato and A. Kudo, *J. Catal.*, 2008, **259**, 133–137.
19. H. Kato, Y. Sasaki, N. Shirakura and A. Kudo, *J. Mater. Chem. A*, 2013, **1**, 12327–12333.
20. Y. Sasaki, H. Kato and A. Kudo, *J. Am. Chem. Soc.*, 2013, **135**, 5441.
21. A. R. Lim, S. H. Choh and M. S. Jang, J. Phys.: *Condens. Matter.*, 1995, **7**, 7309.
22. A. Kudo, K. Omori and H. Kato, *J. Am. Chem. Soc.*, 1999, **121**, 11459.
23. S. Tokunaga, H. Kato and A. Kudo, *Chem. Mater.*, 2001, **13**, 4624–4628.
24. B. Ohtani, O. Mahaney, F. Amano, N. Murakami and R. Abe, *J. Adv. Oxid. Technol.*, 2010, **13**, 247–261.

25. R. S. Roth and J. L. Waring, *Am. Mineral.*, 1963, **48**, 1348.
26. A.W. Sleight, H.Y. Chen, A. Ferretti and D. E. Cox, *Mater. Res. Bull.*, 1979, **14**, 1571.
27. A. Kudo, K. Ueda, H. Kato and I. Mikami, *Catal. Lett*., 1998, **53**, 229.
28. G. Li, D. Zhang and J. C. Yu, *Chem. Mater.*, 2008, **20**, 3983.
29. A. Iwase and A. Kudo, *J. Mater. Chem.*, 2010, **20**, 7536–7542.
30. A. Iwase, H. Kato and A. Kudo, *J. Sol. Energy Eng., B*, 2003, **104**, 36.
31. J. Yu and A. Kudo, *Chem. Lett.*, 2005, **34**, 850.
32. L. Zhang, D. Chen and X. Jial, *J. Phys. Chem. B*, 2006, **110**, 2668.
33. J. Yu and A. Kudo, *Adv. Funct. Mater.*, 2006, **16**, 2163–2169.
34. J. Yu, Y. Zhang and A. Kudo, *J. Solid State. Chem*, 2009, **182**, 223–228.
35. S. Okunaka, H. Tokudome and R. Abe, *J. Mater. Chem. A*, 2015, **3**, 14794–14800.
36. S. Okunaka, H. Tokudome, Y. Hitomi and R. Abe, *J. Mater. Chem. A*, 2015, **3**, 1688–1695.
37. K. Zare, P. Lagrange and J. Lagrange, *J.C.S. Dalton.*, 1978, 1372–1376.
38. M. Bartušek and V. Šustáček, *Collection Czechoslovak Chem. Commun.*, 1983, **48**, 2785–2797.
39. M. M. Caldeira, M. L. Ramos, N. C. Oliveira and V. M. S. Gil, *Can. J. Chem.*, 1987, 65, 2434–2440.
40. K. Popov, A. Vendilo and N. Djatlova, *Mag. Res. Chem.*, 1991, 29, 301-303.
41. S. P. Summers, K. A. A.bboud, S. R. Farrah and G. J. Palenik, *Inorg. Chem.*, 1994, **33**, 88–92.
42. Z. H. Zhou, H. Zhang, Y. Q. Jiang, D. H. Lin, H. L. Wan and K. R. Tsai, *Trans. Metal. Chem.*, 1999, **24**, 605–609.
43. M. Kaliva, C. P. Raptopoulou, A. Terzis and A. Salifoglou, *Inorg. Chem.*, 2004, **43**, 2895–2905.
44. A. R. Khan, D. C. Crans, R. Pauliukaite and E. Norkus, *J. Braz. Chem. Soc.*, 2006, **17**, 895–904.
45. P. Schwendt, A. S. Tracey, J. Tatiersky, J. Galikova and Z. Zak, *Inorg. Chem.*, 2007, **46**, 3971–3983.
46. L. R. Guilherme, A. C. Massabni, A. Cuin, L. A. A. Oliveira, E. E. Castellano, T. A. Heinrich and C. M. Costa-Neto, *J. Coord. Chem*., 2009, **62**, 1561–1571.
47. J. Galikova, P. Schwendt, J. Tatiersky, A. S. Tracey and Z. Zak, *Inorg. Chem.*, 2009, **48**, 8423–8430.
48. Y. K. Kho, W. Y. Teoh, A. Iwase, L. Madler, A. Kudo and R. Amal, *ACS Appl. Mater. Interfaces.*, 2011, **3**, 1997–2004.

49. F. D. Hardcastle and I. E. Wachs, *J. Phys. Chem.* 1991, **95**, 5031–5041.

Chapter 5

Z-scheme Water Splitting into H_2 and O_2 under Visible-light over Photocatalyst Panels Consisting of Rh-doped $SrTiO_3$ and $BiVO_4$ Fine Particles

5.1 Introduction

Photocatalytic water splitting has attracted considerable attention due to the potential application of this reaction to clean hydrogen production from water by utilizing abundant solar light.[1] Heterogeneous photocatalysis systems with suspended semiconductor particles have extensively been studied for this reaction due to the simplicity and/or potential scalability.[2,3] Such suspension systems, however, requires the energy for keeping the semiconductor particles suspended in the solution (e.g., mechanical stirring) in the practical application, as well as the troublesome process in the collection and/or recycling (e.g., filtration or centrifugation) of the used photocatalysts. In contrast, photocatalyst panels, in which films of photocatalyst particles are fixed on an inexpensive substrate (e.g., glass), require neither such energy nor troublesome collection process, and thereby have a potential to be employed as a cost-effective system on large scale.[4–6] For example, Domen et al. demonstrated water splitting using such kind of photocatalyst panels prepared *via* drop-casting or squeegeeing of $Ga_{1-x}N_x$-$Zn_{1-x}O_x$ ($x = 0.18$) photocatalyst particles, which can harvest visible light up to ca. 460 nm.[4] For the practical application, however, it is necessary to harvest wider range of visible light by employing the semiconductor materials having narrower bandgaps. It has been demonstrated that the introduction of Z-scheme mechanism can extend the usable wavelength for water splitting up to 670 nm at maximum by employing two different narrow bandgap photocatalysts combined with a redox mediator such as IO_3^-/I^- or Fe^{3+}/Fe^{2+}.[7,8] Among them, the combination of Rh-doped $SrTiO_3$($SrTiO_3$:Rh) and $BiVO_4$ has been demonstrated to split water into H_2 and O_2 in the presence of various redox couples in solution (e.g., Fe^{3+}/Fe^{2+}, $[Co(bpy)_3]^{3+/2+}$, $[Co(phen)_3]^{3+/2+}$) with relatively high efficiency by harvesting visible light up to 520 nm.[9–13] The availability of solid electron mediator such as RGO and Au was also proven.[14,15] For example, Wang at el. recently demonstrated simultaneous evolution of H_2 and O_2 on a photocatalyst sheet, in which $SrTiO_3$:Rh,La and $BiVO_4$ photocatalyst particles immobilized onto the thin Au layer deposited on substrate; the electron transfer between two photocatalyst proceed through the Au layer. Interestingly, the combination of $SrTiO_3$:Rh and $BiVO_4$ can work even without any redox couples or solid electron mediators; the electron transfer between them proceed directly *via* redox cycle of Rh species that are contained in the $SrTiO_3$:Rh particle.[16,17] These findings have motivated to employ this combination as the component of photocatalyst panels for water splitting under visible light. To achieve efficient water splitting based on such interparticle electron transfer in the films, a greater numbers of hetero-interfaces between these two different

photocatalysts ($SrTiO_3$:Rh and $BiVO_4$) is required. The use of semiconductor particles having well-controlled particle sizes is thus highly desirable to increase the numbers of hetero-interfaces, as well as to control the porous structure that facilitate the transport of the substrates and products, within the films.

As described in Chapter 3, efficient H_2 evolution (half reaction in aqueous methanol solution) using photocatalyst panels prepared *via* simple screen printing of $SrTiO_3$:Rh fine particles on a glass substrate were demonstrated.[6] The use of $SrTiO_3$:Rh particles with homogeneously small size (ca. 50 nm), which were synthesized *via* a newly-developed water-based hetero-chelate (WH) method,[18] enabled the preparation of homogeneous films with controlled structures for effective light absorption and efficient transportation of substances and/or products within the pores. In this chapter, the composite-type porous films consisting of the $SrTiO_3$:Rh and $BiVO_4$ fine particles were fabricated by means of simple screen-printing followed by calcinations, to achieve simultaneous evolution of H_2 and O_2 on such structure-controlled photocatalyst panels under visible light.

5.2 Experimental

5.2.1 Materials

Titanium(IV) tetraisopropoxide (95.0%, TIPT), acetylacetone (99.0%, acac), acetic acid (99.7%, AcOH), strontium acetate hemihydrate ($Sr(OAc)_2 \cdot 0.5H_2O$), rhodium(III) chloride trihydrate ($RhCl_3 \cdot 3H_2O$), lactic acid (85.5–94.5%), rhodium(III) oxide (Rh_2O_3), ammonium vanadate(V) (99%, NH_4VO_3), bismuth(III) nitrate pentahydrate (99.9%, $Bi(NO_3)_3 \cdot 5H_2O$), L(+)-tartalic acid (tart), ethylenediamine tetraacetic acid (edta), silver nitrate (99.5%, $AgNO_3$), α-terpineol, 2-(2-butoxyethoxy)ethanol and poly(vinyl butyral) were purchased from Wako Pure Chemical Industries, Ltd., Osaka, Japan. Acrylic emulsion (VONCOAT (EC-905EF), particle size: 100–150 nm) was purchased from DIC Corporation. Titanium oxide (99.9%, TiO_2) was purchased from Soekawa chemical. Strontium carbonate (99.9%, $SrCO_3$) and aqueous ammonia (28.0–30.0%) were purchased from Kanto chemical. All reagents were used as received, and all the experiments were carried out under ambient condition without eliminating the moisture from the atmosphere.

5.2.2 Preparation of $BiVO_4$ and $SrTiO_3$:Rh particles

Particles of $BiVO_4$ were prepared *via* the following aqueous chelating (AC) method developed in

Chapter 4. An aqueous solution that contains bismuth(III) nitrate pentahydrate ($Bi(NO_3)_3 \cdot 5H_2O$, 0.17 mol/L), ethylenediamine tetraacetic acid (edta, 0.34 mol/L) and ammonia solution (NH_4OH, 0.01 mol/L) was mixed with another aqueous solution that contains ammonium vanadate(V) (NH_4VO_3, 0.17 mol/L) and tartaric acid (tart, 0.17 mol/L), at the ratio of Bi:V = 1:1. After the evaporation of the solution to dryness, the obtained gel was calcined in air at 500℃ for 2 h, yielding $BiVO_4$ particles with monoclinic scheelite structure and relatively small primary particle sizes below ca. 100 nm (see Figure 5-6 (a)), which will be denoted by $BiVO_4$(AC). For comparison, $BiVO_4$ particles were prepared *via* the conventional solid-state (SS) reaction, in which a stoichiometric mixture of NH_4VO_3 and $Bi(NO_3)_3 \cdot 5H_2O$ was calcined at 700℃ for 6h, giving the $BiVO_4$ particles with the same monoclinic scheelite structure but significantly larger particle size (1–10 μm) (see Figure 5-6 (b)). These $BiVO_4$ particles prepared *via* SS reaction will be denoted by $BiVO_4$(SS). It was confirmed that the $BiVO_4$(AC) sample showed higher rate of O_2 evolution than the $BiVO_4$(SS) sample under visible light from aqueous solution containing Ag^+ as an electron acceptor (Figure 4-11).

The fine particles of $SrTiO_3$:Rh(2%) were prepared *via* the water-based hetero-chelate (WH) method, which was developed in Chapter 2.[18] The aqueous titania sol (AA-sol) was prepared by mixing titanium(IV) tetraisopropoxide, an aqueous solution of acetylacetone, and an aqueous solution of acetic acid.[20] The AA-sol was mixed with an aqueous solution containing both $Sr(OAc)_2$ (1.08 mol/L) and lactic acid (2.16 mol/L) and an aqueous solution of $RhCl_3$ (0.24 mol/L) at the ratio of Sr:Ti:Rh = 1.02:0.98:0.02, and stirred for 1 hour at room temperature, yielding an orange transparent sol. The sol was added by an acrylic emulsion (VONCOAT (EC-905EF), particle size: 100–150 nm) and stirred for 15 minutes at room temperature, then dried at 80℃ for 3 hours, and finally calcined at 1000℃ for 10 hours, yielding $SrTiO_3$:Rh(Rh: 2%) particles with pure (cubic) perovskite structure and relatively small primary particle sizes below ca. 50 nm (see Figure 5-6 (c)), which will be denoted by $SrTiO_3$:Rh(WH). For comparison, $SrTiO_3$:Rh(2%) particles were also prepared *via* the solid state (SS) reaction method,[21] in which a stoichiometric mixture of TiO_2, $SrCO_3$ and Rh_2O_3 was calcined at 1000℃ for 10 hours, producing large particles (ca. 300 nm) (see Figure 5-6 (d)), which will be denoted by $SrTiO_3$:Rh(SS). Although some reports have suggested that the addition of excess Sr in the preparation of $SrTiO_3$:Rh particles *via* the SS-method is effective to obtain more active photocatalyst samples, it was confirmed that the $SrTiO_3$:Rh particles prepared *via* the SS-method with excess amount of Sr (Sr/(Ti+Rh) =1.03, for example) showed almost same rate of H_2 evolution as that on the sample

prepared with the stoichiometric ratio(Sr:(Ti+Rh) = 1).[2] Thus in this chapter, the $SrTiO_3$:Rh particles prepared *via* the SS-method with stoichiometric ratio was used for comparison. Small amount (0.7 wt%) of ruthenium (Ru) particles were loaded on all the $SrTiO_3$:Rh samples by mean of in-situ photodeposition method and following H_2-reduction treatment at 200℃ for 30 min.[16]

5.2.3 Preparation of composite-type films

The composite-type films were prepared as follows. The $BiVO_4$(AC) and Ru/$SrTiO_3$:Rh(WH) particles were basically mixed at the weight ratio of 1:1 unless otherwise stated. The mixture was added to an organic vehicle consisting of mixture of α-terpineol, 2-(2-butoxyethoxy)ethanol, and acrylic resin (SPB-TE1) with their weight ratio of 4:10:2. The weight ratio between the mixed particles and the vehicles was set to 1:3. The paste was coated on glass substrate (quartz) by screen-printing using a metal mask (60 μm thick), followed by calcination in air at 300℃ for 30 min unless stated. The TG-DTA analysis confirmed that the organic vehicle used in the present study can be completely burn out by the calcination at 300℃, producing films having enough mechanical strength. The obtained films are denoted as AC-WH film. The composite-type film of $BiVO_4$(SS) and Ru/$SrTiO_3$:Rh(SS) particles was also prepared by the same process for comparison (SS film).

5.2.4 Characterization of composite-type films

The obtained $SrTiO_3$:Rh films were characterized by mean of a scanning electron microscope (SEM, HITACHI, S-4100), an X-ray diffraction (XRD, PANalytical, X'Pert Pro, rotating anode diffractometer, 45 kV, 40 mA, Cu Kα radiation), and , a UV-vis-NIR spectrometer (UV-vis. DRS, Jasco, V-670). Photocatalytic reactions were carried out in a Pyrex-made reaction vessel connected to a closed gas-circulating system. For the Z-scheme water splitting reaction, the composite-type film was horizontally fixed in 100 mL of pure water or a pH-adjusted aqueous solution. The light irradiation was carried out from the top of reactor by a 300W Xe-arc lamp (Perkin-Elmer, Cermax PE300BF) attached with a cut-off filter (Hoya; L42) to eliminate the UV light. The amounts of gas produced were analyzed and quantified by means of an on-line gas chromatograph (GL Science; GC-3200, TCD, Ar carrier, MS-5A column).

5.3 Results and discussion

5.3.1 Characterizations of Composite films prepared *via* screen-printing method

The XRD patterns of the composite-type films (AC-WH film and SS film, see Figure 5-1) showed only the diffraction peaks corresponding to the original $BiVO_4$ and $SrTiO_3$:Rh particles, strongly suggested that any impurity phases were not produced during the calcinations process at 300℃. As for the AC-WH film, any peaks corresponding to impurity phase were not emerged even after calcinations at 500℃. The diffuse reflection spectrum of the composite-type films roughly agreed with the sum of each diffuse reflection spectrum of $BiVO_4$ and Ru/$SrTiO_3$:Rh(2%) even after calcinations at 300–500℃ (Figure 5-2). Figure 5-3 shows the SEM images of the composite-type films (AC-WH and SS). As seen in the cross-section views (a, b), the AC-WH film possessed homogeneous thickness of ca. 10 μm with flat surfaces, whereas the SS film possessed rough surface. The magnified cross-section views (c, d) revealed that both the films have densely packed porous structures. The top-views (Figure 5-4) and elemental mapping images (EDX, see Figure 5-5) of AC-WH and SS film indicated homogenous mixing of $SrTiO_3$:Rh and $BiVO_4$ particles; no significant change in particle sizes compared to the original ones (Figure 5-6) was not observed.

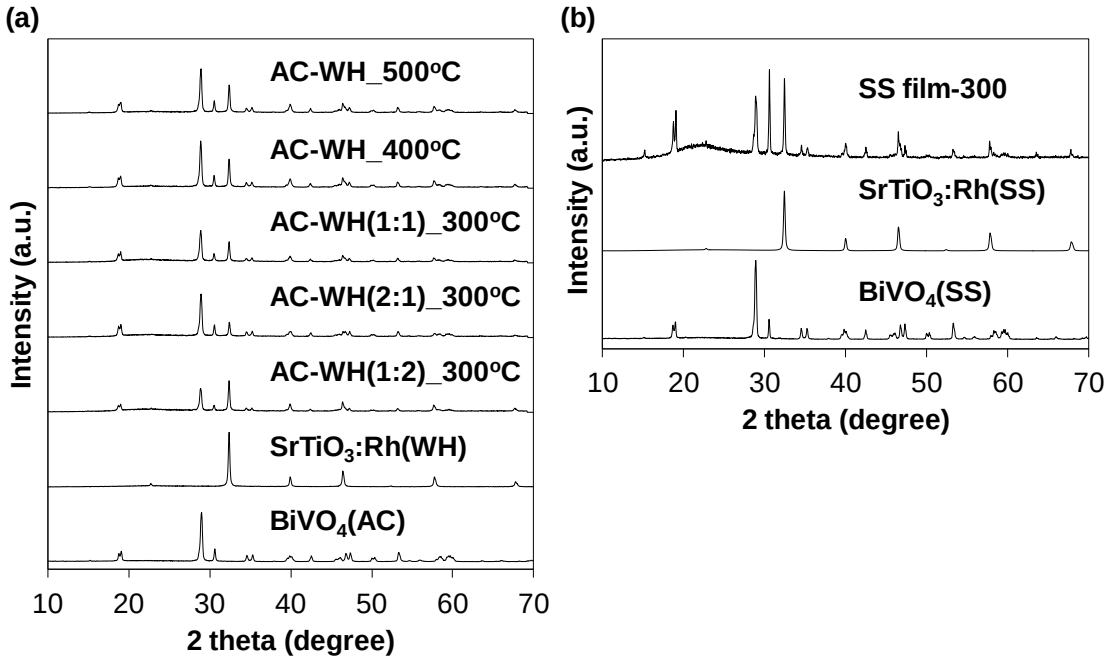

Figure 5-1. XRD patterns of composite-type films ((a) AC-WH films and (b) SS film) prepared by using $SrTiO_3$:Rh and $BiVO_4$ particles.

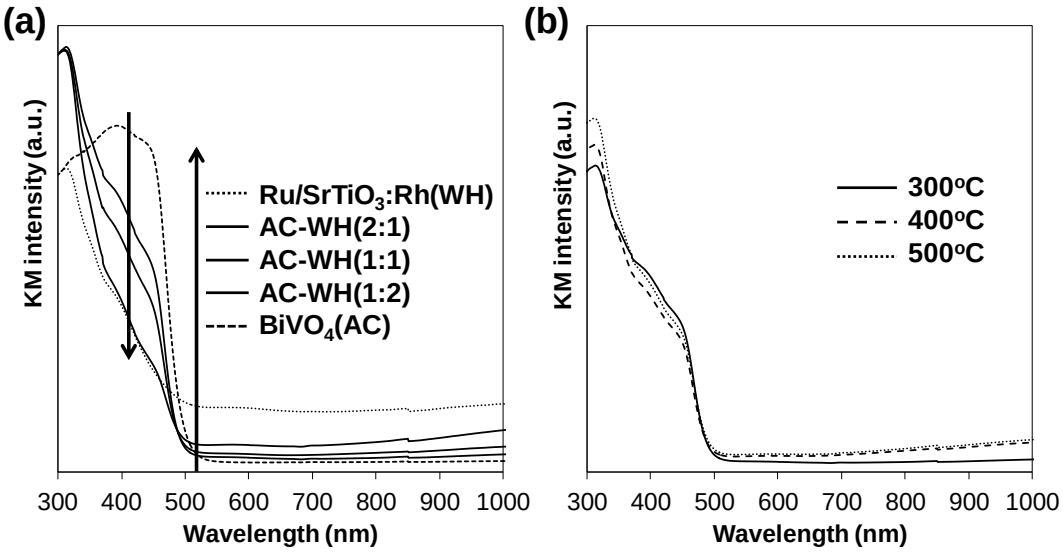

Figure 5-2. UV spectra of composite-type films (a) prepared by mixing at the different weight ratio of $SrTiO_3$:Rh(WH) and $BiVO_4$(AC) particles followed by calcinations at 300℃, (b) prepared by mixing at the 1:1 ratio of $SrTiO_3$:Rh(WH) and $BiVO_4$(AC) particles followed by calcinations at different temperatures.

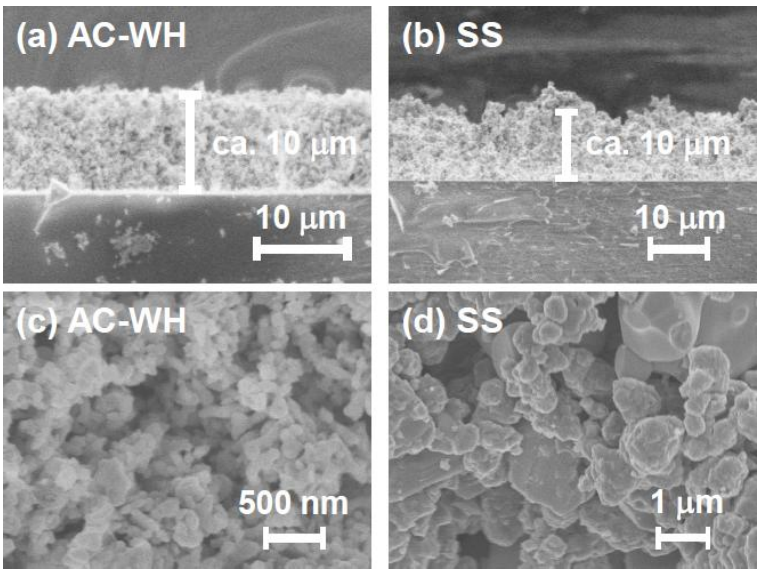

Figure 5-3. Cross-sectional SEM images of composite-type films of (a and c) AC-WH film and (b and d) SS film.

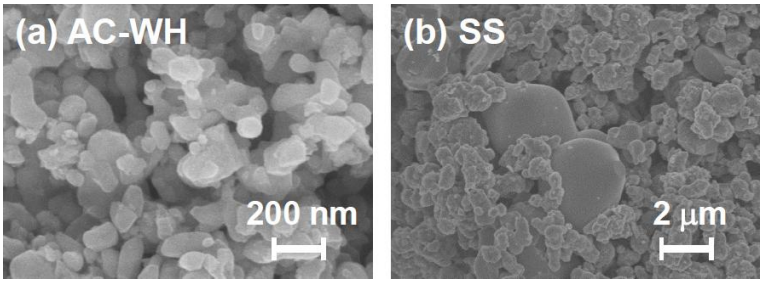

Figure 5-4. Top-view images of composite-type films ((a) AC-WH film and (b) SS film).

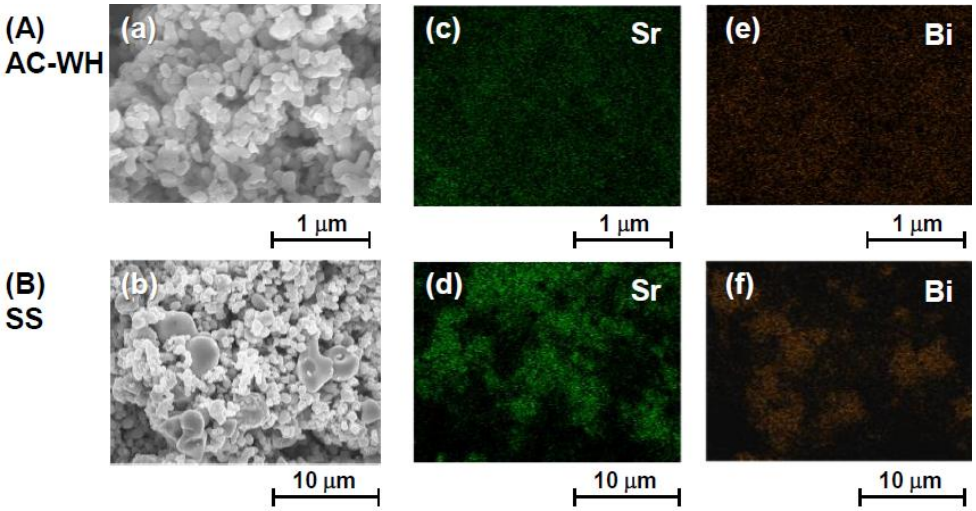

Figure 5-5. Top-view images of composite-type film ((A) AC-WH film, (b) SS film). (a and b) SEM images. (c–f) SEM-EDX mapping images for (c) Bi, (d) Sr.

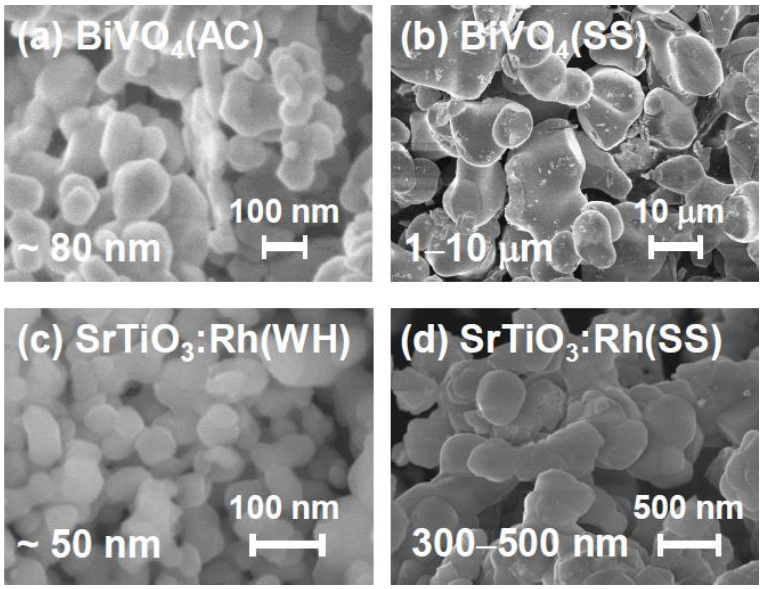

Figure 5-6. SEM images of $BiVO_4$ particles prepared *via* AC process (a) and SS reaction (b). Those of $SrTiO_3$:Rh(2%) particles prepared *via* WH method (c) and SS reaction (d).

5.3.2 Photocatalytic water splitting on composite-type films under visible-light irratiation

The prepared composite-type films were then evaluated as photocatalyst panels for water splitting under visible light. As summarized in Table 5-1, all the composite-type films (AC-WH and SS films, Entries 1–5, 8) generated H_2 and O_2 simultaneously from pure water under visible light irradiation, whereas the films consisted of single photocatalyst (Entries 6, 7) could not generate any gasses. Figure 5-7 shows the time course of gas evolution on the composite-type film prepared *via* the calcination (at 300℃) of the 1:1 mixture of $BiVO_4$(AC) and Ru/$SrTiO_3$:Rh(WH) particles (corresponding to Entry 1). Although O_2 gas was evolved preferentially in the initial period of photoirradiation, H_2 and O_2 gasses simultaneously evolved with steady rates after the evacuation of gas phase, while the gas evolution rates (H_2: 0.71 μmol h^{-1}, O_2: 0.27 μmol h^{-1}) slightly deviated from the stoichiometric value. The total amount of H_2 gas evolved was 31 μmol. The doubled value (i.e., 62 μmol) exceeded the amount of photocatalyst particles ($SrTiO_3$:Rh: 46.1 μmol, $BiVO_4$: 26.4 μmol). These results strongly suggested that the overall water splitting reaction proceeds through the two-step photoexcitation mechanism including interparticle electron transfer. The first step includes the water oxidation to O_2 by the photogenerated holes on the $BiVO_4$ accompanied by the transfer of photoexcited electrons to the neighbor $SrTiO_3$:Rh particles, on which the Rh^{4+} species are reduced to Rh^{3+} by the injected electrons. The second step includes the photoexcitation of the $SrTiO_3$:Rh particles containing the Rh^{3+} species by visible light, generating both the Rh^{4+} species and the photoexcited electrons in the conduction band for water reduction to H_2 on the Ru cocatalysts. The rates of gas evolution on composite-type films were strongly dependent on the calcinations temperature during the preparation process (Entries 1–3 in Table 5-1). As described above, the organic vehicle used in this study can be completely burn out by the calcination at 300℃. The calcination at lower than 250℃ produced residual carbons, resulting in lower activity (not shown). Although the AC-WH film prepared by the calcination at 300℃ exhibited the highest rate of gas evolution, the higher temperatures was found to be detrimental to the activity of composite-type films; the rate of gas evolution significantly decreased with increasing calcination temperature up to 500℃. To clarify the reasons for the lowered activity, the influence of calcination temperature on each photocatalyst was examined. It was found that the calcination at higher temperature was detrimental to the H_2-evolving ability of Ru/$SrTiO_3$:Rh photocatalyst as shown in Table 5-2, in which the rate of H_2 evolution on Ru/$SrTiO_3$:Rh samples from an aqueous methanol solution was obviously decreased by the calcination in air. The most likely reason for this phenomenon

will be that the air-calcination at elevated temperatures causes the oxidation of Ru species loaded on $SrTiO_3$:Rh photocatalyst and consequently lowers their activity as water reduction site. These findings evoked us the necessity of rational design of highly active co-catalysts that are durable against such calcination for improving the efficiency of these photocatalyst panels for water splitting in the future. The water splitting activity of the composite-type films was also dependent on the mixed ratio of $BiVO_4$ and Ru/$SrTiO_3$:Rh. The highest activity was obtained when $BiVO_4$:Ru/$SrTiO_3$:Rh was mixed at 1:1 by weight. This dependence was probably caused by the balance of the numbers of photons absorbed by each photocatalyst, as well as the number of contact points between Ru/$SrTiO_3$:Rh and $BiVO_4$ particles, as suggested by Sasaki and co-workers.[16] The use of fine particles was also confirmed to be effective; the H_2 and O_2 evolution rates on the AC-WH film were about 1.5 times higher than those on the SS film (Entry 8 in Table 5-1). The higher activity of the original fine particles of Ru/$SrTiO_3$:Rh(WH) and $BiVO_4$(AC) than that of samples prepared *via* SS method is undoubtedly favorable for overall efficiency, as well as for the formation of larger numbers of contact between the fine particles.

Table 5-1. Photocatalytic activity of Z-scheme water splitting under visible light irradiation using composite-type films of $BiVO_4$ and $SrTiO_3$: Rh with various modes.

Entry	Synthesis method	$BiVO_4$: $SrTiO_3$:Rh ratio	Calcination temperature (℃)	H_2 evolution rate (μmol/h)	O_2 evolution rate (μmol/h)
1	AC-WH	1:1	300	0.71	0.27
2	AC-WH	1:1	400	0.32	0.16
3	AC-WH	1:1	500	0.16	0.08
4	AC-WH	2:1	300	0.45	0.21
5	AC-WH	1:2	300	0.57	0.25
6	AC-WH	0:1	300	n.d.	n.d.
7	AC-WH	1:0	300	n.d.	n.d.
8	SS	1:1	300	0.54	0.22

*film, 4×4 cm; film thickness, 10 μm; reactant solution, aqueous solution, 100 mL; reactant cell, top-irradiated separable cell; light source, 300 W Xe lamp with cut-off filters (λ > 410 nm).

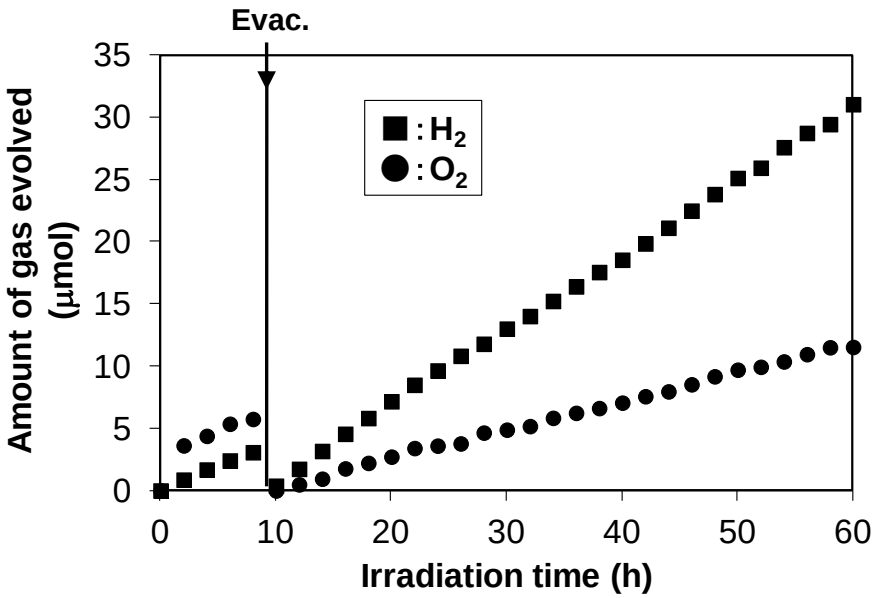

Figure 5-7 Time course of gas evolution on the AC-WH film prepared *via* the calcination (at 300℃) of the 1:1 mixture of $BiVO_4$(AC) and Ru/$SrTiO_3$:Rh(WH) particles. *film, 4×4 cm; film thickness, 10 μm; reactant solution, 100 mL of pure water; reactant cell, top-irradiated separable cell; light source, 300 W Xe lamp with cut-off filters (λ > 410 nm).

Table 5-2. Rate of H_2 evolution from an aqueous methanol solution under visible light irradiation over a Ru/$SrTiO_3$:Rh(WH) particles after calcination at different temperatures (300–500℃).

Calcination temperature (℃)	H_2 evolution rate (μmol/h)
Non	7.8
300	1.6
400	1.4
500	1.3

Conditions: photocatalyst, 0.05g; reactant solution, 50 mL of 10 vol% aqueous methanol solution; reactant cell, top-irradiated separable cell; light source, 300 W Xe lamp with cut-off filters (λ > 410 nm).

To evaluate the influence of immobilization on the performance, the H_2 and O_2 evolution rates on the AC-WH film were compared with those on the suspension systems of photocatalyst particles. In the suspension system of Ru/$SrTiO_3$:Rh and $BiVO_4$ particles, aggregation of the photocatalyst particles occurred upon acidification of the suspension, thus resulting in the highest activity at pH 3.5 where the

effective aggregation for interparticle electron transfer was formed.[20] Thus, the pH value of the reaction solution was adjusted to 3.5, for fair comparison. The water splitting activity on the AC-WH film was almost the same as that on the corresponding suspended particles (Figure 5-8), suggesting the availability of the porous structure in the present composite-type film (AC-WH film) for maintaining the original activity of photocatalyst particles for H_2/O_2 evolution under visible light even after being immobilized on a substrate.

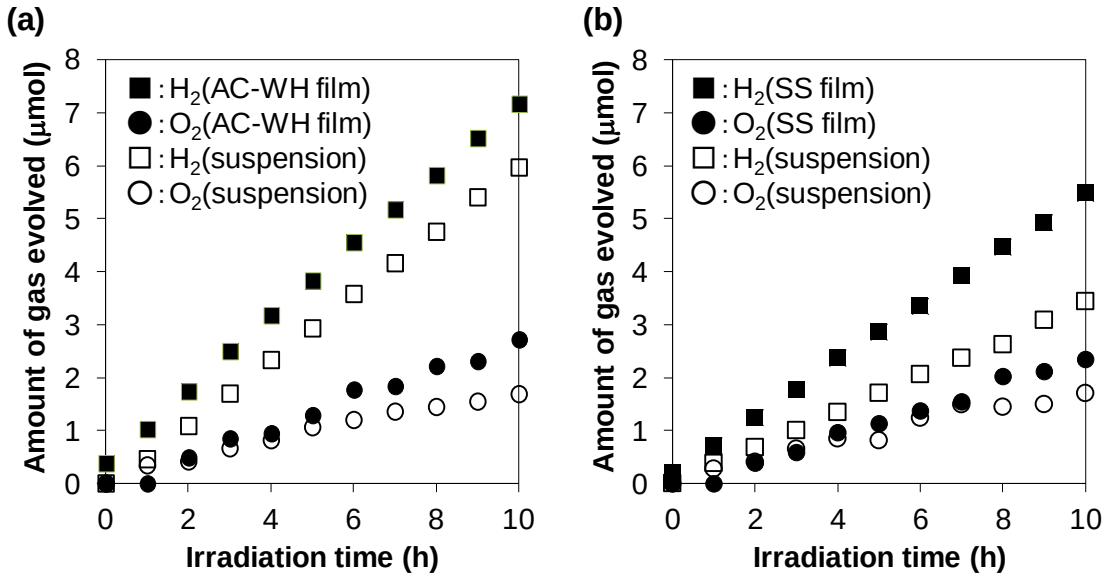

Figure 5-8 H_2 and O_2 evolution from an aqueous solution under visible light irradiation over particle suspension system, and composite-type film calcined at 300℃ using ((a) $Ru/SrTiO_3$:Rh(WH) and $BiVO_4$(AC), (b) $Ru/SrTiO_3$:Rh(SS) and $BiVO_4$(SS)). *film, 4×4 cm , particles: 17 mg $Ru/SrTiO_3$:Rh (8.5 mg) and $BiVO_4$ (8.5 mg); film thickness, 10 μm; reactant solution, aqueous H_2SO_4 solution (pH 3.5), 100 mL; reactant cell, top-irradiated separable cell; light source, 300 W Xe lamp with cut-off filters ($\lambda > 410$ nm).

5.4 Conclusions

In summary, photocatalyst panels that can split water to H_2 and O_2 under visible light were successfully fabricated by employing the composite fine particles of $SrTiO_3$:Rh and $BiVO_4$, both of which were prepared using water based processes. The combination of the fine particles and the screen-printing method enabled the preparation of porous films having enough mechanical strength after calcination in air. Although the improvement in efficiency is still required and challenging, our concept of constructing a highly active porous structure with fine photocatalyst particles *via* simple screen-printing method will open the possibility for the large-scale application of photocatalyst panels in solar-hydrogen production.

References

1. A. Fujishima, K. Honda, *Nature* 1972, **238**, 37.
2. K. Maeda, K. Domen, *J. Phys. Chem. C.*, 2007, **111**, 7851.
3. A. Kudo, Y. Miseki, *Chem. Soc. Rev.*, 2009, **38**, 253.
4. A. Xiong, G. Ma, K. Maeda, T. Takata, T. Hisatomi, T. Setoyama, J. Kubota, K. Domen, *Catal. Sci. Technol.*, 2014, **4**, 325.
5. B.A.Pinaud, J. D. Benck, L. C. Seitz, A. J. Forman, Z. Chen, T. G. Deutsch, B. D. James, K. N. Baum, G. N. Baum, S. Ardo, H. Wang, E. Miller, T. F. Jaramillo, *Energy Environ. Sci.*, 2013, **6**, 1983.
6. S. Okunaka, H. Tokudome, R. Abe, *Catal. Sci. Technol.*, 2016, **6** , 254.
7. R. Abe, *Bull. Chem. Soc. Jpn.*, 2011, **84**, 1000.
8. K. Maeda, *ACS Catal.*, 2013, **3**, 1486.
9. H. Kato, M. Hori, R. Konta, Y. Shimodaira, A. Kudo, *Chem. Lett.*, 2004, **33**, 1348.
10. H. Kato, Y. Sasaki, A. Iwase, A. Kudo, *Bull. Chem. Soc. Jpn.*, 2007, **80**, 2457.
11. Y. Sasaki, A. Iwase, H. Kato, A. Kudo, *J. Catal.*, 2008, **259**, 133.
12. H. Kato, Y. Sasaki, N. Shirakura, A. Kudo, *J. Mater. Chem. A*, 2013, **1**, 12327.
13. Y. Sasaki, H. Kato, A. Kudo, *J. Am. Chem. Soc.*, 2013, 135, 5441.
14. A. Iwase, Y. H. Ng, Y. Ishiguro, A. Kudo, R. Amal, *J. Am. Chem. Soc.*, 2011, **133**, 11054.
15. Q. Wang, Y. Li, T. Hisatomi, M. Nakabayashi, N. Shibata, J. Kubota, K. Domen, *J. Catal.*, 2015, **328**, 308.
16. Y. Sasaki, H. Nemoto, K. Saito, A. Kudo, *J. Phys. Chem. C*, 2009, **113**, 17536.
17. Q. Jia, A. Iwase, A. Kudo, *Chem. Sci.*, 2014, **5**, 1513.
18. S. Okunaka, H. Tokudome, R. Abe, *J. Mater. Chem. A*, 2015, **3**, 14794.
19. J. Yu, Y. Zhang, A. Kudo, *J. Solid State Chem.*, 2009, **182**, 223.
20. S. Okunaka, H. Tokudome, Y. Hitomi, R. Abe, *J. Mater. Chem. A*, 2015, **3**, 1688.
21. R. Konta, T. Ishii, H. Kato, A. Kudo, *J. Phys. Chem. B*, 2004, **108**, 8992.
22. The authors have a patent application (International application number: WO 2014046305 A1) on part of this work: H. Tokudome, S. Okunaka, WO 2014046305 A1, 2014.

Summary and Outlooks

1. Summary of this thesis

In this thesis, the following two themes were studied to achieve efficient photocatalytic water splitting under visible light: (1) the development of new environmentally-friendly water-based processes for preparing fine particles of metal oxide that show high photocatalytic activity, (2) the effective immobilization of such photocatalyst fine particles to the substrates to demonstrate the feasibility of photocatalyst panels. Firstly, a new stable aqueous titania sols were prepared *via* extremely simple process and applied to fabricate highly active TiO_2 film photocatalyst (Chapter 1). Then the stable aqueous titania sols were utilize as precursor of $SrTiO_3$:Rh fine particles that show high activity for photocatalytic H_2 evolution from water under visible light irradiation (Chapter 2). The prepared $SrTiO_3$:Rh fine particles were immobilized onto glass substrates with controlled porous structure *via* simple screen-printing method to demonstrate efficient H_2 evolution from photocatalyst panels (Chapter 3). As an efficient visible-light-responsive photocatalyst for O_2 evolution, fine particles of $BiVO_4$ with scheelite-monoclinic phase were prepared *via* newly developed aqueous process (Chapter 4). Finally, photocatalytic water-splitting into H_2 and O_2 on photocatalyst panel was demonstrated for the first time by using porous and composite type photocatalyst films fabricated *via* simple screen-printing method of the mixed paste of the $SrTiO_3$:Rh and $BiVO_4$ fine particles (Chapter 5). The details of the results described in each chapter were summarized as follows;

Chapter 1;

Highly stable aqueous titania sols were prepared *via* extremely-facile process using titanium tetraisopropoxide under the co-existence of acetylacetone and acetic acid in the water. The co-existence of them enabled the titania colloidal particles in the sol to stably retain the small diameter (average diameter d = ca. 4 nm), due to the effectively suppressed hydrolysis and condensation of titanium tetraisopropoxide even in water. The titania sols could be easily coated on various substrates *via* simple spin-coating method, forming highly homogeneous and transparent TiO_2 films. The TiO_2 thin films prepared from the present new water-base titania sols showed much higher photocatalytic activity for photo-induced superhydrophilicity under UV light irradiation, certainly due to the much lower roughness factor, the smeller size of TiO_2 particle, and the higher content of anatase phase that shows high activity.

Chapter 2;

Fine particles of $SrTiO_3$:Rh were prepared *via* a newly developed facile water-based process, in which the newly synthesized aqueous titana sols as Ti source and their photocatalytic H_2 evolution performance under visible-light irradiation were investigated. The stable aqueous titania sol was mixed with other metal salts and acrylic emulsion in water solvent, then dried and finally calcined in air. The present facile aqueous solution-based process allows to synthesize pure perovskite phase of $SrTiO_3$:Rh at relatively low temperatures (900–1000℃), producing sufficiently small particles of $SrTiO_3$:Rh with primary particle size lower than 50 nm. Such small particles of $SrTiO_3$:Rh could not be obtained by using other water-soluble Ti precursors. The prepared $SrTiO_3$:Rh fine particles exhibited higher efficiency (e.g., 13.2 % of quantum yield at 420 nm) for photocatalytic H_2 evolution under visible light than the best values (ca. 5% at 420 nm) previously reported on $SrTiO_3$:Rh particles prepared *via* conventional solid-state reaction, because of the satisfying both the high crystallinity and high surface area.

Chapter 3;

The prepared $SrTiO_3$:Rh fine particles were immobilized onto glass substrates with controlled porous structure *via* simple spin coating method to demonstrate efficient H_2 evolution from photocatalyst panels. Porous films of $SrTiO_3$:Rh were prepared by simple screen-printing using pastes of fine particles (ca. 50 nm) of $SrTiO_3$:Rh followed by calcination. The screen printing of the paste of $SrTiO_3$:Rh fine particles enabled fabrication of porous films with precisely controlled thickness (1 to 10 μm) and enough mechanical strength. The prepared porous films exhibited high activity for H_2 evolution from aqueous methanol solution under visible light irradiation ($\lambda > 410$ nm), due to the effective utilization of incident photons in visible light region and to the facilitate transfer of substances within the pores. Furthermore, the addition (10–20 wt%) of the large particles to the $SrTiO_3$:Rh films further increased the H_2 evolution rate probably due to the light scattering with large $SrTiO_3$:Rh particles, by which the neighboring small $SrTiO_3$:Rh particles in the films can effectively absorb the scattered light and generate more H_2.

Chapter 4;

Fine particles of $BiVO_4$ with scheelite-monoclinic (s-m) phase, which is known as the most favorable crystal phase for photocatalytic O_2 evolution under visible light irradiation, were prepared *via* a newly developed aqueous process. Stable aqueous solutions that contain both Bi^{3+} and V^{5+} complexes were prepared by simply mixing of two aqueous solutions in which each cation was stabilized with an appropriate chelating agent. The use of chelating agents (glycolic acid (gly), L(+)-tartaric acid (tart), citric acid (cit), or ethylenediamine tetraacetic acid (edta)) was effective to form stable V^{5+} complexes from NH_4VO_3. On the other hand, only the use of two equivalents of edta with $Bi(NO_3)_3 \cdot 5H_2O$ was effective to stabilize the Bi^{3+} complex in water, while the use of other ligands resulted in precipitations. Evaporation of the aqueous solution containing the stable Bi^{3+} and V^{5+} complexes and subsequent calcination in air at 500°C yielded s-m $BiVO_4$ particles smaller than 300 nm, which were much smaller than $BiVO_4$ particles prepared *via* conventional solid-state reactions (1–10 μm). In particular, the $BiVO_4$ particles that were prepared with the tart ligand for V^{5+} stabilization possessed the smallest size (< 80 nm) and exhibited the highest photocatalytic activity for O_2 evolution from an aqueous solution containing an electron acceptor (Ag^+ or Fe^{3+}) under visible-light irradiation. These results strongly suggested that the tart ligand effectively suppresses particle growth during the crystallization process and thereby affords small $BiVO_4$ particles with high crystallinity, both of which are necessary to achieve highly efficient photocatalysis.

Chapter 5;

Finally, the construction of photocatalyst panels that can split water into H_2 and O_2 under visible light was attempted to employ the combination of the developed fine particles of $SrTiO_3$:Rh and $BiVO_4$ as components of interparticle Z-scheme water splitting. The composite-type films were prepared by employing simple screen-printing of the mixed paste of $BiVO_4$ and $SrTiO_3$:Rh fine particles (< 100 nm). The prepared composite-type films were found to possess porous structure and to exhibit high activity for H_2 and O_2 evolution from pure water under visible light irradiation ($\lambda > 410$ nm). The use of fine particles and simple screen-printing method enabled us to prepare the films with controlled structures for both the effective light absorption and the efficient

transportation of substances and/or products within the pores.

2. Outlooks

The goal of this study is the construction of an efficient photocatalysis that is environmentally-friendly and also cost-effective in large scale application. As for the environmental purification using photo-induced surface superhydrophilicity of TiO_2 under UV-light irradiation, the present aqueous titania sols have superior features such as high stability (for more than one year), no use of organic solvents, and mild acidity (pH ~4). The aqueous titania colloidal sols are very convenient for preparing homogeneous and transparent TiO_2 thin films with high photocatalytic activity for photo-induced superhydrophilicity under UV-light irradiation. These superior features of newly developed aqueous titania sols will widen the application of TiO_2 thin films for practical use on a large scale. As for the water-splitting reaction, significant enhancement of the solar-light to hydrogen efficiency is still indispensable for the practical application of this technique for commercial hydrogen production. It is generally suggested that the overall water-splitting system *via* solar-driven with a solar energy conversion efficiency higher than 5% requires an apparent quantum efficiency of as high as 30% and up to 600 nm for the photocatalytic reaction. Although the apparent quantum efficiency still remains at most a few percent at a wavelength around 400 nm, it appears that the efficiency of the present water-splitting system using $SrTiO_3$:Rh and $BiVO_4$ could be improved by extending the visible absorption of photocatalysts toward a longer wavelength. Accordingly, it is necessary to develop more efficient photocatalytic materials by decreasing the intrinsic band gap to be as narrow as 2 eV (corresponding to 600 nm) or by introducing doing levels of metal ions to harvest long wavelength light. It is generally accepted that particle sizes influence the photocatalytic reaction. The distance that photo-excited carriers have to migrate to reach the active surface sites is shorter, and therefore charge recombination is probably lower when the particle size is smaller. The fine particles synthesized by the present water-based process actually enhance the photocatalytic activity under visible-light irradiation. This research offers useful concepts for the preparation of active metal oxide photocatalysts. The present aqueous titania colloidal sols are very convenient to be used as a metal source of mixed material. As mentioned in general introduction, the precursors of many photocatalysts include transition material oxides consisting of d^0 cations, such as Ti^{4+}, Ta^{5+}, and Nb^{5+}. The present water-based

processes based on coordination chemistry are environmentally friendly and can be applied to metal oxides including not only Ti but also other transition metals such as Ta and Nb.

For large-scale applications, the development of techniques for immobilizing photocatalyst particles onto substrates is indispensable, in addition to improving the efficiency of photocatalytic particles. In particular, studies of photocatalyst panels have recently been promoted. The concept of constructing a highly active porous structure with fine photocatalyst particles *via* a simple screen-printing method will open the possibility for the large-scale application of photocatalyst panels in solar-hydrogen production.

For visible-light driven overall water-splitting reaction, further development of photocatalysts requires advanced knowledge of materials preparation and system design. The author hopes that the results presented in this dissertation will provide useful information for improving the photocatalytic performance of photocatalysis.

List of publications (Peer Reviewed Papers)

1. Sayuri Okunaka, Hiromasa Tokudome, Yutaka Hitomi, Ryu Abe:
   ″Facile preparation of stable aqueous titania sols for fabrication of highly active TiO_2 photocatalyst thin films″
   J. Mater. Chem. A, **2015**, *3*, 1688–1695.

2. Sayuri Okunaka, Hiromasa Tokudome, Ryu Abe:
   ″Facile Water-based Preparation of Rh-doped $SrTiO_3$ Nanoparticles for Efficient Photocatalytic H_2 Evolution under Visible Light Irradiation″
   J. Mater. Chem. A, **2015**, *3*, 14794–14800.

3. Sayuri Okunaka, Hiromasa Tokudome, Ryu Abe:
   ″Structure-controlled Porous Films of Nanoparticulate Rh-doped $SrTiO_3$ Photocatalyst toward Efficient H_2 Evolution under Visible-light Irradiation″
   Catal. Sci. Technol., **2016**, *6*, 254–260.

4. Sayuri Okunaka, Hiromasa Tokudome, Yutaka Hitomi, Ryu Abe:
   ″Preparation of Fine Particles of Sheelite-Monoclinic Phase $BiVO_4$ *via* an Aqueous Chelating Method for Efficient Photocatalytic Oxygen Evolution under Visible-light Irradiation″
   J. Mater. Chem. A, under revision.

5. Sayuri Okunaka, Hiromasa Tokudome, Ryu Abe:
   ″Z-scheme Water Splitting into H_2 and O_2 under visible light over Photocatalyst Panels consisting of Rh-doped $SrTiO_3$ and $BiVO_4$ Fine Particles″
   Chem. Lett., **2016**, *45*, 57–59.

Acknowledgements

This thesis is based on experimental work carried out in the Research Institute of TOTO Ltd. and the Laboratory of Professor Abe (Department of Energy and Hydrocarbon Chemistry, Kyoto University). It has been a great opportunity to conduct research in the photocatalysis field.

The author would like to express her sincere gratitude to Professor Ryu Abe (Department of Energy and Hydrocarbon Chemistry, Kyoto University) for accepting her as a doctoral student in his laboratory and guiding the author's study with beneficial discussions, continuous guidance, and kind encouragement. This remarkable experience in the Professor Abe's laboratory will help the author develop future research studies.

The author would also like to appreciate to Professor Hiroshi Kageyama (Department of Energy and Hydrocarbon Chemistry, Kyoto University) and Professor Tsunehiro Tanaka (Department of Molecular Engineering, Kyoto University) for taking time from their busy schedules to carefully read the present thesis and to provide their valuable comments.

The author would like to express her deepest, sincerest gratitude to Dr. Hiromasa Tokudome (Research Institute, TOTO Ltd.) for his many heartwarming suggestions, valuable discussions, and continuous encouragement. The author learned the spirit of scientific research from him and will never forget this passion for research.

The author also wish to specially acknowledge Professor Yutaka Hitomi (Department of Molecular Chemistry and Biochemistry, Doshisha University), not only for his support in helping with experiments involving NMR measurements but also for his heartfelt suggestions, meaningful discussions and continuous encouragement.

The author appreciates Assosiate Professor Masanobu Higashi (Department of Energy and Hydrocarbon Chemistry, Kyoto University) for helping with the BET measurements and Mr. Masashi Kondo (Yokohama National University) and Ms. Ayako Ikezawa (Research Institute, TOTO Ltd.) for helping with the TEM observations in Chapter 2. Grateful acknowledgements are also extended to Professor Kazunari Domen (Department of Chemical System Engineering, The University of Tokyo) and Professor Akihiko Kudo (Department of Applied Chemistry, Tokyo University of Science) for their heartfelt support and kind encouragement. The author also deeply grateful to Mr. Yukihiro Fukuda, Mr. Eiichi Kojima, Mr. Nobuhiko Kanekuni and Mr. Nobuhiro Shouno (Research Institute, TOTO Ltd.) for

giving her chance to study in the Professor Abe’s laboratory. The author also appreciates Emeritus Professor Koji Kano (Department of Molecular Chemistry and Biochemistry, Doshisha University) for supporting her research life, even after the master's program graduation. Sincere guidance is also expressed to all the members of the Professor Abe’s laboratory and research institute of TOTO Ltd. for their kind supports and encouragements.

Finally, the author would like to express her special thanks to her parents, grandparents and brother for their warm encouragement and deep understanding toward accomplishing this work.

Sayuri Okunaka

2016